

Interlinked signaling feedback loops and self-regulation during vertebrate limb development

Inauguraldissertation

zur
Erlangung der Würde eines Doktors der Philosophie
vorgelegt der
Philosophisch-Naturwissenschaftlichen Fakultät
der Universität Basel

von

Jean-Denis Bénazet

aus Cahors, Frankreich

Basel, 2009

Original document stored on the publication server of the University of Basel
edoc.unibas.ch

This work is licenced under the agreement „Attribution Non-Commercial No Derivatives –
2.5 Switzerland“. The complete text may be viewed here:
creativecommons.org/licenses/by-nc-nd/2.5/ch/deed.en



Attribution-Noncommercial-No Derivative Works 2.5 Switzerland

You are free:



to Share — to copy, distribute and transmit the work

Under the following conditions:



Attribution. You must attribute the work in the manner specified by the author or licensor (but not in any way that suggests that they endorse you or your use of the work).



Noncommercial. You may not use this work for commercial purposes.



No Derivative Works. You may not alter, transform, or build upon this work.

- For any reuse or distribution, you must make clear to others the license terms of this work. The best way to do this is with a link to this web page.
- Any of the above conditions can be waived if you get permission from the copyright holder.
- Nothing in this license impairs or restricts the author's moral rights.

Your fair dealing and other rights are in no way affected by the above.

This is a human-readable summary of the Legal Code (the full license) available in German:
<http://creativecommons.org/licenses/by-nc-nd/2.5/ch/legalcode.de>

Disclaimer:

The Commons Deed is not a license. It is simply a handy reference for understanding the Legal Code (the full license) — it is a human-readable expression of some of its key terms. Think of it as the user-friendly interface to the Legal Code beneath. This Deed itself has no legal value, and its contents do not appear in the actual license. Creative Commons is not a law firm and does not provide legal services. Distributing of, displaying of, or linking to this Commons Deed does not create an attorney-client relationship.

Genehmigt von der Philosophisch-Naturwissenschaftlichen Fakultät

auf Antrag von

Prof. Dr. Markus Affolter, Prof. Dr. Rolf Zeller

Basel, den 17. Februar 2009

Prof. Dr. Eberhard Parlow

Dekan

I. TABLE OF CONTENTS

I. TABLE OF CONTENTS	p3
II. LIST OF ABBREVIATIONS	p6
III. ABSTRACT	p9
IV. INTRODUCTION	p10
A historical appreciation of the progress zone and morphogen gradient models	p10
<i>The AER controls outgrowth and patterning of the proximo-distal limb bud axis</i>	p12
<i>The ZPA is an organizer that controls antero-posterior limb bud patterning</i>	p13
Retinoic acid and FGFs: evidence that two opposing signaling gradients control proximo-distal limb axis specification	p14
<i>RA acts as a proximalizing morphogenetic signal</i>	p14
<i>AER-FGF signaling promotes distal progression of limb bud morphogenesis</i>	p15
<i>Early specification and progressive expansion/differentiation front models</i>	p16
Of space and time: How the SHH morphogen specifies the antero-posterior limb axis and digits identities	p19
<i>Setting up the ZPA and morphogenetic SHH signaling</i>	p19
<i>Cellular response to morphogenetic SHH signaling</i>	p22
Back to the future: How and when are digits specified and/or determined?	p23
Temporal regulation of BMP signaling and integration of proximo-distal and antero-posterior patterning by interacting signaling systems with self-regulatory properties	p25
V. AIMS OF THE THESIS	p27
VI. MATERIAL AND METHODS	p29
Homologous recombination in mouse embryonic stem cells	p29
<i>Preparation of MEF</i>	p29

<i>ES cells expansion and electroporation</i>	p30
<i>Drug selection</i>	p30
<i>Colony picking</i>	p30
<i>Freezing clones</i>	p31
<i>Generating chimeras</i>	p31
<i>REAGENTS AND PROTOCOLS</i>	p31
Genetic analysis of <i>Grem1-Bmp2</i> and <i>Grem1-Bmp7</i> interactions	p36
Genetic analysis of <i>Bmp4</i> functions and interactions	p37
Tamoxifen (TM)-mediated activation of Cre recombinase in embryos carrying the TM-Cre transgene	p37
Skeletal staining	p39
Whole mount <i>in situ</i> mRNA hybridization	p39
X-Gal staining	p41
Cell death detection using LysoTracker Red	p43
Quantitative real-time PCR analysis	p44
Grafting and culturing of mouse limb buds	p45
DiI labeling of posterior mesenchymal cells in cultured mouse limb buds	p46
Mathematical modeling	p47
Parameter sensitivity analysis	p50
VII. GENERATION OF A <i>HAND2</i> CONDITIONAL NULL ALLELE	p53
Introduction	p53
<i>Hand</i> genes and murine heart development	p54
<i>Hand2</i> functions during limb development	p56
<i>Limb bud prepattern</i>	p56
<i>Hand2 and the establishment of the SHH polarizing activity</i>	p57
Homologous recombination of the <i>Hand2</i> locus	p60
VIII. A SELF-REGULATORY SYSTEM OF INTERLINKED SIGNALING FEEDBACK LOOPS CONTROLS VERTEBRATE LIMB PATTERNING	p63
Introduction	p63
Results	p66

<i>Reduction of BMP4 activity enables SHH-dependent specification of digit identities</i>	p66
<i>Self-regulation of the BMP4/GREMI interactions</i>	p73
<i>Interlinked feedback loops control specification of digit identities</i>	p76
<i>Mesenchymal BMP4 is required during the onset of limb bud development</i>	p80
<i>Prx1-Cre mediated inactivation of Bmp4 in the forelimb bud mesenchyme using different genetic make-ups</i>	p81
<i>Supplementary figures</i>	p85
Discussion	p92
IX. CONCLUSION AND OUTLOOK	p97
X. ACKNOWLEDGEMENTS	p101
XI. REFERENCES	p103
XII. CURRICULUM VITAE AND PUBLICATION LIST	p116

II. LIST OF ABBREVIATIONS

Δ	Null allele
Δc	Conditionally induced null allele
Δc -Jfm	Conditionally induced null allele from James Martin's laboratory
AER	Apical Ectodermal Ridge
AER-FGFs	FGFs expressed by the AER
Ant	Anterior
AP	Antero-posterior
B4	Bmp4
BAC	Bacterial Artificial Chromosome
BBBA	Benzyl-benzoate benzyl-alcohol
bHLH	basic Helix Loop Helix
BMP	Bone Morphogenetic Protein
BMPR IA	BMP Receptor type IA
bp	base pair
BSA	Bovine serum albumin
cDNA	complementary DNA
CHAPS	3-[(3-Cholamidopropyl)dimethylammonio]-1-propanesulfonate
ChIP	Chromatin immunoprecipitation
Cl	Clavicle
DiI	1,1'-dioctadecyl-3,3,3'-tetramethylindocarbocyanine perchlorate
Dist	Distal
DMEM	Dubelcco's Modified Eagle's Medium
DNA	Deoxyribonucleic acid
DV	Dorso-ventral
EDTA	Ethylenediaminetetraacetic acid
e-m	epithelial-mesenchymal
ES	Embryonic Stem
FGF	Fibroblast Growth Factor
f-Jfm	Conditional allele generated in James Martin's laboratory

Frt	FLP recognition target
GLI3	GLI-Kruppel family member GLI3 (Greig cephalopolysyndactyly syndrome)
GLI3R	Repressor form of the transcription factor GLI3
GREM1, G1	Gremlin1
HAND	Heart, autonomic nervous system, and other neural crest-derived tissues
HBSS	Hanks' Balanced Salt Solution
hf	hypomorphic floxed (conditional) allele
Hox	Homeobox gene
Hu	Humerus
ID	Interdigital
kb	kilobase
LacZ	Lactose operon gene Z
LIF	Leukemia Inhibiting Factor
Matlab	Matrix Laboratory
MEF	Mouse Embryonic Fibroblast
Msx	Muscle segment homeobox homolog
Neo	Neomycin resistance gene
NMRI	Naval Medical Research Institute
ODE	Ordinary Differential Equation
PABA	4-Aminobenzoic acid (also known as para-aminobenzoic acid)
PBS	Phosphate Buffer Saline
PBT	PBS with 0.1% Tween 20
PCR	Polymerase Chain Reaction
PD	Proximo-Distal
PFA	Paraformaldehyde
PFR	Phalanx Forming Region
Pgk	Phosphoglycerate kinase
Post	Posterior
Prox	Proximal
Ptc1	Patched1
r, Ra	Radius

RA	Retinoic Acid
RNA	Ribonucleic Acid
RPL 19	Ribosomal protein large 19
rpm	Revolution per minutes
r/u	Fused radius and ulna
RALDH	Retinaldehyde dehydrogenase
Sc	Scapula
Smad	Mothers Against Decapentaplegic homolog
SHH	Sonic Hedgehog
Sox9	SRY (sex determining region Y)-box 9
Spry4	Sprouty 4
tg	transgene
TM	Tamoxifen
tRNA	Transfer RNA
TUNEL	Terminal deoxynucleotidyl transferase dUTP nick end labeling
u, Ul	ulna
Wt	Wild type
ZPA	Zone of Polarizing Activity

III. ABSTRACT

Reliable organ and tissue morphogenesis seems to depend on self-regulatory mechanisms that are able to buffer spontaneous and/or genetic variations. While the analysis of the interactions of BMPs with their antagonists during gastrulation has provided insights into the self-regulatory capacity of early embryos, few other mechanisms endowing developmental programmes with robustness have been identified. Limb development and digit specification are regulated by epithelial-mesenchymal (e-m) interactions involving instructive SHH and FGF signaling. The BMP antagonist Gremlin1 (GREM1) is key to establishing these interactions. By combining genetics with ex vivo manipulation and mathematical modeling, we establish that both BMP4 and SHH positively regulate *Grem1* expression, defining this antagonist as a critical node that links a fast and self-regulatory BMP4/GREM1 module to the SHH/GREM1/FGF e-m feedback loop. This network architecture allows a self-regulative switch from BMP4- to SHH-driven limb development and endows limb patterning with robustness against variations in gene activity due to interconnectivity between the BMP, SHH and FGF signaling pathways. The establishment of this robust signaling network may have contributed to the appearance and stabilization of pentadactyly in tetrapods.

IV. INTRODUCTION

A historical appreciation of the progress zone and morphogen gradient models

For more than half a century, manipulation and analysis of vertebrate limb development in different animal models has yielded seminal discoveries that further our knowledge of how growth, specification and determination are coordinately controlled during embryogenesis. The developing limb bud is a large embryonic field whose cells receive proliferative and positional cues from signals emanating from two instructive signaling centers (organizers). The fore- and hindlimb buds emerge at defined somite positions perpendicular to the primary body axis due to continued growth of the flank mesoderm. The developing limb bud is patterned along three axes, the antero-posterior (AP), dorso-ventral (DV) and proximo-distal (PD) axes as is apparent from the morphology of the definitive limb skeleton (Fig. 1A, B). While limb skeletal morphology varies greatly among tetrapods, the underlying basic bauplan is conserved and provides an excellent read-out for normal and altered limb morphogenesis (Shubin et al. 1997). Three main limb skeletal compartments characterize the PD axis: the proximal stylopod, followed by the zeugopod and the distal autopod (Fig. 1A, B). The AP limb axis is congruent with the primary body axis and manifests itself best in the skeletal morphology of the zeugopod (radius/ulna and tibia/fibula) and in the distinct identities of the digits bearing autopod (Fig. 1A, B). Five distinct digits form in mice and humans with digit 1 (thumb) having the most anterior and digit 5 (little finger) the most posterior identities. AP digit identities are morphologically defined by their position and the number, length, and shapes of metacarpal bones and phalanges (Fig. 1A). It is generally accepted that the identities of the limb skeletal elements reflect the establishment of positional identities during limb bud development. While this thesis focuses on the role of the graded signaling interactions that

control establishment of the PD and AP limb bud axes, during outgrowth the limb bud is also polarized along its DV axis from early developmental stages onwards (reviewed by Zeller and Duboule 1997; Niswander 2003).

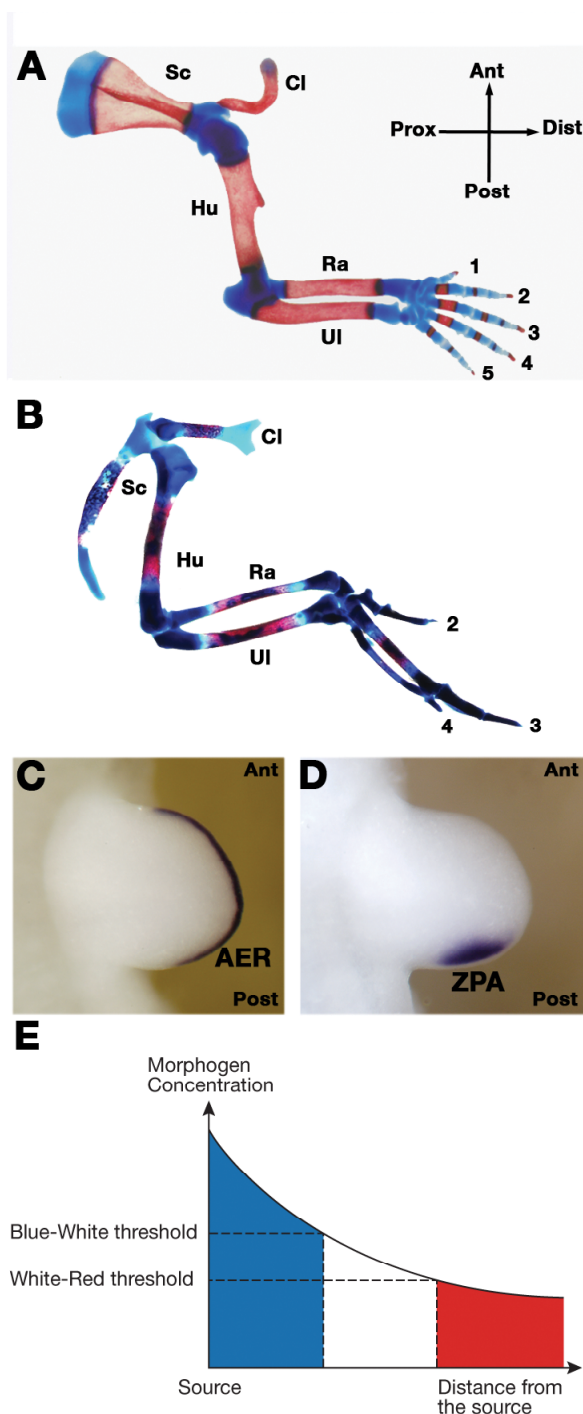


Fig. 1. Two morpho-regulatory signaling centers control vertebrate limb bud development.

(A) Skeletal preparation of a mouse forelimb at birth. (B) Skeletal preparation of a fetal chicken wing at day 15 of embryonic development. Red and blue histological stains mark ossified bone and cartilage, respectively. Despite morphological differences, the basic bauplan along both axes is conserved Prox-Dist, proximo-distal axis; Ant-Post, antero-posterior axis; Sc, scapula; Cl, clavicle; Hu, humerus; Ra, radius; UI, ulna. Numbers indicate digit identities. (C) Visualization of the AER by in situ detection of *Fgf8* transcripts in a mouse limb bud. (D) The ZPA expresses the *Shh* morphogen. (E) Wolpert's French flag model: A concentration gradient forms by diffusion of a morphogen from a source and positional information is determined in groups of cells by inducing distinct responses to specific concentration thresholds (indicated by blue, white, red).

The AER controls outgrowth and patterning of the proximo-distal limb bud axis

The emerging limb bud consists of an ectodermal pocket initially “filled” with apparently naïve and undetermined mesenchymal cells that derive from the embryonic flank mesoderm. During the onset of outgrowth, a morphologically distinct ectodermal thickening that consists of a partially stratified epithelium forms at the distal tip, which is called the apical ectodermal ridge (AER; Fig. 1C). Saunders carried out a series of microsurgical experiments in chicken limb buds 60 years ago, establishing that removal of the AER causes a developmental arrest, which truncates the chicken wing skeleton (Saunders 1948). Removing the AER at progressively earlier stages results in truncations of the limb skeleton at progressively more proximal levels. From these experiments, Saunders concluded that the AER is required for outgrowth and patterning of the PD limb axis. In particular, it seemed that the time mesodermal cells spend under the influence of the AER is relevant with respect to their subsequent PD identities, such that the distal-most cells depend on the AER for the longest time. Furthermore, grafts of an AER to a recipient limb bud induces ectopic PD outgrowth, revealing its strong growth promoting potential, while its removal causes cell death (Fallon et al. 1983). These and other studies led Summerbell and Wolpert to formulate the so-called progress zone model (Fig. 2A; Summerbell et al. 1973; Wolpert et al. 1979). This model, which has only recently been challenged and modified as a consequence of extensive molecular analysis (see later) predicts that acquisition of PD identities depends on the time spent by proliferating, undetermined cells in the distal mesenchyme (= progress zone) under the influence of AER signals. As the progress zone is displaced distally, the more proximal cells are no longer under the influence of the AER, which causes determination of their positional identities. Mesenchymal cells “left behind” early acquire more proximal identities while progenitor cells staying under influence of the AER longer acquire progressively more

distal identities (Fig. 2A). The progress zone model introduced for the first time the notion of time as an important component of morphogenetic signaling. In 1993, Niswander and colleagues identified fibroblast growth factors (FGFs) as the relevant signals produced by the AER to induce PD limb axis formation. In particular, PD outgrowth is rescued by exogenous application of FGFs upon AER removal and FGFs are normally expressed by the AER (Fig. 1C; Niswander et al. 1993). This study provided the first molecular insights into how AER-FGF signaling controls PD outgrowth and patterning.

The ZPA is an organizer that controls antero-posterior limb bud patterning

About 50 years ago, Zwilling (1956) was trying to understand how the AER is maintained and in the course of these studies he identified a region within the posterior mesenchyme with the property to produce an AER maintenance factor. A good decade later, Saunders and Gasseling (1968) discovered that transplantation of this posterior mesenchyme to the anterior margin of recipient chicken wing buds results in induction of mirror image duplications of all digits, while grafts to more posterior positions result in progressively less complete duplications (Tickle et al. 1975; Summerbell 1979). This re-specification activity was termed “polarizing activity” and the posterior region was called the Zone of Polarizing Activity (ZPA) or Polarizing Region (Fig. 1D) due to its properties of a classical embryonic organizer. Wolpert (1969) proposed that the ZPA specifies positional information in the limb bud mesenchyme by secreting a diffusible molecule that forms a posterior (high) to anterior (low) gradient. Wolpert’s model became famous as the “French Flag model”, as it proposes that mesenchymal cells receive their positional identities by responding to specific thresholds of the morphogen gradient (Fig. 1E). In contrast to other proposals (see e.g. French et al. 1976), Wolpert’s morphogen hypothesis was able to explain the different patterns of digit

duplications observed by grafting ZPAs into various positions in recipient limb buds. In support, Tickle (1981) established that the numbers and identities of duplicated digits depend on the number of ZPA cells grafted. A small number of ZPA cells (~30) induce digits with anterior identities, while specification of additional posterior digits requires many more cells (≥ 150). With the dawn of molecular biology, the hunt for Wolpert's morphogen was initiated and retinoic acid (RA) was first identified as a diffusible molecule that is able to induce digit duplications comparable to ZPA grafts (Tickle et al. 1982; Summerbell and Harvey 1983). Despite initial claims (Thaller and Eichele 1987), it was never shown that endogenous RA is produced or secreted by ZPA cells to form a posterior to anterior gradient, which together with other experimental results excluded it from being the morphogen produced by the ZPA (Wanek and Bryant 1991). In 1993, Tabin and coworkers succeeded in identifying Sonic Hedgehog (SHH) as the true morpho-regulatory signal peptide produced by the ZPA (Fig. 1D; Riddle et al. 1993).

Retinoic acid and FGFs: evidence that two opposing signaling gradients control proximo-distal limb axis specification

RA acts as a proximalizing morphogenetic signal

Although a direct role for RA in specifying the AP axis has been excluded, experimental manipulation of chicken limb buds and genetic analysis in the mouse show that RA functions in specification of the PD axis for which there are now good molecular markers. For example, the expression domains of the *Meis1/2* transcription factors mark the proximal limb bud mesenchyme corresponding roughly to the future stylopod, while *Hoxa11* and *Hoxa13* mark the prospective zeugopod and autopod territories (Fig. 2C; reviewed by Tabin and Wolpert 2007). Their expression is altered by ectopic RA signaling such that the expression

of *Meis1/2* expands distally upon RA treatment (Mercader et al. 2000) or genetic inactivation of CYP26B1, an enzyme involved in the degradation of RA (Yashiro et al. 2004). Concurrently, the distal expression of *Hox* genes is reduced, revealing that exogenous RA proximalizes the limb bud mesenchyme (Mercader et al. 2000). RA is synthesized by retinaldehyde dehydrogenases (RALDH) and in particular, RALDH2 is expressed in the limb bud flank mesenchyme during onset of outgrowth. In the mouse, inactivation of the *Raldh2* gene arrests embryogenesis and disrupts initiation of limb bud development (Niederreither et al. 1999; Niederreither et al. 2002). The latter is rescued by providing exogenous RA during the onset of limb bud development (Niederreither et al. 2002). Taken together, these studies indicate that RA is synthesized in the proximal mesenchyme and spreads into the distal limb bud, where it is actively degraded (Yashiro et al. 2004). This is presumed to result in a proximo-distal gradient of RA activity, whereby high levels of RA would specify proximal cell fates and inhibit distal ones (Fig. 2C).

AER-FGF signaling promotes distal progression of limb bud morphogenesis

The seminal discovery that FGFs can replace the AER and restore distal outgrowth upon AER removal in chicken limb buds (Niswander et al. 1993) resulted in the systematic genetic analysis of the essential FGF signaling function during mouse limb bud development. *Fgf10* is expressed by the limb bud mesenchyme and is essential to establish AER-FGF signaling, which is in turn required to maintain *Fgf10* expression (Ohuchi 1997; Sun et al. 2002). Indeed, development of *Fgf10* deficient limb buds is arrested at a very early stage resulting in agenesis of limbs (Min et al. 1998; Sekine et al. 1999). Four *Fgf* ligands (*Fgf4,-8,-9,-17*) are expressed by the AER (reviewed by Martin 1998) and extensive genetic analysis has provided insight into their overlapping, respectively redundant functions during outgrowth

and PD patterning of mouse limb buds. Rather unexpectedly, concurrent inactivation of all three *Fgfs* expressed predominantly by the posterior AER (*Fgf4,-9,-17*) does not alter limb bud development (Mariani et al. 2008). In contrast loss of *Fgf8*, which is the first and only *Fgf* ligand expressed by the entire AER from early stages onwards (Fig. 1C) disrupts formation of the proximal most limb skeletal element, the stylopod (Lewandoski et al. 2000; Moon and Capecchi 2000). This unexpected early and transient disruption of PD outgrowth is rescued by precocious and uniform activation of *Fgf4* in the *Fgf8*-deficient AER, which enables almost normal development of the more distal limb skeleton (Lu et al. 2006). Indeed, concurrent inactivation of both *Fgf8* and *Fgf4* causes a complete arrest of limb bud development and limb agenesis (Sun et al. 2002; Boulet et al. 2004). These genetic studies also revealed that transient expression of *Fgf8* and *Fgf4* during initiation of limb bud outgrowth is sufficient for specification of the entire PD axis, but the progressive proliferative expansion of such specified limb segments is disrupted (Sun et al. 2002). A recent genetic study shows that the other AER-FGFs, in particular FGF9, contribute to this proliferative expansion of the early specified PD axis such that higher AER-FGF levels are required for formation of more distal limb skeletal structures (Fig. 2B, C; Mariani et al. 2008). Taken together, this genetic analysis reveals an instructive role of AER-FGF signaling in the specification and proliferative expansion of the PD limb bud axis.

Early specification and progressive expansion/differentiation front models

These results, in particular the loss of proximal but not distal skeletal elements in *Fgf8* deficient mouse limb buds (Lewandoski et al. 2000), were difficult to reconcile with the classical progress zone model (Fig. 2A). Furthermore, fate-mapping studies in chicken limb

buds provided good additional evidence that progenitor pools with distinct PD identities are specified very early and then expanded sequentially by proliferation (Dudley et al. 2002).

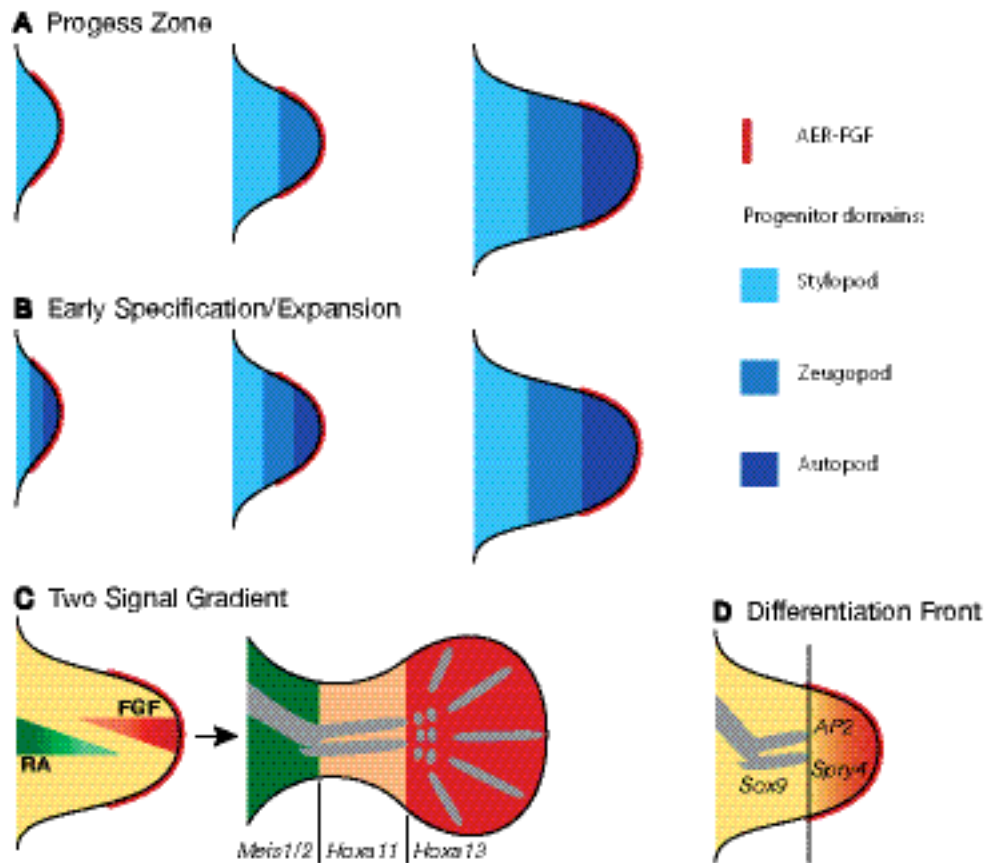


Fig. 2. Models and mechanisms of PD limb axis morphogenesis.

(A) The original progress zone model. PD positional information values depend on the time cells have spent in the progress zone under the influence of the AER. Stylopod identity is acquired early while zeugopod and autopod identities are specified at progressively later time points. The sequence of skeletal elements is specified from proximal to distal. (B) Early specification/expansion model. PD positional information is specified very early during initiation of limb bud development and the specified territories expand sequentially during distal progression of limb bud outgrowth. (C) Two signal gradient model. Cells are specified by a proximal to distal RA gradient emanating from the embryonic flank/proximal limb bud and by a distal to proximal gradient of AER-FGF signaling. Integration of these two signals over space and time provides the cells with their positional values. The *Meis1/2*, *Hoxa11* and *Hoxa13* expression domains mark the three PD territories. (D) The differentiation front model. AER-FGF signaling keeps the distal mesenchyme in an undifferentiated state. *Sprouty4* (*Spry4*) and *AP2* are molecular markers of this undifferentiated zone, while *Sox9* marks differentiating chondrocytes. The differentiation front separates these two domains and is displaced distally during progression of limb bud outgrowth.

Removal of the AER at progressively later stages simply eliminates the distal mesenchyme containing the specified but not yet expanded progenitor pools. Taken together, these studies provide a straightforward alternative explanation for the loss of distal skeletal elements following AER extirpation (Dudley et al. 2002). These and other results led to the proposal of the early specification/expansion model as a valid alternative to the progress zone model (Fig. 2B; Dudley et al. 2002; Sun et al. 2002). According to this model, AER-FGF signaling controls survival and sequential proliferative expansion of PD territories in a dose- and time-dependent fashion. Although, no molecular markers for the proposed early specification phase are known, it has been shown that this early specification indeed occurs and endows mesenchymal cells with the potential to sort themselves out according to their PD identities (Barna and Niswander 2007). Furthermore, these studies corroborate the proposal by Mercader et al. (2000), which states that PD limb bud identities are specified by two early, opposing signals, namely RA and AER-FGFs as proximalizing and distalizing signals respectively (Fig. 2C). PD positional identities are likely specified as a consequence of cells integrating these signaling cues. During the onset of limb bud development, the source of RA and AER-FGFs are very close, but their distance increases with outgrowth of the limb bud, such that proximal cells are exposed to RA for much longer than AER-FGFs, while the reverse applies to distal cells. Similar to specification of AP positional identities (see below), the integration of the dose and time of exposure to both signals likely provides cells with their PD positional cues (Fig. 2C). In an attempt to integrate the molecular and genetic knowledge with the classical experimental studies, Tabin and Wolpert (2007) proposed a modified model that better approximates all known experimental facts (Fig. 2D). This model states that during the proliferative expansion of the PD axis, distal mesenchymal cells maintain an undifferentiated state due to exposure to AER-FGFs. As the PD limb axis

expands distally, proximal mesenchymal cells are no longer under the influence of AER-FGFs, which results in the determination of their PD fates and initiation of differentiation. Therefore, the proximal limit of cells receiving AER-FGFs signals at a given development time point defines a “differentiation front”. This differentiation front prefigures the PD sequence by which the chondrogenic elements of the limb skeleton become apparent during subsequent mesenchymal condensation of the cartilage models (Fig. 2D).

Of space and time: How the SHH morphogen specifies the antero-posterior limb axis and digit identities

Setting up the ZPA and morphogenetic SHH signaling

As described before, the ZPA is located in the posterior limb bud mesenchyme and specifies AP identities in the mesenchyme by morphogenetic SHH signaling (Fig. 1D). Mapping of polarizing activity by grafting experiments in chicken embryos established that diffuse polarizing activity is already present in the presumptive limb field (Hornbruch and Wolpert 1991; Tanaka et al. 2000). During subsequent activation of *Shh* expression and initiation of limb bud outgrowth, polarizing activity is posteriorly restricted and vastly up-regulated. While genetic evidence in the mouse implicates both RA and FGF8 in *Shh* activation (Lewandoski et al. 2000; Niederreither et al. 2002), these two signals are unlikely to restrict polarizing activity posteriorly. During emergence of the limb bud, the expression of the 5'most members of the *Hoxd* gene cluster is activated within the posterior limb bud mesenchyme. Genetic analysis has shown that the 5'*Hoxd* transcriptional regulators are essential for activation of *Shh* expression in the posterior limb bud mesenchyme (Tarchini et al. 2006). Indeed, cell biochemical studies have revealed a direct interaction of Hoxd proteins with the *cis*-regulatory limb bud enhancer region of the *Shh* gene (Capellini et al. 2006). In

addition, the dynamic expression of the *Hand2* transcription factor in the limb field mesenchyme and its posterior restriction during onset of limb bud development parallels the posterior restriction of polarizing activity. Genetic studies in mouse and zebrafish embryos have indeed implicated HAND2 in the activation of *Shh* expression in both limb and fin buds (reviewed by Cohn 2000). Additional genetic studies in the mouse revealed a mutual antagonistic interaction of HAND2 with GLI3, which suggest a potential mechanism by which these two transcriptional regulators pre-pattern the limb field prior to activation of *Shh* expression (Fig. 3A; Ros et al. 1996; te Welscher et al. 2002a). This pre-patterning mechanism may not only restrict *Shh* activation to the posterior mesenchyme, but also specify anterior and posterior limb bud compartments already during the onset of limb bud development (Fig. 3A).

SHH is one of the three vertebrate homologues of the segment polarity gene *Hedgehog* and its genetic analysis has revealed essential functions in a large number of morpho-regulatory processes (reviewed by Varjosalo and Taipale 2008). During limb bud development, *Shh* expression domain marks the ZPA and naïve fibroblasts engineered to express SHH are endowed with polarizing activity as grafts induce complete mirror image duplications (Riddle et al. 1993). Genetic inactivation of *Shh* disrupts establishment of the AP limb axis as the zeugopod is reduced to one anterior bone, the radius, and the autopod is lost with exception of the anterior-most digit 1 (Fig. 3B; Chiang et al. 2001; Kraus et al. 2001).

The active SHH signaling peptide is generated by autoproteolytic cleavage of the full-length protein and is covalently modified by the addition of cholesterol and palmitate moieties (Mann and Beachy 2004). This modified peptide forms a posterior to anterior gradient in the developing limb bud (Zeng et al. 2001). Genetic alteration such that the active SHH peptide is no longer cholesterated increases its spread, which results in formation of additional

anterior digits (pre-axial polydactyly; Li et al. 2006). In contrast, the palmitoyl modification increasing long-range signaling by promoting the formation of multimeric SHH ligand

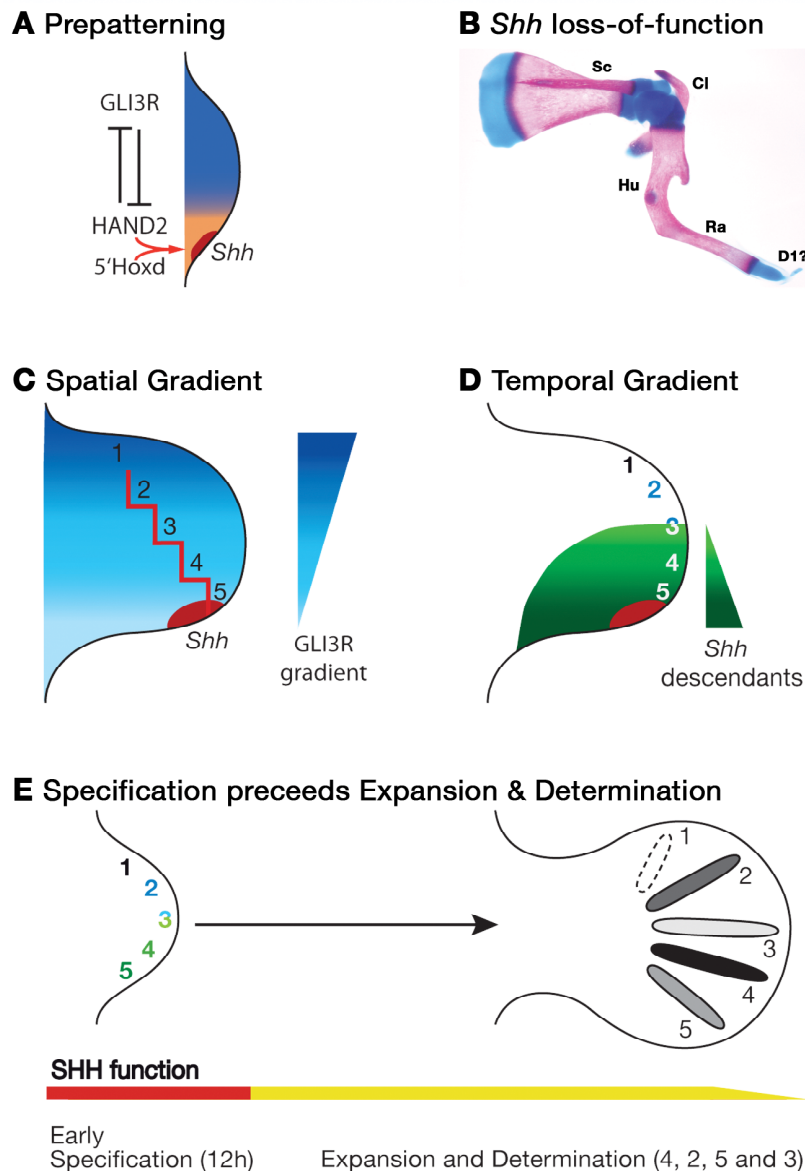


Fig. 3. Models and mechanisms for SHH-mediated AP limb axis patterning.

(A) The early limb bud is already pre-patterned by an antagonistic interaction between HAND2 (orange) and the repressor form of GLI3 (GLI3R, dark blue) transcription factors. Nested expression of 5'*Hoxd* genes and *Hand2* participate in activation of *Shh* expression. (B) Skeletal preparation of a *Shh* deficient mouse limb at birth. (C) Spatial gradient model. Diffusion of the SHH peptide secreted by the ZPA generates a GLI3R gradient across the limb bud (graded blue) by inhibiting processing of full-length GLI3. The red line indicates the threshold values predicted by Wolpert's French flag model (Fig. 1E).

(D) Temporal gradient model. Descendants of *Shh* expressing ZPA cells contribute to the progenitor domains of digit 3 to 5. Cell having expressed *Shh* for a short time contribute to digit 3, while the progenitor domains of digits 4 and 5 contain cells having expressed *Shh* for progressively longer times. Progenitors forming digit 2 and parts of digit 3 are specified by long-range SHH signaling. (E) Genetic analysis of the temporal requirement of SHH in the mouse shows digit identities are specified early. Subsequently, SHH is required for proliferative expansion of progenitor pools and determination of specified identities. Determination of digit identities in the mouse occurs in the following sequence: digit 4 (first), 2, 5 and 3 (last). Sc, scapula; Cl, clavicle; Hu, humerus; Ra, radius; Ul, ulna; D1?, digit 1?.

complexes (Chen et al. 2004). Limb buds of mouse embryos deficient in the enzyme for palmitoylation lack digit 2 and display fusions of digits 3 and 4, which is indicative of reduced long-range signaling (Chen et al. 2004).

Cellular response to morphogenetic SHH signaling

Cells responding to SHH will transduce the signal to the nucleus via activation of the GLI1/2 transcriptional activators and inhibition of the GLI3 transcriptional repressor (GLI3R). Genetic analysis shows that *Gli1* and *Gli2* are not essential for limb bud development (for more details see Ahn and Joyner 2004). In contrast, inactivation of *Gli3* results in the formation of several additional digits with no AP identities, which reveals the essential role of GLI3 in specifying the number and identity of digits (reviewed by Theil et al. 1999). A polydactylous autopod also forms when both *Shh* and *Gli3* are inactivated together, which indicates that one of the main functions of SHH is to counteract GLI3R (Litingtung et al. 2002; te Welscher et al. 2002b). In absence of SHH signaling, the full-length GLI3 protein is constitutively processed to GLI3R, while this process is inhibited by SHH signaling (reviewed by Varjosalo and Taipale 2008). Indeed, evidence for the existence of an intracellular, anterior (high) to posterior (low) GLI3R gradient opposing SHH has been obtained in the limb bud mesenchyme (Fig. 3C; Wang et al. 2000). This GLI3R repressor gradient seems required to establish the polarized expression of genes involved in AP patterning such as e.g. *5'Hoxd* genes (Zuniga and Zeller 1999; Litingtung et al. 2002; te Welscher et al. 2002b).

The notion of opposing spatial gradients of SHH and GLI3R (Fig. 3C) is complicated by the fact that the descendants of *Shh* expressing cells give rise to the posterior half of the limb bud, namely digits 3 to 5 as revealed by genetic cell lineage marking experiments (Fig. 3D,

compare to Fig. 3C; Harfe et al. 2004). Descendants born early, i.e. derived from ZPA cells having expressed *Shh* for only a short time, will be incorporated into digit 3 together with anterior cells having responded to long-range SHH signaling. Descendants of cells having expressed *Shh* for longer times will be incorporated into the posterior digits 4 and 5 (Fig. 3D; Harfe et al. 2004). In contrast, the anterior digit 2 is specified in response to long-range SHH signaling (Ahn and Joyner 2004; Harfe et al. 2004). In agreement, limiting morphogenetic SHH signaling to a short time window is sufficient to pattern anterior, but not posterior digits (Scherz et al. 2007). In contrast, decreasing overall SHH activity without altering the time of signaling is sufficient to specify posterior digits, but the proliferative expansion of the autopod territory is affected. These studies indicate that the time spent expressing *Shh* provides cells with a kinetic memory relevant to specification of their AP identities (Fig. 3D; Harfe et al. 2004; Zeller 2004; Scherz et al. 2007). However, mesenchymal cells not only integrate their response to SHH, but they also modulate their responsiveness (Ahn and Joyner 2004; Scherz et al. 2007). Posterior cells are exposed to much higher levels of SHH for longer times than anterior cells, which results in them being desensitized in comparison to anterior cells. These studies reveal the complexity by which the response to SHH signaling is integrated over time and space in an expanding system such as the autopod territory.

Back to the future: How and when are digits specified and/or determined?

Wolpert's French flag model (Fig. 1E) provided a simple conceptual framework for understanding how and when digit identities are specified/determined by the limb patterning system. This question has been revisited recently in several studies. Cycloamine-mediated blocking of SHH signal transduction shortly after its initiation inhibits proliferation and patterning of the posterior-most digits as a consequence of shortening the exposure to SHH

signaling (Towers et al. 2008), which agrees with the temporal gradient model (Fig. 3D). If proliferation of the digit progenitor pool is, however, blocked by a cell-cycle inhibitor, then the expansion of the presumptive digit territory is inhibited. As a consequence, only digits with posterior identities form due to exposure of the remaining small autopod territory to high levels of SHH signaling (Towers et al. 2008). In addition, genetic inactivation of *Shh* from defined developmental time points onwards induces digit losses in a sequence not consistent with a morphogen gradient type patterning mechanism (Zhu et al. 2008). Rather, the sequence of digit loss reflects the sequence by which the digits normally condense. This study indicates that SHH-mediated specification of digit identities occurs within the first 12 hours of SHH signaling and that SHH activity is continuously required to generate the required number of cartilage progenitor cells (Zhu et al. 2008).

Furthermore, evidence is accumulating that digit identities are fixed (= determined) much after specification and expansion of their progenitors domains. In chicken limb buds, this late determination process is governed by instructive BMP signaling from the interdigital (ID) mesenchyme prior to its elimination by cell death (blue shaded regions in Fig. 4). This became evident as a consequence of the serendipitous discovery that digit identities can still be altered at late developmental stages by manipulating BMP signaling in the footplate of chicken hindlimb buds (Dahn and Fallon 2000). The targets of this instructive BMP signaling from the ID mesenchyme are the cells located at the distal tip of the forming digit models. This region of mesenchyme located directly under the AER is called the phalanx-forming region (PFR; Suzuki et al. 2008). Suzuki and coworkers established that PFR of a particular digit is characterized by its unique BMP activity signature (Suzuki et al. 2008). The activities of SMAD proteins are higher in posterior than anterior PFRs, with the exception of the most posterior digit 4 (Fig. 4). In addition, FGF signaling from the AER also participates in this

late determinative process by regulating the number of phalanges formed, which is a defining hallmark of digit identities (Sanz-Ezquerro and Tickle 2003). At present, it is not known which BMP ligands generate these activity signatures and how BMP signaling is integrated with AER-FGF signaling.

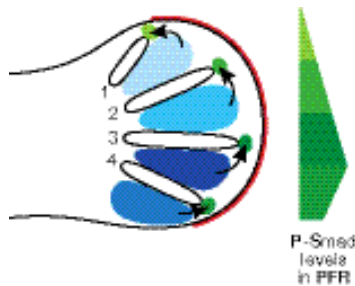


Fig. 4. The role BMP signaling from the interdigital mesenchyme in determination of digit identities.

Graded BMP signaling from the interdigital (ID) mesenchyme (blue) in the chicken foot primordia is involved in determining the identities of digits 1 to 4 at late developmental stages. The distal phalanx of individual digits form from the sub-AER mesenchyme, which is therefore called phalanx forming region (PFR). The activity of phosphorylated SMAD (pSMAD) proteins, which are the intracellular mediators of BMP signal transduction, is graded within the PFR (green), such that each digit has its characteristic pSMAD activity signature. Note that the pSMAD activity in the PFR of the posterior-most digit 4 is lower than the one of digit 3.

Temporal regulation of BMP signaling and integration of proximo-distal and antero-posterior patterning by interacting signaling systems with self-regulatory properties

Tickle (1981) already observed that polarizing grafts are most potent when placed in direct contact with the AER. Subsequently, it was discovered that maintenance and propagation of *Shh* expression requires AER-FGF signaling as part of a positive epithelial-mesenchymal (e-m) feedback loop operating between the ZPA and the AER (Laufer et al. 1994; Niswander et al. 1994). The BMP antagonist Gremlin1 (GREM1) was identified as a crucial mesenchymal component in this e-m feedback signaling system (Zuniga et al. 1999; Khokha et al. 2003; Michos et al. 2004). GREM1 is required to up-regulate AER-FGF signaling and to establish SHH/GREM1/FGF e-m feedback signaling. In *Greml1* deficient mouse limb buds, establishment of e-m feedback signaling is disrupted, which in turn interferes with specification and expansion of the distal limb bud compartments (Khokha et al. 2003; Michos

et al. 2004). During initiation of limb bud development, BMP signaling is however required to induce formation of a functional AER (Ahn et al. 2001; Ovchinnikov et al. 2006) and later is able to up-regulate the expression of its own antagonist *Grem1* (Nissim et al. 2006). Thus, BMP activity and its regulation appear to be crucial for inducing and propagating morphogenetic signaling during limb development.

This introduction is part of the publication:

Jean-Denis Bénazet and Rolf Zeller. **Vertebrate limb development: moving from classical morphogen gradients to an integrated 4D patterning system.** In **Generating and Interpreting gradient during development.** Cold Spring Harbor Laboratory Press 2009, *in press*.

V. AIMS OF THE THESIS

Joining the laboratory of Rolf Zeller in Basel was for me a unique opportunity to bring together two aspects of experimental biology I learned during my undergraduate studies. As a student of the university Paul Sabatier in Toulouse, I spent several months in the laboratory of Dr. Fabienne Pituello working on the development of the chicken embryo. In particular, I was studying the influence of the paraxial mesoderm on the expression of cell cycle genes in the early spinal cord using microsurgery techniques on cultured embryos. I completed my training in the laboratory of Dr. François Payre working on signaling and cell morphogenesis during development using the genetic model *Drosophila melanogaster*. Mouse development and more particularly limb morphogenesis was a model of choice to combine these two complementary approaches to study embryological processes.

During my thesis, I was involved in two projects aspiring to further our knowledge on distinct phases of limb development and more globally on the general principles of cell communication and patterning during animal organogenesis. One aim was to generate a genetic tool to study the mechanism pre patterning the early limb bud. Although the instructive roles of the SHH and FGFs peptides, secreted by the ZPA and the AER respectively, have been clearly demonstrated during specification of the limb skeletal pattern, the upstream mechanisms responsible for the activation of these signals as well as the differential responsiveness of mesenchymal cells receiving these signals are less understood. Genetic interaction between the transcription factors HAND2 and GLI3 has suggested that these two genes are involved in positioning the *Shh* expression domain as well as creating an anterior and a posterior compartment in the limb mesenchyme prior to SHH signaling. Unfortunately, the lethality of *Hand2* deficient embryos due to heart anomalies during the

onset of limb development has precluded in depth analysis of *Hand2* functions in this process. To circumvent this problem, I have generated a *Hand2* conditional null allele under the supervision of Dr. Antonella Galli, by homologous recombination in mouse embryonic stem cells. This conditional allele has allowed Dr. A. Galli to produce limb-specific *Hand2* mutant embryos using the *Prx1*-Cre line and gain insights into *Hand2* functions during limb development. In addition this allele allows the study of possible *Hand2* functions in a tissue specific manner in all other organs not accessible previously due to embryonic lethality.

One of the consequences of the initial early events of limb development is the establishment of an epithelial-mesenchymal positive feedback loop between the AER and the ZPA involving *Fgfs* and *Shh* genes respectively. The BMP antagonist *Grem1* is essential for mediating this feedback signaling in the distal mesenchyme. *Bmp2*, *Bmp4* and *Bmp7* are the three BMPs ligands expressed during limb development from early stages onwards. BMP signaling has been implicated in a variety of processes such as dorso-ventral and antero-posterior patterning as well as AER induction and maturation, interdigital cell death and bone morphogenesis. However, the genetic analysis of single *Bmp* gene functions was complicated by the early lethality of *Bmp2* and *Bmp4* deficient embryos and possible functional redundancy was suspected. The second aim of my thesis was to analyze the functions of *Bmp* ligands during early limb development by studying their interactions with *Grem1* and with the SHH/FGFs feedback loop. To reach this goal I combined genetic analysis, manipulation of embryos in culture and mathematical simulation of signaling interactions in collaboration with Mirko Bischofberger from the group of Felix Naef and Alexandre Gonçalves and Eva Tiecke in our group.

VI. MATERIAL AND METHODS

Homologous recombination in mouse embryonic stem cells

For the generation of the mice carrying the *Hand2* conditional null allele, male R1 (10th passage, 129 hybrid background) embryonic stem (ES) cells were used.

During most of the procedure ES are grown on mouse embryonic fibroblasts (MEF) feeder layer. ES cells are fed every day.

Preparation of MEF:

MEF were conserved in liquid nitrogen. A vial was defrosted several minutes in a water bath at 37°C. The freezing medium was washed away by transferring MEF in freshly made warm MEF culture medium (see recipe below), centrifuged (5min, 1200 rpm) and resuspended in 8 ml of warm medium (pipet up and down several times smoothly with 3 ml and add 5 more ml). MEF were seeded in four 10 cm dishes (10 ml/dish) and two 6 cm dishes. After 3 days of growth, cells from the 10 cm dishes were diluted 1:6 in 10 cm dishes after obtaining cell suspensions following a trypsin (Sigma T-3924) treatment (see detailed protocol). These MEF were used to expand ES cells before electroporation. MEF can be split only twice. Before receiving ES cells MEF from the two 6 cm dishes were treated with mitomycin C (Sigma M-0503) to stop proliferation (see detailed protocol). After this treatment cells can be kept for 1 week (media change every 3 days) and split in multiwells plates (MEF must rest a couple of hours after splitting). One 10 cm dish of MEF is enough for a 48 wells plate. The amount of MEF to be prepared has to be adjusted to the amount of ES cells.

ES cell expansion and electroporation:

A vial of ES cells was thawed and cells were expanded on a MEF-coated dish (see detailed protocol). The day of electroporation, cells were treated with Trypsine and resuspended in a falcon tube. Cell concentration was evaluated by counting a 1/10th dilution in ES medium in a hemocytometer while the rest was centrifuged 10 min at 1000rpm. Cells were resuspended at a final concentration of 18.75x10⁶/ml in PBS (single cell suspension). 0.8 ml was electroporated per cuvette (Biorad Gene Pulser 165-2088). One 10 cm dish corresponds roughly to one cuvette. 4 cuvettes were electroporated with 35 µg of targeting vector and one was electroporated with water control. This cuvette was used to assess the efficiency of the antibiotic selection. After electroporation (capacitance 475 µF, voltage 0.24 V) cells were left on ice for 20 min in the cuvettes. Cells from each cuvette with DNA were transferred in tubes containing 5ml ES medium with LIF, mixed and plated on 10 cm dishes coated with gelatin (5 dishes per cuvettes, 10 ml total). Cells were left to recover for two days before antibiotic selection.

Drug selection:

Cells were cultured for 10 days in G418 containing ES cell medium. G418 is generally used at 200-400µg/ml but it is better to test the efficiency of each batch before ES electroporation. After 4 or 5 days the cells electroporated without DNA should have all die.

Colony picking:

ES cell colonies were picked in PBS using a Gilson P200 and transferred in 48-wells plates containing MEF and 500µl of ES cell medium. Colonies were broken up by pipetting up and down few times. This allows a faster growth.

Freezing clones:

ES cells clones that were growing fast were directly split on gelatin coated and MEF coated 48-wells plate. Cells on gelatin were grown to confluency in ES medium without LIF and used to prepare DNA for southern blot analysis. Cells on MEF were frozen at -80°C just after reaching confluency, waiting for the result of the Southern blot screen. Clones growing slower were treated with 75 µl of trypsin for 15 min, resuspended in 500µl of ES medium and transferred to new 48-well plate coated with MEF.

Generating chimeras:

The two positive colonies were thawed, expanded in several dishes and frozen. These cells were used to generate chimeras by injection in blastocysts. This worked was done in the Transgenic Mouse Core Facility of the Biozentrum of Basel.

REAGENTS AND PROTOCOLS (Aimee Zuniga):*Incubator:*

37°C, 7.5% CO₂

MEF culture medium:

DMEM + 4.5g/l Glucose (Gibco 41966029)	500 ml	
Fetal Calf Serum	58 ml	(10%)
Penicillin-Streptomycin (100u-0.1mg/ml) (Sigma P-0781)	5.8 ml	
L-Glutamin (200mM) (Sigma G-7513)	5.8 ml	

Trypsine treatment for MEF:

Rinse with 4 ml trypsin and incubate 5 min in 3 ml trypsin at 37°C, collect cells after adding 7 ml of medium and spin 5 min. 1200 rpm. Resuspend pellet in small volume, dilute and seed at around 1:5-1:6.

Mitomycine C treatment:

Stock solution (store at 4°C in foil-wrapped tube, stable for approx. 2 weeks): dissolve mitomycin C (Sigma M-0503) in PBS at 1mg/ml, ie introduce 2 ml PBS in a 2mg vial, using syringe needle through the rubber cap, mitomycine C is very toxic, avoid contact with the powder/solution.

Treatment: confluent plates of MEF are treated with MEF media containing 10 mg/ml mitomycine C (5 ml medium+50 µl stock mitomycine C for a 10 cm plate). Incubate the plates at 37°C (in 7.5% CO₂ incubator) for 2 hours (not longer than 2.5 h). Remove media, rinse 3 times with PBS, add media, return to incubator or seed ES-cells on.

NB: - The MEF can kept for one week after the mitomycine C treatment, with media changes (every 3 days) but if not used within this period of time, they should be discarded (anyway, always check under microscope before use, after one week they look sick).

-These cells can be used like this or split on another type of plate (10 cm plate = 48-well plate or 24-well plate or 6-well plate or 3 X 6 cm plates) To prevent cell clumping and uneven plating, cells should not be overgrown at time of trypsin and/or mitomycine C treatment. Allow the cells to attach for at least a couple of hours before using. After overnight plating, they should form a confluent monolayer.

Unused cells treated with mitomycin C can be trypsinized and frozen, if mitomycin C treatment is not older than a day. Freeze one vial per plate. This is worth it in case of "emergency".

Thawing ES cells for Electroporation:

Day 0. Remove medium of a 6 cm mitomycin treated MEF plate (see below) and add 4-5 ml of ES medium.

Thaw quickly cell vial at 37 °C and as soon as the last crystals are disappearing, wipe the vial with Ethanol and take the cells into a 15 ml falcon tube containing 10 ml of complete ES medium.

Spin 5 min. at 1200 rpm, remove the medium except for 100-200 µl liquid.

Add 2 ml ES medium and resuspend the cells well. Plate onto the MEF plate.

Incubate at 37 °C, 7.5% CO₂ for 24h.

Day 1: Next day, change medium.

Day 2: Split cells as described below onto 2 x 10 cm plates

Day 3: Change medium.

Day 4: Split each plate 1:5-1:7 depending on confluency and on cells. Depending on transfection, you may need to split only one plate. In this case, freeze the other plate.

Day 5: Change medium

Day 6: Electroporate

ES cell culture medium:

Make it directly in the bottle

DMEM + 4.5g/l Glucose (Gibco 41966029)	500 ml	
Fetal Calf Serum	94 ml	(15%)
<u>Not</u> heat inactivated. 4 X 23.5 ml		
Penicillin-Streptomycin (100u-0.1mg/ml)	6.25 ml	
(Gibco 15140-122)		
L-Glutamin (200mM)	6.25 ml	
(Gibco 25030-024)		
b Mercapto-Ethanol (ie 50 mM stock is 500X)	1.25 ml	
(Gibco 31350-010)		
Leukemia Inhibitory Factor (LIF)**(10^7 u/ml)	62.5 ml	
(EsGRO LIF TM Gibco 13275-029)		
Non Essential Amino Acids (100X)	10 ml	
(Gibco 11140-035)		
Sodium Pyruvate (100mM)	10 ml	
(Gibco 11360-039)		

Splitting ES cells (protocol by Aimee Zuniga)

Rinse quickly the plates with Trypsine/EDTA (Sigma T-3924), prewarmed or RT:

4 ml for 10 cm plate

2ml for 6 well-plate

300 μ l for 24 well-plate

75 μ l for 48 well-plate

Gelatin coating:

Stock solution : make 0.1% solution of gelatin (Sigma G-2500) in double distilled water.

Weigh 100 mg and add to 100 ml Gibco water in a 100 ml glass bottle. A total of 5 bottles is enough for a targeting. Autoclave (will dissolve gelatin) and store at 4°C (or room temperature if air conditioning).

Coating plates : use enough gelatin to cover the surface of the plates, let stand 5-10 min at room temperature, aspirate the gelatin solution leaving a thin film on the plates. Let dry 5-10 minutes before use.

Freezing ES cells colonies:

48-well plates containing ES cells on MEF were frozen at confluency.

Remove media, place plate on ice, add 400 µl of freezing medium (25% Fetal Calf Serum, 10% DMSO in DMEM), wrap the plate in parafilm and store at -80°C in a plastic bag in a Styrofoam box during the southern blot screening.

Genetic analysis of *Grem1-Bmp2* and *Grem1-Bmp7* interactions

The *Grem1*, *Bmp2* and *Bmp7* loci are all located on mouse chromosome 2, mice carrying the *Grem1*^Δ null allele (Michos et al. 2004) were crossed with mice carrying the *Bmp2*^Δ (Ma and Martin 2005) and the *Bmp7*^Δ (Karsenty et al. 1996) null alleles and their offspring crossed to wild-type mice. The resulting F2 offspring were screened for mice carrying both mutations in *cis* due to germline recombination. Males carrying both mutations in *cis* were then mated to *Grem1*^{Δ/+} females to produce *Grem1*^{Δ/Δ}*Bmp2*^{Δ/+} and *Grem1*^{Δ/Δ}*Bmp7*^{Δ/+} embryos. *Grem1*^{Δ/Δ}*Bmp7*^{Δ/Δ} double homozygous embryos were generated by inter-crossing double

heterozygous males and females, while the generation of *Grem1-Bmp2* double mutant embryos was precluded due to early lethality of embryos homozygous for the *Bmp2*^Δ null allele. The primer pairs used for genotyping all alleles (wild-type and mutant) are listed in table 1 (p38).

Genetic analysis of *Bmp4* functions and interactions

Bmp4^{Δ/hf} embryos were obtained by crossing mice carrying the *Bmp4*^{hf} allele with mice heterozygous for the *Bmp4*^Δ null allele (*Bmp4*^{ΔlacZ}) (Kulesa and Hogan 2002). Compound mutant embryos were generated by mating *Grem1*^{Δ/+}*Bmp4*^{hf/+} or *Grem1*^{Δ/+}*Bmp4*^{hf/hf} females with *Grem1*^{Δ/Δ}*Bmp4*^{Δ/+} or *Shh*^{Δ/+}*Grem1*^{Δ/Δ}*Bmp4*^{Δ/+} males. The compound mutant strains used were kept in the C57BL/6 genetic background; with the exception of the *Shh* allele (St-Jacques et al. 1998) that was kept in a NMRI outbred background. *Bmp4*^{f-Jfm} refers to the non-hypomorphic *Bmp4* conditional allele generated in James Martin's laboratory. All mice and embryos were genotyped by PCR amplification of diagnostic fragments (for primers see table 1, p38) using DNA prepared from tail clips (mice at weaning), head tissue and/or extra-embryonic membranes (embryos).

Tamoxifen (TM)-mediated activation of the Cre recombinase in embryos carrying the TM-Cre transgene (Hayashi and McMahon 2002) (studies performed by Alexandre Gonçalves)

A stock solution of 100 mg/ml TM (Sigma) in ethanol was diluted in sterilized corn oil (Sigma, 1h at 100°C) to achieve a 20 mg/ml final concentration. 40 mg/ml of progesterone (Sigma) was added to attenuate a possible abortive effect of TM. After emulsion through

sonication in a glass vial, 150 μ l of TM-progesterone solution was injected intraperitoneally into pregnant females (3mg TM/mouse (30g)).

Table1: genotyping primers

Gene	forward primer	reverse primer	Allele
<i>Bmp2</i>	5'-GCTTGGTCTGGTAATCTTCCT-3'	5'-AGGGATGCTGCTGTTTCTGGA-3'	Wt
		5'-AAGCGCCTCCCCTACCCGGTA-3'	null
<i>Bmp4</i>	5'-GTGTGTGTAGGGTGTGAGGGAGAAA-3'	5'-CCCGGTCTCAGGTATCAAAGTAGCA-3'	Wt/hf
		5'-CCCAGTCACGACGTTGTAAAACGAC-3'	null
<i>Bmp4</i>	GCTAAGTTTTGCTGGTTTGC	GCCCATGAGCTTTTCTGAGA	Wt / f-Jfm
<i>Bmp7</i>	5'-TTGTGCTGTGTAGACTGGGTG-3' 5'-TGTTCTCCTCTTCCTCATCTCC-3'	5'-TTTGTAGGAGTGGTAGGGTGC-3'	Wt
		5'-ACCCTTTCCAAATCCTCAGC-3'	null
<i>Grem1</i>	5'-ATGAATCGCACCCGCATACACTG-3' 5'-GGCACATGGCTGAATATCGACGG-3'	5'-TCCAAGTCGATGGATATGCAACG-3'	Wt
		5'-AAGCGCCTCCCCTACCCGGTA-3'	null
<i>Shh</i>	5'-GAAGAGATCAAGGCAAGCTCTGGC-3' 5'-ATGCTGGCTCGCCTGGCTGTGGAA-3'	5'-GGACACCATTCTATGCAGGG-3'	Wt
			null
CRE	5'-GCCTGCATTACCGGTTCGATGCAACGA-3'	5'-GTGGCAGATGGCGCGGCAACACCATT-3'	Tg

Skeletal staining

Embryos were collected in PBS at E14.5 and fixed in technical grade ethanol 95% for 3 days. Cartilages were stained by incubating the embryos in a solution of 80% ethanol 95% and 20% acetic acid containing 0.3 g/l of alcian blue powder (Sigma A3157) during 36 hours. Embryos were rinsed twice in ethanol 95% and left in ethanol 95% overnight. The next day, ethanol was replaced by a solution of 1% KOH in water for 30 min. Bones were stained by incubating the embryos in a 1% KOH solution containing 0.05 g/l of Alizarin Red powder for 1 hour. After rinsing for 30 min in 1% KOH, embryos were cleared in glycerol series: 2 days in 80% 1% KOH/ 20% glycerol, 2 days in 50% 1% KOH/ 50% glycerol, 2 days 20% 1% KOH/ 80% glycerol. Skeletal preparations were photographed and stored indefinitely in 80% glycerol in water.

For older embryos and newborns, the skin must be removed before fixation in ethanol and incubation time has to be extended.

Whole mount *in situ* mRNA hybridization

Embryos were collected in PBS and fixed overnight at 4°C in 4% paraformaldehyde (PFA Sigma)/PBS and dehydrated in a methanol/PBS 0.1% Tween 20 (PBT) series and stored in methanol at -20°C. Embryos are handled in 10 ml glass vial. After genotyping and age matching, embryos were rehydrated in the reverse methanol/PBT series. Embryos were bleached 15 min in 6% H₂O₂ (Sigma) and washed in PBT 3 times 5 min. Embryos were incubated in Proteinase K in PBT: 15 min, 10 µg/ml for detection in limb mesenchyme from E9.0 to E11.0 and 30 min at E12.5 and 4 min, 5 µg/ml for detection in the ectoderm. Proteinase K was inhibited by incubating the embryos in a solution of glycine in PBT (2mg/ml) for 5 min. After rinsing twice 5 min in PBT, embryos were fixed 20 min in 4%

PFA in PBT with 0.2% glutaraldehyde (Sigma). After rinsing twice 5 min in PBT, embryos were transferred in 2 ml tubes containing the hybridization buffer and prehybridized 3 hours at 65°C. Embryos can be stored at -20°C at this stage. The prehybridization solution was replaced by prewarmed hybridization buffer containing 10 µl/l of digoxigenin-labelled RNA probe and incubated overnight at 70°C in a rotating oven.

The next day, embryos were progressively brought into 2X SSC through a hybridization buffer/2X SSC series at 70°C. After incubating twice 30 min in 2X SSC 0.1% CHAPS at 70°C, single stranded RNA molecules were digested with RNase A (20µg/ml) in 2X SSC 0.1% CHAPS during 45 min at 37°C. Embryos were washed twice 10 min in 100 mM maleic acid, 150 mM NaCl ph 7.5 at room temperature. Embryos were washed twice 30 min in 100 mM maleic acid, 150 mM NaCl ph 7.5 at 70°C. Embryos were washed twice 10 min in PBS and once 5 min at room temperature in PBT. Embryos were blocked with 10% sheep serum, 1% Bovine Serum Albumin (BSA) in PBT for two to three hours before adding the anti-digoxigenin antibody (Fab fragments Roche). The antibody was blocked for a similar time in the same solution containing 3 mg/ml of embryo powder at 4°C. The blocking solution was replaced by the solution containing the antibody and the embryos were incubated overnight at 4°C.

The next day, embryos were washed 5 times 45 min in PBT, 0.1% BSA, twice 30 min in PBT and three times 10 min in NTMT. The signal was revealed after incubation of the samples in BM purple solution (Roche). Colorations were monitored visually and stopped in NTMT followed by several PBT washes. Embryos were then stored in 4% PFA in PBS.

Hybridization buffer:

50% formamide (deionized, extra pure)

5X SSC pH 4.5 (from a 20X stock: 3 M NaCl, 0.3 M tri-sodium citrate dehydrate)

2% Blocking Reagent (Roche)

0.1% Tween 20

0.5% CHAPS

5 mM EDTA 50

50 µg/ml yeast tRNA

50 µg/ml heparin

NTMT:

100 mM NaCl

100 mM Tris HCl pH 9.5

50 mM MgCl₂

0.1% Tween 20

X-Gal staining

Embryos were collected in PBS in 2 ml tubes. PBS was replaced by the fixative solution and embryos were fixed 25 min at 4°C on a rocking platform. Embryos were rinsed three times 5 min in PBS at room temperature. At the same time, solutions X, K3 and K4 were brought to room temperature away from light. PBS was replaced by the staining solution and embryos were stained at 37°C in a rotating oven (from several hours to overnight) and the reaction was stopped by PBS washes.

Fixing solution:

37% Formaldehyde	1.35 ml
25% Glutaraldehyde	400 μ l
10% NP40	100 μ l
1% Sodium deoxycholate	500 μ l
Add PBS to 50 ml	

Staining solution for embryos up to E12.5

Solution X (Xgal 40 mg/ml)	625 μ l
*Solution K3 (500 mM $K_3Fe(CN_6)$)	25 μ l
*Solution K4 (500 mM $K_4Fe(CN_6)$)	25 μ l
10% NP40	50 μ l
MgCl ₂ (1 M)	20 μ l
Add PBS to 50 ml	

Staining solution for older embryos (E13.5 or older)

Solution X (Xgal 40 mg/ml)	625 μ l
*Solution K3 (500 mM $K_3Fe(CN_6)$)	25 μ l
*Solution K4 (500 mM $K_4Fe(CN_6)$)	25 μ l
10% NP40	50 μ l
MgCl ₂ (1 M)	20 μ l
1% Sodium deoxycholate	500 μ l
Add PBS to 50 ml	

*For genes expressed highly, use 10X as much.

Stocks:

X-Gal: dissolved in dimethyl formamide at 40mg/ml, stored at -20°C.

500 mM potassium ferricyanide (K3) dissolved in PBS (3.3 g in 20 ml PBS, stored in 1ml aliquots at -20°C and do not re-freeze)

500 mM potassium ferrocyanide (K4) dissolved in PBS (4.2 g in 20 ml PBS, stored in 1ml aliquots at -20°C and do not re-freeze)

Cell death detection using LysoTracker Red (Molecular Probe)

LysoTracker Red is a dye that accumulates in lysosomes and becomes fluorescent in these acidic conditions. In the embryo, this dye stains macrophage-like cells engulfing apoptotic bodies. Colocalisation of LysoTracker Red and TUNEL signals is well established in mouse embryos (Zucker et al. 1999).

Uteri of pregnant females were dissected in prewarmed (37°C) HBSS buffer (Gibco). Once the embryonic membranes are discarded (used for genotyping), embryos were transferred into 2 ml tubes filled with a prewarmed solution of LysoTracker Red in HBSS (5 µM) and incubated for 45 min at 37°C. Embryos were extensively washed (5 times in minimally 1 hour) and fixed overnight in 4% PFA at 4°C. The next day, samples were dehydrated in a methanol/PBT series. The embryos were cleared in order to avoid diffraction of the fluorescent signal in Benzyl Benzoate/Benzyl Alcohol (2:1, BBBA): 30 min in 50% methanol/50% BBBA and then 100% BBBA. The signal was detected by epifluorescence.

Table 2: Primers for real time PCR

cDNA	forward primers	reverse primers
<i>Shh</i>	5'-GATGACTCAGAGGTGCAAAGACAA-3'	5'-TGGTTCATCACAGAGATGGCC-3'
<i>Ptc1</i>	5'-CTTTTAATGCTGCGACAACCTCAGG-3'	5'-CAACACCAAGAGAAGAAACGG-3'
<i>Gli1</i>	5'-CAAGTGCACGTTTGAAG-3'	5'-CAACCTTCTTGCTCACACATGTAAG-3'
<i>Bmp2</i>	5'-ATGTGGAGACTCTCTCAATG-3'	5'-ACGCTAGAAGACAGCGGTC-3'
<i>Bmp4</i>	5'-AGCCGAGCCAACACTGTGA-3'	5'-GTTCTCCAGATGTTCTTCGTGATG-3'
<i>Bmp7</i>	5'-TGTGGCAGAAAACAGCAGCA-3'	5'-TCAGGTGCAATGATCCAGTCC-3'
<i>Grem1</i>	5'-CCCACGGAAGTGACAGAATGA-3'	5'-AAGCAACGCTCCCACAGTGTA-3'
<i>Msx2</i>	5'-ATACAGGAGCCCGGCAGATACT-3'	5'-TCCGGTTGGTCTTGTGTTTCC-3'
<i>Fgf8</i>	5'-TAATTGCCAAGAGCAACGGC-3'	5'-GCACGATCTCTGTGAATACGCA-3'
<i>RLP 19</i>	5'-ACCCTGGCCCGACGG-3'	5'-TACCCTTTCCTCTTCCCTATGCC-3'

Quantitative real-time PCR Analysis

Pairs of forelimb buds from littermates in the same genetic background were collected at E10.5-10.75 (34-39 somites) and stored in RNAlater (Ambion). Total RNA was isolated using the RNeasy Micro kit (Qiagen) and cDNA synthesized using Superscript III (Invitrogen). Transcript levels were quantified by real time PCR using the ABI Prism 7000 in combination with the Power SYBR Green PCR Master Mix (Applied Biosystems; primers

are listed in Table S2, p44). Relative transcript levels were normalized using transcripts of the mouse *ribosomal protein L19* (RPL 19) as internal standard. Transcript levels in mutant forelimb buds are shown relative to the ones of wild-type forelimb buds (mean value set at 100%). Each result represents the mean of nine independent samples per genotype (+/- standard deviation). All values of a particular experiment were first evaluated with respect to their Gaussian distribution using the Kolmogorov-Smirnov and Shapiro-Wilk tests. The statistical significance of all differences was then assessed using the two-tailed, unpaired t-test with Welch's correction in case of unequal variance (F-test). Note that the values of the *Shh-Grem1-Bmp4* triple mutant limb buds and the corresponding controls (Fig. 2C to 2E) vary slightly from all others due to the mixed NMRI/C57BL/6 background used, but this does not affect the conclusions.

Grafting and culturing of mouse limb buds (trunk cultures) (performed by Eva Tiecke)

Mouse forelimb buds were cultured as described (Zuniga et al. 1999) with the following modifications. Wild-type, *Grem1*^{ln2/ln2} (limb bud-specific *Grem1* loss-of-function allele, Zuniga et al. 2004) and *Bmp4*^{Δ^{hf}} mutant embryos were used at E10.5 (33-35 somites). Heparin beads were soaked in recombinant BMP4 (0.1 mg/ml) or GREM1 protein (0.2 mg/ml) and Affigel-blue beads in recombinant SHH protein (5 mg/ml; all from R&D systems). Beads loaded with protein were grafted into the right forelimb bud, while the contra-lateral forelimb bud was not grafted to serve as an internal control. In addition, a small number of limb buds grafted with beads alone were analyzed, but no alteration of gene expression was observed (data not shown). Trunks were cultured between 1-6 hours in defined medium (see below). During this time period, mouse limb buds in culture develop

with kinetics identical to embryonic limb buds *in utero* (Boot et al. 2008). No cell death was observed following grafts of beads. Each of the results shown is representative of minimally three independent embryos per genotype and type of manipulation.

DiI labeling of posterior mesenchymal cells in cultured mouse limb buds

Small DiI crystals (D3911, Invitrogen) were inserted into the sub-ectodermal mesenchyme in the vicinity of the polarizing region in forelimb buds of wild-type and *Grem1*^{ln2/ln2} embryos at E10.5 (34-35 somites). Limb buds were cultured for 48 hrs with one medium change after 24 hours (see below for medium recipe). The expansion of the DiI labeled cell population in the posterior limb bud mesenchyme was monitored photographically at 4, 24 and 48 hours.

Culture medium (500ml):

This medium is prepared fresh on the day of use

- 500 ml DMEM (1X), liquid (high glucose) (Cat. 41966-029, Gibco)
- 5 ml L-glutamine (Cat. 25030-024, Gibco)
- 2.5 ml penicillin-Streptomycin (Cat. 15140-122, Gibco)
- 5 ml non-essential amino acids (Cat. 11140-035, Gibco)
- 5 ml sodium pyruvate (Cat. 11360-039, Gibco)
- 5 ml D-glucose (45% solution) (Cat. G8769, Sigma)
- 0.5 ml L-ascorbic acid ¹ (Cat. A4034, Sigma)
- 5 ml lactic acid ² (Cat. L4388, Sigma)
- 0.5 ml d-biotin/vitamin B12 ³ (Cat. B4639 and V6629 respectively, Sigma)
- 0.5 ml PABA ⁴ (Cat A9878, Sigma)

¹ Dissolve 1 gram of L-ascorbic acid in 5 ml PBS, filter through 0.22 μ m filter and add 0.5 ml to the medium. Make fresh.

² Dissolve 0.2 gram of lactic acid in 5 ml of DMEM, filter through 0.22 μ m filter and add 5 ml to the medium. Make fresh.

³ Make stock of 0.2 mg d-biotin and 40 μ g vitamin B12 per ml DMEM. Filter through 0.22 μ m filter. Make 0.5 ml aliquots and store at -20°C

⁴ Make a stock of 2 mg PABA per 1 ml of PBS. Filter through 0.22 μ m filter. Make 0.5 ml aliquots and store at -20°C .

Mathematical modeling (studies performed by Mirko Birschofberger and Felix Naef)

To model the dual time feedback loops shown in Fig. 6A the following experimental facts were considered. The results shown in Fig. S7 establish that *Bmp4* expression precedes the one of *Shh* and *Grem1* in the mesenchyme and acts genetically upstream of *Shh* and *Grem1*. At this stage only low levels of *Fgf8* are expressed by the forming AER (Fig. S7), while expression of all other AER-*Fgfs* is activated during subsequent limb bud stages (Martin 1998). Therefore, the starting conditions for the simulations were accordingly set as “high” BMP4 and “low” SHH, GREM1 and AER-FGF activities (Fig. 7H). Nissim et al. (2006) showed previously that BMP2 beads soaked in 0.1mg/ml recombinant BMP2 induce *Grem1* expression around the bead. Beads soaked in 1mg/ml BMP2 activate *Grem1* at a distance, while *Grem1* expression around the bead is inhibited (at concentrations ≥ 0.2 mg/ml). The initial BMP4 activity (High) in all simulations (Fig. 7H, Fig. S9 and Fig. S11) is defined as being able to up-regulate *Grem1* expression (Fig. 3H) in accordance with our grafting experiments (Fig. 5, using beads soaked in 0.1 mg/ml BMP4). Finally the equations do not take into account any potential direct cross-talk between the signals that regulate *Grem1*

expression (e.g. between SHH and BMP4, see Fig. S7). To describe the temporal dynamics of BMP4, GREM1, SHH and AER-FGF activities the following ordinary differential equation (ODE) model was constructed:

$$\begin{aligned}\dot{B} &= l - d \cdot G \cdot \left(\frac{B}{B+K_0} \right) - a_B \cdot B \\ \dot{G} &= p_{G1} \left(\frac{B^n}{B^n + K_1^n} \right) + p_{G2} \left(\frac{S^n}{S^n + K_2^n} \right) - a_G \cdot G \\ \dot{S} &= p_S \left(\frac{F^n}{F^n + K_4^n} \right) - a_S \cdot S \\ \dot{F} &= p_F \left(\frac{K_3^n}{K_3^n + B^n} \right) - a_F \cdot F\end{aligned}$$

The equations are based on the following facts and assumptions: BMP4 activity levels (B) depend negatively on GREM1 (G). In particular, BMP4 activity is inhibited by GREM1 following Michaelis-Menten kinetics with d being the maximum inhibition rate per unit of G ; saturation in function of B occurs at K_0 (half saturation). The half-life of the BMP4 protein is defined as $1/a_B$ and BMP4 levels are increased at the constant rate l . *Grem1* expression and thereby its concentration and activity are positively controlled by both BMP4 and SHH (S), which is modeled by Hill functions with the maximal velocities p_{G1} and p_{G2} , while the half maximal induction concentrations correspond to K_1 and K_2 , respectively. The half-life of GREM1 is defined as $1/a_G$. In summary, GREM1 activity is increased via BMP4 (fast) and SHH (slow) following sigmoidal activation functions. The negative regulation of AER-*Fgfs* expression and activity (F) by BMPs is modeled by a Hill function with the maximal velocity p_F and the half maximal induction concentration K_3 . The half-life of FGFs protein is defined as $1/a_F$. Finally, the positive regulation of *Shh* expression and activity (S) by AER-FGFs is also modeled by a Hill function with maximal velocity p_S , half maximal induction

concentration K_4 and a half-life of SHH defined as $1/a_S$. A common Hill exponent n is used in all equations (see table 3 for sensitivity analysis, p51).

The values for all parameters are listed in table 3 (p51). The equations were simulated using the ODE 45 differential equation solver from Matlab. To simulate the signaling interactions in the different mutant genotypes (Fig. 7E and Fig. S8) $p_{G1}=0$ was used to disrupt the BMP4/Grem1 module and $p_{G2}=0$ was used to disrupt the SHH/GREM1/FGF e-m feedback loop as indicated. Signaling in $Grem1^{\Delta/\Delta}$ limb buds was simulated by setting $p_{G1}=p_{G2}=0$, while the decrease in $Bmp4$ gene dosage was simulated by setting the activation coefficient l to 0.25 of its reference value in $Bmp4^{\Delta/hf}$ and to 0.5 in $Bmp4^{\Delta/+}$ limb buds. Sensitivity analysis with respect to the ordering of stable SHH plateau activities revealed that the model predictions are fairly insensitive to changes in the values of particular parameters, which is indicative of a certain robustness of the limb patterning system.

To model the termination phase of the feedback signaling interactions (Fig. 7H and Fig. 9), the simulations were extended to include FGF-dependent repressor X, which mediates the proposed inhibitory effect of FGF signaling on $Grem1$ expression. This requires the addition of second degradation term to the equation describing the GREM1 kinetics:

$$\dot{G} = p_{G1} \left(\frac{B^n}{B^n + K_1^n} \right) + p_{G2} \left(\frac{S^n}{S^n + K_2^n} \right) - a_G \cdot G - d_G G \left(\frac{X^m}{X^m + K_5^m} \right)$$

The FGF-dependent repressor X is governed by the following equation:

$$\dot{X} = p_X \left(\frac{F^m}{F^m + K_6^m} \right) - a_X X$$

The additional required parameters for these equations are included in table 4 (p52). All other parameters are as listed in table 3 (p51) with the exception of the degradation rate of BMP (a_B), which is reduced in its sensitivity range. The simulated activities of the key regulatory

signals during progression of limb bud development are shown in Fig. 9.

Parameter sensitivity analysis (studies performed by Mirko Birschofberger and Felix Naef)

Parameter sensitivity analysis (table 3, third column, p51) shows that the degradation/inactivation rates of the different signals appear as most relevant to maintaining the hierarchy of SHH activities in the different mutant backgrounds (Fig. 7E). A few of the other threshold values are also rather sensitive, such as the threshold of BMP4-mediated repression of AER-FGF activity (K_3) or the threshold of AER-FGF-mediated activation of SHH (K_4). In contrast, many other parameters are very insensitive. For example, an increase in GREM1 activity (by increasing the positive contributions of P_{G1} , P_{G2} and P_S ; see table 3, p51) will not alter the properties of the model after the highest levels of GREM1-mediated repression of BMP4 activity have been reached.

B^0 , G^0 , F^0 and S^0 (table 3, p51) are reference activities that can be set to 1 (=100 %) in the simulations. The ranges given in the third column indicate the parameter interval in which the ordering of the stable plateau activities of SHH (by E10.0) is preserved among the four compound mutant genotypes shown in Fig. 6E. In this interval variation analysis the remaining parameters were kept fixed. These simulations use a fixed Hill coefficient n , but in addition an individual sensitivity analysis was performed for all four Hill coefficients (see third column for range). The Hill coefficient n_1 is used for simulations of the positive regulation of *Grem1* activity by BMP4; n_2 for SHH-mediated regulation of *Grem1*; n_3 for repression of AER-*Fgf* activity by BMP4 and n_4 for positive *Shh* regulation by FGFs.

Table 3: Parameter values used for modeling the dual-time feedback loops and the corresponding sensitivity ranges (Fig. 6, Fig. 9 and Fig. S8).

Parameter	Value	Sensitivity Range (Fig. 6E; units as in column 2)
p_{G1}	$0.25 \cdot G^0$	0.03 – >1
p_{G2}	$0.25 \cdot G^0$	0.08 – >1
p_F	$0.25 \cdot F^0$	0.07 – 0.41
p_S	$0.25 \cdot S^0$	0.06 – >1
a_B	0.25 hrs^{-1} (half life = $\log(2)/a=2.8$ hrs)	0.11 – 0.43
a_G	0.25 hrs^{-1}	0 – 0.68
a_F	0.25 hrs^{-1}	0.16 – 0.95
a_S	0.25 hrs^{-1}	0.05 – 1
K_0	$0.4 \cdot B^0$	0 – 1.4
K_1	$0.5 \cdot B^0$	0 – 1.8
K_2	$0.3 \cdot S^0$	0 – 1.2
K_3	$0.45 \cdot B^0$	0.2 – 0.78
K_4	$0.35 \cdot F^0$	0.26 – 1.27
n	3	1, 2, 3, 4
l	$0.25 \cdot B^0$	0.15 – 0.56
d	1.5 hrs^{-1}	0.6 – >100
n_1	3	1 – >150
n_2	3	1 – >150
n_3	3	1 – 4
n_4	3	1 – 5

table 4: Additional parameters required to model the termination phase (Fig. 7H and Fig. 9).

Parameter	Value
p_X	$0.001 \cdot X^0$
a_X	0.01 hrs^{-1}
d_G	100 hrs^{-1}
K_5	$0.1 \cdot X^0$
K_6	$0.3 \cdot F^0$
a_B	0.125 hrs^{-1}
m	6

X^0 is a reference activity that can be set to 1 (=100 %).

VII. GENERATION OF A *HAND2* CONDITIONAL NULL ALLELE

Introduction

In vertebrates, the family of *Hand* transcription factors consists of two members: *Hand1* also known as *Hxt*, *Thing1* and *eHAND* (because of its expression in extra-embryonic membrane, heart, autonomic nervous system, and other neural crest-derived tissues) and *Hand2* (*Hed*, *Thing2* and *dHAND* for deciduum, heart, autonomic nervous system, and other neural crest-derived tissues). They are transcription factors belonging to the basic helix-loop-helix (bHLH) superfamily. These proteins are implicated in a variety of processes during embryonic development (for review see Massari and Murre 2000). bHLH proteins can be divided in two classes. The class A factors are represented by the E-proteins such as E12, which are broadly expressed in the embryo. *Hand1* and *Hand2* genes (like *MyoD* or *Twist1*) belong to the class B that includes transcriptional regulators with more restricted expression patterns. The current model is that bHLH transcription factors function as heterodimers of class A and B proteins (Firulli 2003). However, functional dimerisation of class B partners has also been reported (Firulli et al. 2005). bHLH proteins dimerize by interactions of α helices while the preceding basic domain is responsible for DNA binding ability of the dimer. bHLH protein dimers interact with specific DNA sequences called E-boxes (consensus sequence: 5'-CANNTG-3', Firulli 2003).

Hand1 and *Hand2* were identified and cloned as part of a mouse in yeast two-hybrid screen using E-protein domains as baits (Cross et al. 1995; Cserjesi et al. 1995; Hollenberg et al. 1995). The genomic organization of *Hand* genes is well conserved between zebrafish, chick, mouse and human and are transcription units of two exons separated by an intron (Fig. 1A), as well as the amino-acid sequence of HAND proteins (Fig. 1B). Partially overlapping

expression patterns suggest that their functions have been conserved and that *Hand1* and *Hand2* may be partially redundant with respect to their functions during development (Firulli 2003; McFadden et al. 2005).

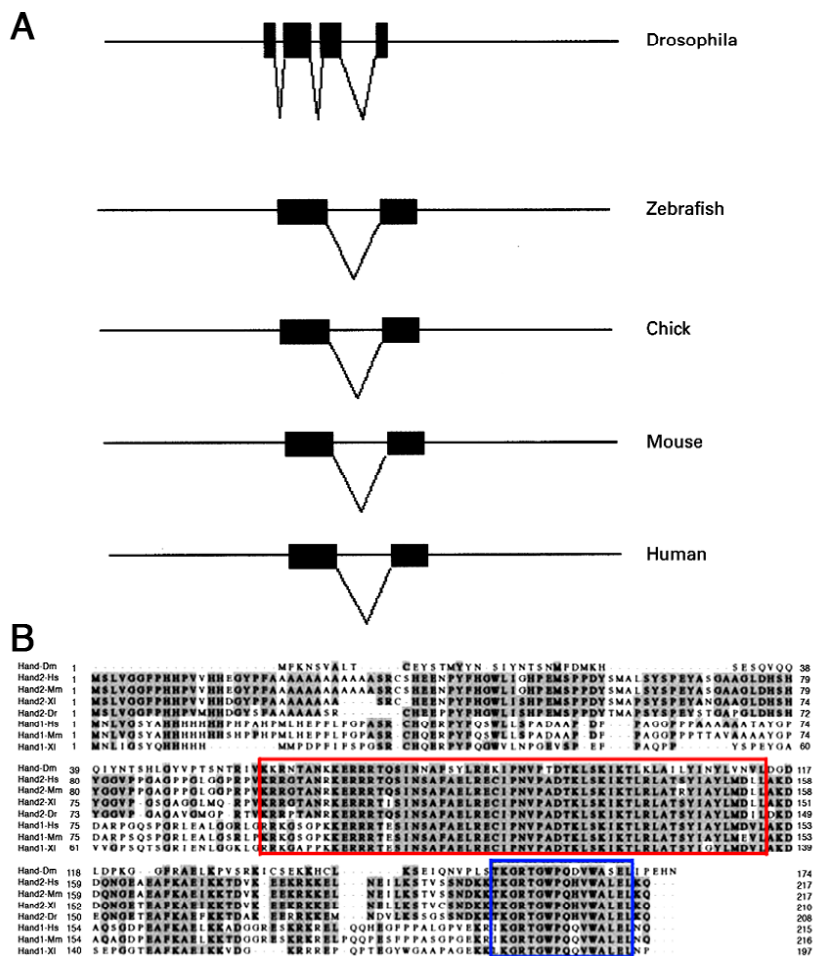


Fig. 1. Gene structures and conservation of HAND proteins. (A) Schematic diagrams of *Hand* genes. DNA is depicted as a solid line and exons are shown as black boxes. Species are indicated to the right (Firulli, 2003). (B) *Drosophila* HAND was aligned to several vertebrate HAND proteins. The conservation is most prominent within the bHLH-domain (red box). And the so-called Hand-domain, which is highly specific for this subclass of bHLH proteins (blue box). Identical residues are shaded. Dm: *Drosophila melanogaster*; Hs: *Homo sapiens*; Mm: *Mus musculus*; Xl: *Xenopus laevis*; Dr: *Danio rerio*. (From Kolsch and Paululat 2002).

Hand genes and murine heart development

Complete loss-of-function alleles of both genes have been generated by homologous recombination in mouse embryonic stem cells and have allowed the genetic analysis of the early functions *Hand* genes. *Hand1* deficient embryos die between E8.5 and E9.5 and exhibit yolk sac abnormalities due to a deficiency in extra-embryonic mesoderm. The yolk sac is

lacking proper vascularization and the expression of the *placental lactogen 1* gene in the trophoblast is strongly reduced. The resulting poor nutrient supply is probably responsible for the observed growth retardation and death of the embryo. In addition to these extra-embryonic defects, heart development is impaired in *Hand1* deficient embryos. The heart tube forms in mutant embryos but fails to undergo its normal looping morphogenesis (Firulli et al. 1998).

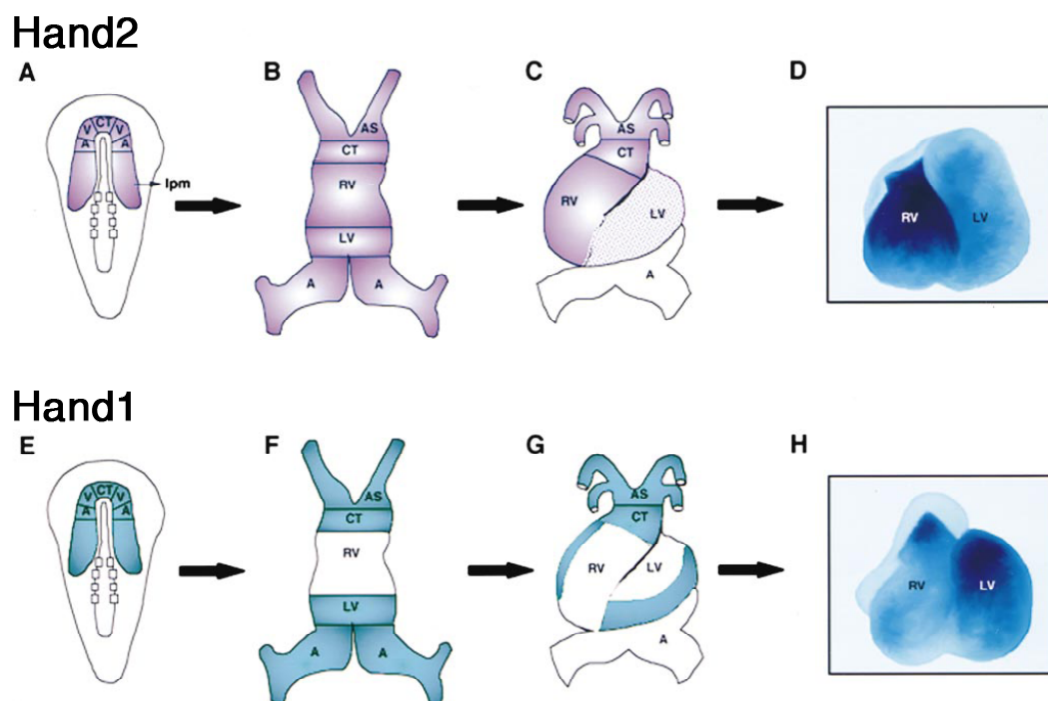


Fig. 2. Summary of *Hand2* and *Hand1* expression patterns during mouse cardiogenesis.

Hand2 (purple) and *Hand1* (blue) are uniformly expressed in cardiac progenitor cells (A-E) and in the left and right lateral plate mesoderm (lpm) but become restricted to the future right and left ventricle-forming regions, respectively, as the heart tube loops. *Hand2* is expressed throughout the linear heart tube (B) but becomes predominately right sided after looping (C). *Hand1* is expressed in the conotruncus (CT) and left ventricle (LV)-forming regions of the linear heart tube (F); the anterior-posterior interrupted pattern becomes left-right by virtue of cardiac looping (G). Expression is non-concentric and is along the outer curvature of the heart (G). RNA in situ hybridization with isolated E10.0 mouse hearts shows expression of *Hand2* in the right ventricle (D) and *Hand1* in the left ventricle (H) (frontal views). Both genes are expressed in the aortic sac (AS) that gives rise to the aorta and pulmonary arteries, but are down-regulated in the myocardium of the heart once formation is complete. RV, right ventricle; A, atria. (From Srivastava 1999).

Hand2 deficient embryos die a bit later, around E9.5-E10. Embryonic development arrests due to a failure in right ventricle development and additional heart and vascular defects (Srivastava et al. 1997). *Hand1* and *Hand2* are co-expressed by the precardiogenic mesoderm (Fig. 2A and 2E) where they could fulfill partially redundant roles as heart morphogenesis is initiated in both mutants. However as heart development continues, their respective expression domains become restricted to complementary regions of the heart tube (Fig. 2B-D and 2F-H). *Hand2* is specifically expressed in the future right ventricle as the tube loops and acts upstream of the cardiogenic transcription factor GATA4. Thus *Hand2* is an early and essential component of the genetic network controlling right ventricle development (Srivastava et al. 1997). *Hand1* expression is restricted to the future left ventricle during looping of the heart tube, but the early lethality of *Hand1* null mutants precludes analysis of possible function of *Hand1* in left ventricle development (Firulli et al. 1998).

***Hand2* functions during limb development**

Limb bud prepatterning

Both *Hand* genes are expressed during limb development. In mouse, *Hand1* is detectable only at late stages (E11.5). Its expression pattern is restricted to a small region of the antero-ventral mesenchyme. In chicken limb buds *Hand1* is expressed earlier and in a more complex expression pattern (Fernandez-Teran et al. 2003). Overexpression experiments showed that *Hand1* can induce ectopic digits with a variable efficiency, in both fore and hind limbs (Fernandez-Teran et al. 2003; Firulli et al. 2003).

In both mouse and chicken, *Hand2* is expressed at early stages in a dynamically changing expression pattern throughout limb bud development. Initially, *Hand2* is expressed in the whole lateral plate mesoderm, thus encompassing the prospective limb field. As the limb bud

emerges, *Hand2* expression becomes rapidly restricted to the posterior mesenchyme. Later, a second expression domain is detected in the distal limb bud. *Hand2* is widely expressed in the autopod territory with the exception of the anterior most mesenchyme, region of the presumptive digit 1. During later stages *Hand2* expression gets restricted to all condensing digits (Fig. 3, Charité et al. 2000; Fernandez-Teran et al. 2000).

The posterior restriction of *Hand2* expression in the early limb bud is due to an interaction with the repressor form of the *Gli3* transcription factor (Gli3R). Genetic analysis of *Gli3* and *Hand2* deficient buds showed that a mutual genetic antagonism restricts *Gli3* and *Hand2* expression to the anterior and posterior mesenchyme respectively. Thus this antagonistic interaction polarizes the early limb bud prior to SHH signaling by defining an anterior (GLI3R) and a posterior compartment (HAND2). In addition, this mechanism prepatterns the limb bud by setting up the competence to express other genes such as *Alx4* in the anterior mesenchyme and 5'*Hoxd* genes, *Bmp2* and *Shh* in the posterior mesenchyme. In addition, overexpression of HAND2 protein enhances the expression of the BMP antagonist *Grem1* (te Welscher et al. 2002a). *Hand2* expression is not expanded distally in *Shh* loss-of-function mutant limb buds suggesting that SHH-mediated upregulation of *Hand2* after initiation of limb bud development sustains ZPA/AER feedback signaling through positive regulation of *Grem1* expression (te Welscher et al. 2002a).

Hand2 and the establishment of SHH polarizing activity

Interestingly, the restriction of *Hand2* expression from the whole limb field to the posterior mesenchyme parallels tissue competence to establish the SHH expressing polarizing region. Transplantation experiments in the chick embryo have shown that a weak polarizing activity is present in the whole limb field prior to limb budding. As limb bud outgrowth is initiated,

polarizing activity increases and is progressively restricted to more posterior cells in the limb bud and adjacent posterior lateral plate mesoderm (Hornbruch and Wolpert 1991). These observations make *Hand2* a good candidate for the establishment and positioning of the ZPA and *Shh* expression.

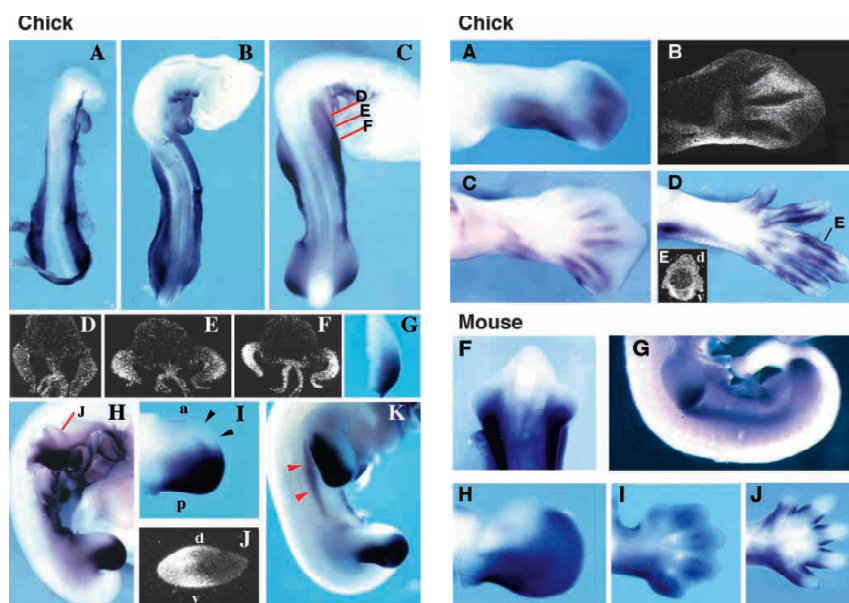


Fig. 3. *Hand2* expression pattern during chick and mouse limb development. Left; *Hand2* expression pattern during early chick limb bud development. (A) Stage 14 embryo showing expression of *Hand2* in the lateral plate mesoderm. (B,C) Expression of *Hand2* in stage 17 and 19 embryos respectively. Note the establishment of the gradient of expression along

the anterior-posterior axis of the emerging limb bud. (D-F) Sequential transverse sections (level of section indicated in C by the red lines) clearly showing the highest level of expression posteriorly (F). (G) Stage 19-20 wing bud. (H) Expression of *Hand2* in stage 23 embryo. Transcripts are observed in the posterior half of both wing and leg. (I) Ventral view of a stage 22 wing bud showing *Hand2* expression. The arrowheads indicate the lack of expression in the AER. (J) *Hand2* expression pattern in a transverse section through the middle of a stage 23 wing bud (level of section indicated in (H) by the red line). (K) *Hand2* expression pattern in a stage 26 embryo. Arrowheads indicate the domain of expression at the flank. A, anterior; p, posterior; d, dorsal; v, ventral. Right; *Hand2* expression at later stages of chick and mouse limb development. (A) *Hand2* expression pattern in a stage 28 leg bud. Note the transverse band devoid of transcripts at the tarsus level. (B) Frontal section of a stage 30 leg bud showing expression in the interdigit area and in the periphery of the digital cartilages. (C) Subsequently, *Hand2* expression is downregulated in the interdigits but persists in the periphery of the digits. (D) At stage 35, *Hand2* expression encompasses the developing tendons with a marked ventral bias, better appreciated in section E. (E-F) *Hand2* expression during mouse limb development. (F) A dorsal view of the forelimbs of an E10.0 mouse embryo showing expression of *Hand2* in the posterior mesoderm. (G) Lateral view of an E11.0 day mouse embryo. (H-J) Ventral views of forelimbs of E12.0 (H), E13.0 (I) and E14.0 (J). In all the panels except E and G, anterior is up (From Fernandez-Teran et al. 2000).

Widespread ectopic expression of *Hand2* in early limb bud using a *Hand2* transgene under the control of the *Prx1* limb enhancer induces an ectopic ZPA (characterized by *Shh* expression) and mirror image duplications of the digit skeletal pattern (Charité et al. 2000). Ectopic expression in chicken wing bud leads to similar results (Fernandez-Teran et al. 2000). It is important to note that *Hox* genes from the Abdominal A and B groups (called *5'Hox* genes in vertebrates) are also able to induce *Shh* expression and digit duplication when ectopically expressed (Charité et al. 1994; Knezevic et al. 1997; Zakany et al. 2004). Interestingly, *5'Hoxd* genes are co-expressed with *Hand2* in the early posterior limb bud prior to initiation of *Shh* transcription. Complete loss of function of *Hoxa* and *5'Hoxd* paralogues abrogates transcriptional activation of *Shh* activation in limb bud (Kmita et al. 2005). In *Hand2* loss-of-function mutant embryos, *Shh* expression is not detectable in limb buds by *in situ* mRNA hybridization suggesting that *Hand2* might participate in induction of *Shh* expression. However, massive apoptosis occurs in limb buds and in the rest of the embryo prior to activation of *Shh* expression, which may thereby very indirectly interfere with activation of *Shh* transcription.

Altogether these (and other) results suggest that in the early limb bud, *5'Hoxd* genes and the *Gli3/Hand2* pre patterning system cooperate to control mesenchyme polarization and the establishment of *Shh* expression in the ZPA. Afterwards, SHH signaling positively regulates *5'Hoxd* genes and *Hand2* for propagation of the epithelial-mesenchymal signaling and patterning of the distal limb. Because of the early lethality of the constitutive loss-of-function *Hand2* allele, we have generated a conditional null allele to specifically remove HAND2 activity from the limb bud mesenchyme and analyze the effects on gene expression and skeletal pattern.

Homologous recombination of the *Hand2* locus

Hand2 is located on chromosome 2 and spans approximately 3.5 kb. Exon 1 (1479 bp) and exon 2 (756 bp) are separated by an intron of 1300 bp. The open reading frame (654 bp) spans over the two exons and encodes a protein of 217 amino acids. To generate the conditional null *Hand2* allele, we constructed a targeting vector that contains LoxP sites flanking the entire transcription unit. Upon Cre-mediated recombination activity the entire gene will be deleted, resulting in a loss of function allele (Fig. 4). The *Hand2* genomic DNA locus was isolated from a BAC library. A 7.1 kb XhoI-NotI fragment containing 6.4 kb of upstream sequence and a part of the coding exon 1 were subcloned in a pGEM vector. This fragment was modified by the introduction of an EcoRV restriction site and the LoxP site in a NarI site 74 bp upstream of the transcriptional start. The rest of the gene and 5 kb of downstream sequence were subcloned as a NotI-XhoI fragment in a pGEM vector. A second LoxP site followed by a Neomycin-resistance gene under control of the PGK promoter and flanked by Frt sequences (LoxP-Frt-Pgk-Neo-Frt cassette) was inserted in a BamHI site 440 bp downstream of the polyA signal. The definitive targeting vector (20 kb) was constructed by assembling these two fragments (see Fig. 4.).

The targeting vector was digested with XhoI, separating the pGEM backbone from the modified allele. The DNA was cleaned by one phenol/chloroform and 2 chloroform/isoamyl alcohol extractions using the Phase Lock Gel kit from Eppendorf, which eliminates traces of organic solvents. The targeting vector was electroporated into mouse embryonic stem (ES) cells and ES cells clones were selected in G418 containing medium. Homologous recombination events were identified by a Southern blot screen in surviving clones. DNA from ES clones was digested with EcoRV for 5' screening. The wild-type allele was detected by the 5' external probe as a genomic fragment of 15 kb while homologous recombination

events generate an 8 kb fragment (Fig. 4, blue lines and boxes). Positive ES cells clones from the 5' end screen were then retested with respect to the 3' end of the locus. DNA was digested with *PacI*. The wild-type and the recombined alleles were detected as a 7 kb and 9 kb fragments respectively by the 3' external probe (Fig. 4, orange lines and boxes).

Out of 1224 clones analyzed, only clones 4D7 and 10C3 had undergone homologous recombination. The frequency is similar to the one obtained generating the constitutive *Hand2* null allele (1:500, Srivastava et al. 1997). Clones 4D7 and 10C3 were expanded and injected into blastocystes to generate chimeras. Following breeding for germline transmission, F1 animals carrying the recombined locus were intercrossed and homozygous animals were found at a normal frequency indicating that the P_{gk}-Neo cassette and LoxP sites do not significantly interfere with normal *Hand2* functions.

Mice carrying the recombined locus were crossed with mice expressing a transgenic F_lp recombinase (F_lpase, Dymecki 1996) to excise the P_{gk}-Neo cassette (Fig. 4). Offspring carrying this *Hand2* floxed allele were then mated with mice expressing the Cre recombinase under the control of the ubiquitous CMV minimal promoter (Schwenk et al. 1995) to generate offspring carrying the *Hand2* null allele (Fig. 4).

These alleles will allow the analysis of *Hand2* functions in a conditional manner by generating embryos carrying a tissue specific Cre transgene and both *Hand2* null and conditional alleles. Limb mesenchyme specific mutants can be obtained using the *Prx1*-Cre transgene (Logan et al. 2002). Moreover, temporal requirement of *Hand2* can be assessed using a Tamoxifen inducible Cre transgene (Hayashi and McMahon 2002).

This work was performed under the supervision of Dr. A. Galli.

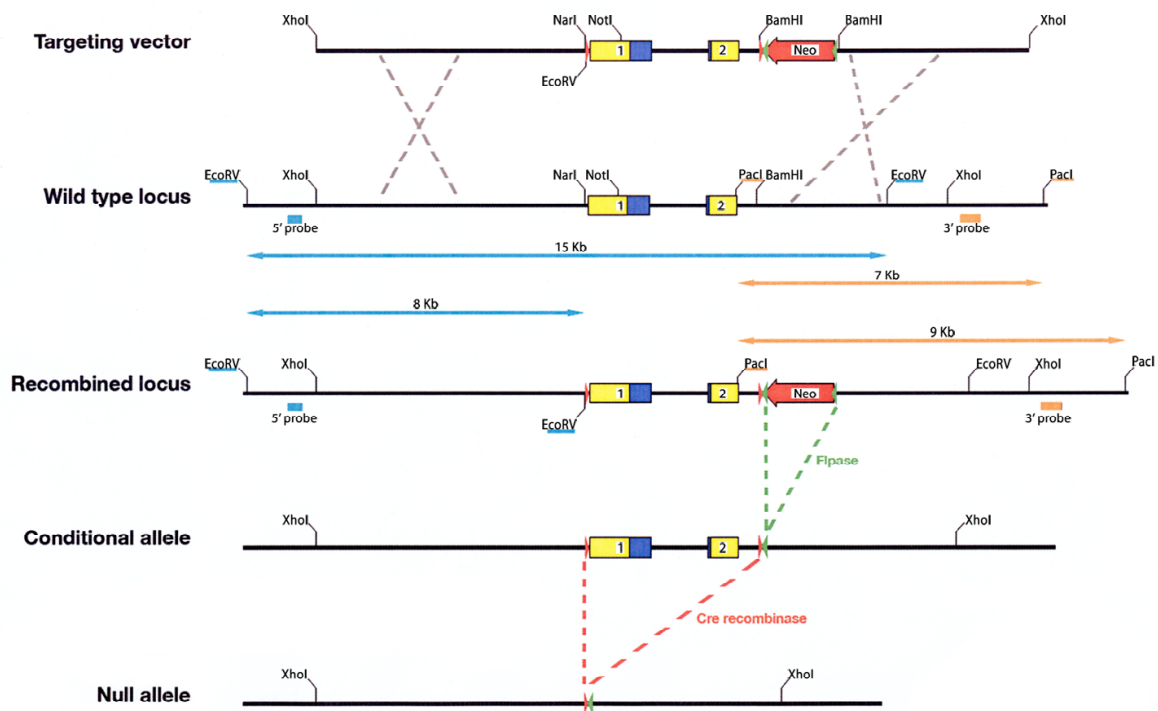


Fig. 4. Generation of the *Hand2* conditional and null alleles.

The wild type locus was modified by homologous recombination in mouse ES cells after electroporation of the targeting vector. Following selection for Neomycin resistance, positive ES clones were screened by Southern blot at both ends of the locus (blue lines: DNA fragments detected after EcoRV digestion and hybridization with the 5' end DNA probe (blue box), endogenous locus: 15 kb, recombined locus: 8 kb; Orange lines: DNA fragments detected after Pacl digestion and hybridization with the 3' end DNA probe (orange box), endogenous locus: 7 kb, recombined locus: 9 kb). The Neomycin resistance cassette was removed by FLPase mediated recombination of the FRT sites (green triangles) to generate the *Hand2* conditional allele. Under Cre recombinase activity, the LoxP sites (red triangles) were recombined leading to the deletion of the two exons of the *Hand2* gene, generating a null allele.

Publication:

Antonella Galli, Dimitri Robay, Marco Osterwalder, Jean-Denis B nazet, Susan Mackem and Rolf Zeller. **Genetic dissection of the pre-patterning mechanism initiating polarity and *Shh* expression in mouse limb buds.** *In preparation.*

VIII. A SELF-REGULATORY SYSTEM OF INTERLINKED SIGNALING FEEDBACK LOOPS CONTROLS VERTEBRATE LIMB PATTERNING

Introduction

During embryonic development, complex tissues and organs are reliably generated, which implies that large groups of cells have to be co-coordinated with respect to their proliferation, survival and differentiation potential to assure development of a functional structure or organ. While molecular and genetic analysis in combination with experimental manipulation have uncovered key regulatory molecules, it has been rather difficult to gain insight into the potentially complex systems and network interactions that endow developmental programs with robustness (Eldar et al. 2003; Kerszberg 2004) against perturbations that could cause congenital malformations and/or death of the embryo. For example, Spemann's organizer and an opposing ventral signaling centre secrete BMP type signals and antagonists that interact to generate a self-regulating morphogenetic field, which in turn controls gastrulation of amphibian embryos (Reversade and De Robertis 2005). These studies provide the first molecular insights into the self-regulatory capacity of embryos in situations such as axis duplications and twinning (De Robertis 2006). Little is currently known about the processes that endow organogenesis and tissue patterning with such self-regulatory properties. Identification of the underlying molecular networks is required and will be of relevance to the understanding of the pathogenesis of congenital malformations and for tissue engineering.

The developing limb is a paradigm to study how growth, patterning and differentiation are co-coordinately regulated in amniote embryos (Zeller 2004; Zuniga and Galli 2005; Tickle 2006; Zakany and Duboule 2007). Limb bud development is controlled in part by epithelial-mesenchymal (e-m) feedback signaling interactions between two

instructive signaling centers, the limb bud organizer located in the posterior mesenchyme (polarizing region or zone of polarizing activity; ZPA) and the apical ectodermal ridge (AER) at the distal tip. The ZPA produces the Sonic Hedgehog (SHH) morphogen, which is required to specify digits 2 to 5 of the pentadactylous autopod (Chiang et al. 2001; Kraus et al. 2001; Ahn and Joyner 2004). In mouse embryos, SHH acts long-range to specify anterior digits (2 and parts of 3), while the posterior digits (3 to 5) are derived from descendants of *Shh* expressing cells that seem to acquire their identities by the duration of their exposure to SHH (Lewis et al. 2001; Harfe et al. 2004; Zeller 2004; Li et al. 2006; Scherz et al. 2007). In particular, SHH signaling by the ZPA fulfills a dual function by integrating the early specification of digit progenitors with their proliferation and progressive distal-anterior expansion of the autopod territory (Towers et al. 2008; Zhu et al. 2008). In response to SHH signaling, the expression of the Bone Morphogenetic Protein (BMP) antagonist *Gremlin1* (*Grem1*) is up-regulated specifically in the dorsal and ventral subectodermal mesenchyme within the expanding population of the distal limb bud (Zuniga et al. 1999; Panman et al. 2006), while *Shh* descendants in the posterior mesenchyme are refractory to *Grem1* expression (Scherz et al. 2004; Nissim et al. 2006). GREM1-mediated BMP antagonism is required to relay morphogenetic SHH signaling to the AER and up-regulates the expression of several Fibroblast Growth Factors (FGFs; Zuniga et al. 1999; Panman et al. 2006). In turn the FGFs produced by the AER (AER-FGFs) instruct the proximo-distal pattern in the limb bud mesenchyme (Mariani et al. 2008) and maintain *Shh* expression by the ZPA. In *Grem1* deficient mouse embryos, this SHH/GREM1/FGF e-m feedback loop is not established, which disrupts both signaling centers, resulting in mesenchymal cell death, fusion of ulna and radius and loss of SHH-dependent specification of digit identities (Khokha et al. 2003; Michos et al. 2004). In addition, ectopic BMP signaling in chicken limb buds can directly

induce *Grem1* expression (Capdevila et al. 1999; Nissim et al. 2006), although the functional relevance of BMP-mediated regulation of *Grem1* expression remains unclear.

Three BMP ligands (BMP2, -4, -7) are expressed during limb bud development and the functions of the BMP signaling pathway have been investigated, but results were rather conflicting (reviewed by Robert 2007). Experimental manipulation of BMP signaling (Pizette et al. 2001) and conditional inactivation of the BMP receptor 1A in the limb bud ectoderm (BMPR-1A; Ahn et al. 2001) provided evidence that BMP signaling activity participates in establishment of the dorso-ventral axis and AER formation. However, the origin and identity of the potentially involved BMP ligands remained unknown. Manipulation of chicken limb buds indicated that BMP2 is a positive secondary signal required for specification of digit identities in response to SHH signaling (Drossopoulou et al. 2000) and that digit identities are determined/fixed rather late by BMP signaling from the interdigital mesenchyme (Dahn and Fallon 2000). A positive role of BMPs in digit specification was supported by mesenchyme-specific inactivation of the *Bmp receptor 1A* (*Bmpr-1A*), which disrupts distal limb and digit patterning (Ovchinnikov et al. 2006). Two other studies corroborated this evidence as the weak and variable digit polydactylies in *Bmp7* (Hofmann et al. 1996) and *Bmp4* (Selever et al. 2004) deficient mouse limb buds seem to arise as a consequence of expanded AER-FGF signaling. Bandyopadhyay et al. (2006) concluded that inactivation of *Bmp2* and *Bmp4* expressed by the limb bud mesenchyme expands AER-*Fgfs* and *Shh* expression and affects initiation of chondrogenesis, resulting in loss of posterior digits.

In the present study, we identify BMP4 as the ligand, whose differential activity is critical to normal progression of mouse limb bud development. Firstly, we show that reduction of the *Bmp4* gene dosage in *Grem1* deficient embryos progressively restores distal limb and autopod development in contrast to *Bmp2* and *Bmp7*. In *Grem1* deficient limb buds,

BMP4 activity remains high as assessed by elevated *Msx2* levels and interferes with SHH-mediated specification of digit identities. We show that the restoration of the pentadactylous autopod in *Grem1-Bmp4* compound mutant embryos is - in contrast to the wild-type - very fragile towards additional inactivation of one *Shh* allele. Secondly, we establish that BMP4 is first required during initiation of limb bud development as its inactivation from early stages onwards disrupts establishment of a functional AER and initiation of e-m feedback signaling. This early loss of *Bmp4* causes apoptosis of the mesenchymal progenitors such that the limb skeleton is truncated distal to the scapula. Thirdly, we show that BMP4 positively regulates early *Grem1* expression and that GREM1-mediated lowering of BMP4 activity is essential for subsequent, SHH-dependent specification of digit identities. In combination with mathematical modeling, we establish that differential regulation of *Grem1* expression by BMP4 and SHH couples a fast BMP4/GREM1 module to the slower SHH/GREM1/FGF e-m feedback loop resulting in a self-regulatory switch from BMP4- to SHH-dependent signaling. Taken together, our analysis reveals the self-regulatory nature of the distal limb and digit patterning system and how the interconnectivity of the involved signaling pathways endows distal limb development with distributed robustness.

Results

Reduction of BMP4 activity enables SHH-dependent specification of digit identities

Three BMP ligands are expressed in limb buds (Fig. S1) and we have generated compound mutant embryos lacking *Grem1* and one functional allele of either *Bmp2*, *Bmp4* or *Bmp7* (Hofmann et al. 1996; Kulesa and Hogan 2002; Ma and Martin 2005) to determine genetically which ones are preferentially antagonized by GREM1. The resulting limb skeletons were initially analyzed at embryonic day E14.5 (Fig. 1A). Halving either the *Bmp2*

or *Bmp7* gene dosage only slightly improves distal limb development in comparison to *Grem1* deficient limb buds (Fig. 1A). In contrast, inactivation of one *Bmp4* allele in *Grem1* deficient limb buds restores the zeugopod (ulna, radius) and promotes formation of four digits, two of them with distinct posterior identities (digits 4, 5 Fig. 1B; n=24/24), similar to complete inactivation of *Bmp7* (*Grem1^{ΔΔ}Bmp7^{ΔΔ}* in Fig. S2). Furthermore, genetic lowering of one *Bmp* in a *Grem1* deficient limb bud does not affect the expression of the other *Bmps* (Fig. S1 and S2). Hindlimb development is restored to a similar extent (data not shown), but our study focuses on forelimb buds as the *Grem1* phenotypes have been molecularly best characterized during their development.

Taken together, antagonism of BMP4 by GREM1 appears as functionally most relevant for distal limb development, while the antagonism of BMP2 and BMP7 contributes to a much lesser extent. Therefore, we focused our analysis on the genetic interaction of *Grem1* with *Bmp4* during mouse forelimb development. Interestingly, the genetic activity of the conditional *Bmp4* allele used is significantly reduced, which clearly reveals its hypomorphic nature (Kulesa and Hogan 2002; Jiao et al. 2003). Therefore, we took advantage of this hypomorphic and floxed *Bmp4* allele (*Bmp4^{hf}*) to generate an allelic series in context of *Grem1* deficiency (Fig. 1B). Introduction of the hypomorphic *Bmp4^{hf}* allele into *Grem1^{ΔΔ}* embryos is phenotypically similar to inactivating one allele of *Bmp2* or *Bmp7* (Fig. 1B; compare to Fig. 1A). Complete inactivation of one *Bmp4* allele enables SHH-dependent specification of posterior digits (*Grem1^{ΔΔ}Bmp4^{Δ+}*; Fig. 1B), while complete restoration of pentadactyly requires further genetic reduction of BMP4 activity in *Grem1* deficient limb buds (*Grem1^{ΔΔ}Bmp4^{Δ/hf}* embryos in Fig. 1B; n=10/14). In about one third, digit formation is almost perfectly restored (n=3/10), while in the others digits 2 and 3 remain proximally fused (n=7/10; Fig.1B). As digit morphologies are rather similar at this stage of development, we

used carpal bone pattern as an additional criteria to assess the antero-posterior polarization of mutant handplates (Fig. S3). Moreover, the restoration of the autopod is already apparent earlier when digit identities are determined (Zhu et al. 2008) and chondrogenesis initiated (*Sox9* expression, Fig. S3). Thus, this stepwise reduction of the *Bmp4* gene dosage in *Grem1* deficient embryos restores forelimb development with proximal to distal and posterior to anterior sequence. At the cellular level, the massive apoptosis apparent in the distal-anterior mesenchyme of *Grem1* deficient limb buds by E10.75, is progressively suppressed by lowering *Bmp4* levels (arrowheads in Fig. 1C). In contrast, the posterior mesenchyme encompassing the *Shh* descendants (contributing to formation of digits 3-5; Harfe et al. 2004) is devoid of apoptosis and expands normally (Fig. 1C and Fig. S4). The expression of 5' *Hoxd* genes in the digit forming area hallmarks digit specification (Zakany et al. 1997; Zakany and Duboule 2007) and their reverse collinear establishment is significantly delayed in *Grem1*^{ΔΔ} mouse limb buds in comparison to wild-types (Fig. 1D, E; for details see Haramis et al. 1995; Panman et al. 2006). In contrast, their distal-anterior expansion is restored to wild-type levels in *Grem1*^{ΔΔ}*Bmp4*^{Δhf} limb buds (Fig. 1D, E), which provides a likely molecular explanation for the observed restoration of distal limb development (Fig. 1B).

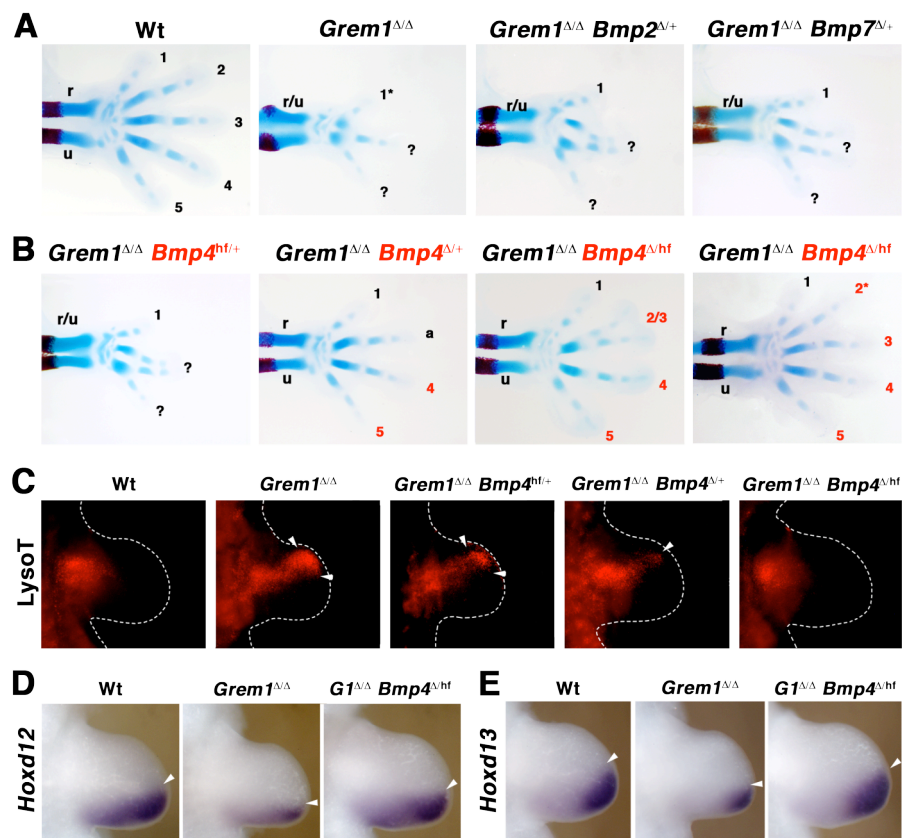


Fig. 1. Genetic reduction of BMP4 activity preferentially restores digit specification, cell survival and 5' *Hoxd* gene expression in *Grem1* deficient forelimb buds.

(A, B) Alcian blue and alizarin red stained skeletal preparations of mouse forelimbs at embryonic day E14.5. Digit identities are indicated by numbers 1 (thumb, anterior) to 5 (little finger, posterior). Question mark: digit with unknown identity - a hallmark of the *Grem1* loss-of-function mutation, a: anterior digit (2 or 3), 2/3: proximally fused digits 2 and 3, asterisks: hypoplastic digits. Zeugopod: r: radius, u: ulna, r/u: (partially) fused radius and ulna- another hallmark of the *Grem1* loss-of-function mutation (for details see (Khokha et al. 2003; Michos et al. 2004)). (A) Wt: wild-type forelimb; *Grem1*^{ΔΔ}: *Grem1* deficient forelimb; *Grem1*^{ΔΔ} *Bmp2*^{Δ/+} and *Grem1*^{ΔΔ} *Bmp7*^{Δ/+}: *Grem1* deficient forelimbs heterozygous for *Bmp2* and *Bmp7*, respectively. (B) *Grem1* deficient forelimbs in which the *Bmp4* gene dosage is gradually reduced in the mesenchyme and ectoderm by introducing either the hypomorphic (*Grem1*^{ΔΔ} *Bmp4*^{hf/+}) or the loss-of-function (*Grem1*^{ΔΔ} *Bmp4*^{Δ/+}) allele or the combination of both (*Grem1*^{ΔΔ} *Bmp4*^{Δ/hf}, *G1*^{ΔΔ} *Bmp4*^{Δ/hf}). Note that the genetic activity of one hypomorphic *Bmp4*^{hf} allele appears as slightly more than 50% (Fig S1). Digit identities were determined using morphological criteria in combination with the associated patterning of carpal elements and *Sox9* expression at earlier stages (Fig. S3). Digits indicated in red correspond to the ones with restored identities. (C) Detection of apoptosis in forelimb buds at E10.75 (38 somites) by LysoTracker Red. Arrowheads point to the ectopic cell death domain. (D, E) Detection of *Hoxd12* and *Hoxd13* transcripts in forelimb buds at E11.0 (39 to 40 somites). White arrowheads indicate the anterior expression boundaries. All panels are oriented anterior to the top and posterior to the bottom.

Levels and spatial distribution of *Msx2* transcripts, a direct and early target of BMP signaling (Brugger et al. 2004), were assessed to quantify alterations in BMP activity. In limb buds lacking *Grem1*, *Bmps* expression are also reduced (Fig. 2A, B; Fig. S1; Michos et al. 2004), but nevertheless the overall BMP activity is significantly increased as indicated by the about two-fold higher *Msx2* transcript levels (Fig. 2C, D). *In situ* hybridization analysis shows that *Msx2* transcription is much increased in both the anterior and posterior mesenchyme (Fig. 2C, panel *Grem1*^{Δ/Δ}). Genetic reduction of *Bmp4* in *Grem1*^{Δ/Δ}*Bmp4*^{Δ/hf} embryos reduces *Msx2* expression to about wild-type levels in both the anterior and posterior mesenchyme (Fig. 2C, D). The distal mesenchyme of *Grem1*^{Δ/Δ}*Bmp4*^{Δ/hf} limb buds is largely devoid of *Msx2* transcripts, while its aberrant expression in the distal mesenchyme of *Grem1* deficient limb buds (Fig. 2C) likely induces apoptosis (Fig. 1C; Marazzi et al. 1997; Ferrari et al. 1998). Similar results were obtained by analyzing *Msx1*, another target of BMP signaling in the limb bud (data not shown). These results are indicative of a primary effect of the antagonistic GREM1-BMP4 interactions in the limb bud mesenchyme, where GREM1 is normally required for establishment of the SHH/GREM1/FGF e-m feedback loop. Indeed, in *Grem1* deficient limb buds, *Shh* expression is drastically reduced (Fig. 2E, F) and SHH signal transduction is roughly halved as measured by the decrease in *Gli1* transcription (Fig. 2G, H) and *Ptc1* (Fig. S5). In *Grem1*^{Δ/Δ}*Bmp4*^{Δ/hf} limb buds, SHH signal transduction is partially, but not completely, restored (to about 75%; Fig. 2H and Fig. S5). Concordantly, *Fgf8* expression is also partially restored, while *Fgf4* expression is reactivated, but remains at low levels in the AER of *Grem1*^{Δ/Δ}*Bmp4*^{Δ/hf} limb buds (Fig. 2I-J and Fig. S3). Taken together, these results (Fig.1 and Fig. 2) show that aberrantly high BMP4 activity in *Grem1*^{Δ/Δ} limb buds opposes distal progression of development and specification of digit identities by interfering with the

transcriptional up-regulation of the instructive SHH (Towers et al. 2008; Zhu et al. 2008) and AER-FGF signals (Mariani et al. 2008).

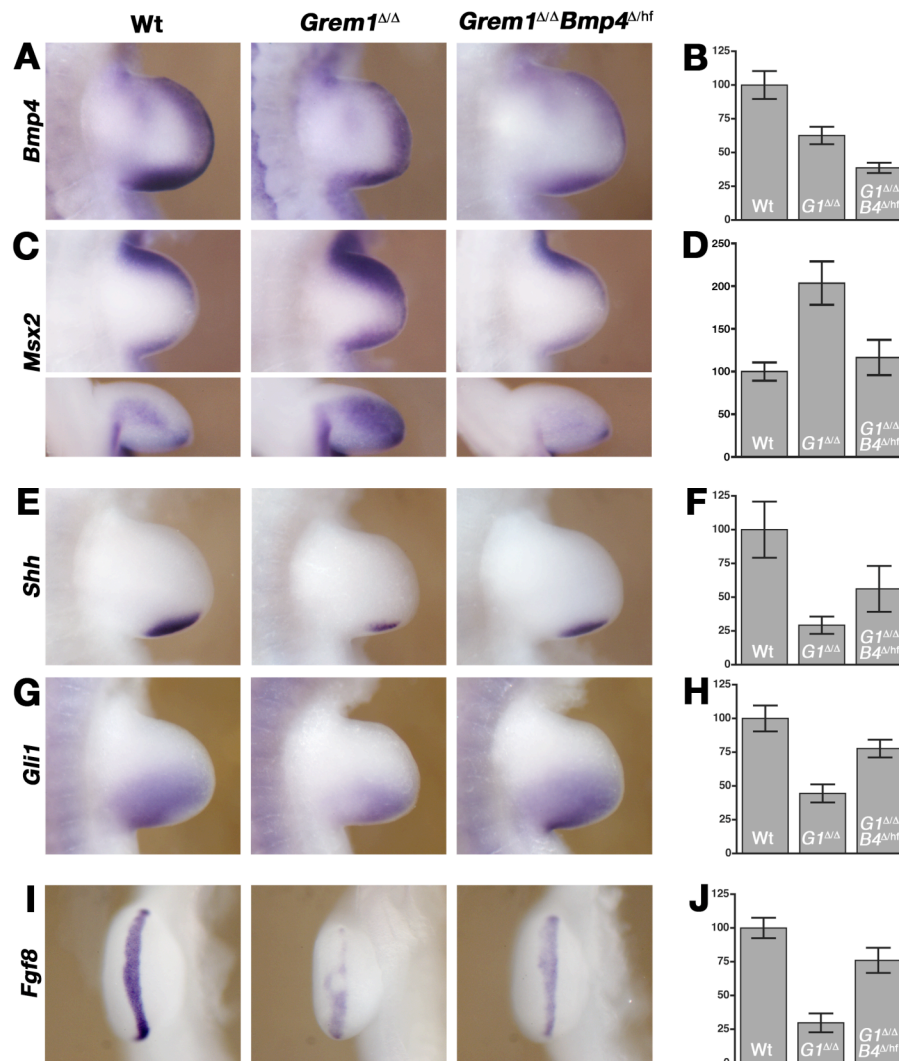


Fig. 2. Reduction of BMP4 activity is required for partial restoration of SHH signaling and *Fgfs* expression in *Grem1* deficient limb buds.

(A, C, E, G, I) Detection of *Bmp4*, *Msx2*, *Shh*, *Gli1* and *Fgf8* transcripts by in situ hybridization in wild-type (Wt), *Grem1*^{ΔΔ} and *Grem1*^{ΔΔ}*Bmp4*^{Δ/hf} forelimb buds at E10.75 (36-37 somites). Lower panels in (C) are posterior views (dorsal: top; ventral: bottom) of the limb buds in the upper panels. Note that *Msx2* expression is up-regulated in the distal and posterior mesenchyme of *Grem1*^{ΔΔ} limb buds. (B, D, F, H, J) Q-PCR was used to determine the relative expression levels of *Bmp4*, *Msx2*, *Shh*, *Gli1* and *Fgf8* in limb bud extracts (n=9 at E10.75, 36-39 somites). Wt: wild-type; *G1*^{ΔΔ}: *Grem1*^{ΔΔ}; *G1*^{ΔΔ}*B4*^{Δ/hf}: *Grem1*^{ΔΔ}*Bmp4*^{Δ/hf}. P values for all quantifications are ≤ 0.001 with one obvious exception: the difference in *Msx2* transcript levels between wild-type and *Grem1*^{ΔΔ}*Bmp4*^{Δ/hf} limb buds (panel D) is not significant (P≥0.05) as BMP4 activity is reduced to wild-type levels in *Grem1*^{ΔΔ}*Bmp4*^{Δ/hf} limb buds.

To further analyze the possible functional relevance of the interconnectivity between the BMP and SHH signaling pathways, we inactivated one *Shh* allele (St-Jacques et al. 1998) in different genetic make-ups (Fig. 3). Inactivation of one *Shh* allele in *Shh*^{Δ/+} limb buds (Fig. 3A) is compensated such that *Shh* transcript levels are at about 70% of wild-types and neither *Gli1* expression as an indicator of SHH signal transduction nor digit specification are affected. Normal digit specification in the context of heterozygosity for *Shh* reveals the stability and robustness of the underlying regulatory networks. In contrast, heterozygosity for *Shh* in *Grem1*^{Δ/Δ}*Bmp4* compound mutant limb buds reduces *Shh* expression by again about 30% (Fig. 3B, C), but in contrast to the *Shh*^{Δ/+} limb buds this reduction is no longer compensated. Inactivation of one *Shh* allele in *Grem1*^{Δ/Δ}*Bmp4*^{Δ/hf} limb buds causes loss of anterior digit identities (with the exception of digit 1; Fig. 3B) as a likely consequence of the significant reduction in SHH signal transduction (as assessed by quantifying *Gli1* expression levels). Furthermore, *Shh* heterozygosity in *Grem1*^{Δ/Δ}*Bmp4*^{Δ/+} limb buds disrupts specification of posterior digit identities (Fig. 3C). In such triple mutant limb buds, *Shh* expression is reduced to similar levels as in *Grem1*^{Δ/Δ} limb buds (Fig. 2F) and BMP signal transduction has increased significantly in comparison to *Grem1*^{Δ/Δ}*Bmp4*^{Δ/+} limb buds (by about 30-40% as assessed by *Msx2* expression; Fig. 3C). These results corroborate the proposal that BMP and SHH activities are opposing one another. In addition, these results show that intact e-m feedback signaling buffers heterozygosity for *Shh* (Fig. 3A), while its disruption renders digit patterning sensitive to gene dosage (Fig. 3B, C). It appears that GREM1-mediated interlinking of SHH with BMP and AER-FGF signaling endows the digit patterning system with robustness towards genetic variation.

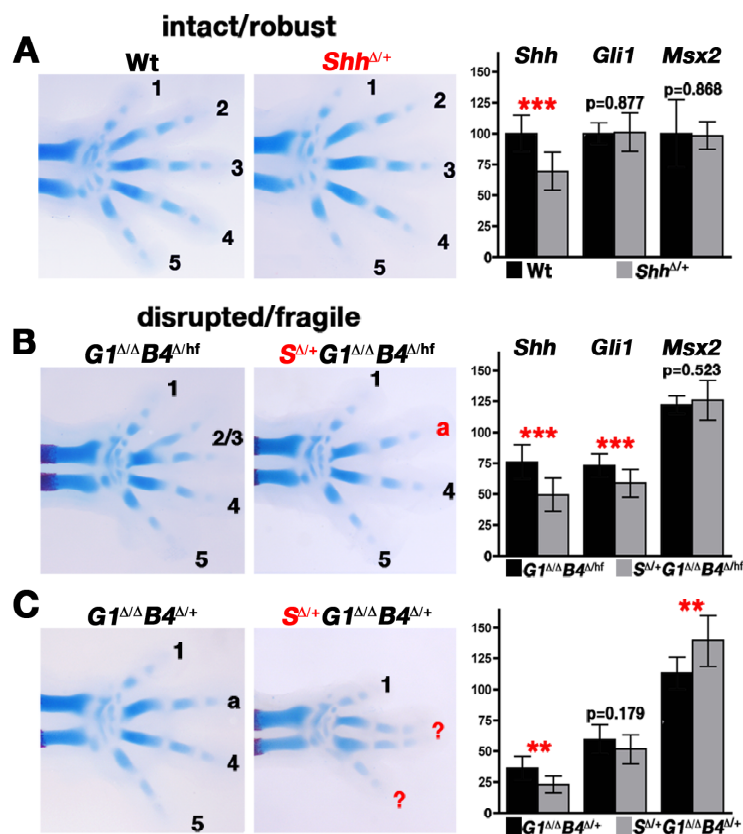


Fig. 3. The restoration of digit identities in *Grem1*^{ΔΔ} limb buds with reduced *Bmp4* levels is highly sensitive to changes in the *Shh* gene dosage.

(A) Digits are specified normally in *Shh*^{Δ/+} forelimbs. (B) Reduction of digit numbers and loss of anterior identities (digits 2, 3) in *Shh*^{Δ/+}*Grem1*^{ΔΔ}*Bmp4*^{Δ/hf} forelimbs (*S*^{Δ/+}*G1*^{ΔΔ}*B4*^{Δ/hf}). (C) Further loss of digit identities in *Shh*^{Δ/+}*Grem1*^{ΔΔ}*Bmp4*^{Δ/+} forelimbs (*S*^{Δ/+}*G1*^{ΔΔ}*B4*^{Δ/+}). All skeletal stains were carried out at E14.5 (for assignment of digit identities see Fig. 1 and Fig. S1). Left panels: forelimb skeletons; right-most panels: Q - PCR

of *Shh*, *Gli1* and *Msx2* transcript levels; bars represent the average of the independent measurements of 9 limb bud pairs at E10.5-10.75 (34-39 somites) with standard deviations. *G1*^{ΔΔ}*B4*^{Δ/hf}: *Grem1*^{ΔΔ}*Bmp4*^{Δ/hf}; *S*^{Δ/+}*G1*^{ΔΔ}*B4*^{Δ/hf}: *Shh*^{Δ/+}*Grem1*^{ΔΔ}*Bmp4*^{Δ/hf}; *G1*^{ΔΔ}*B4*^{Δ/+}: *Grem1*^{ΔΔ}*Bmp4*^{Δ/+}; *S*^{Δ/+}*G1*^{ΔΔ}*B4*^{Δ/+}: *Shh*^{Δ/+}*Grem1*^{ΔΔ}*Bmp4*^{Δ/+}. *Shh* transcription is reduced about 30% (panels A, B: p<0.001; panel C: p<0.01) in the different genetic make-ups. Digit specification, *Gli1* and *Msx2* transcription are not affected by heterozygosity for *Shh* when e-m feedback signaling is intact (panel A). In contrast, disruption of e-m feedback signaling (panels B, C) renders digit specification and sensors for SHH (*Gli1*) and BMP signal transduction (*Msx2*) sensitive to the *Shh* gene dosage (panel B: *Gli1* p<0.001; panel C: *Msx2* p<0.01).

Self-regulation of the BMP4/GREM1 interactions

To gain further insights into the molecular nature of this buffering mechanism, we assessed the potential effects of reducing the *Bmp4* gene dosage alone. No striking alterations of limb development are observed in *Bmp4*^{Δ/hf} embryos (Fig. 4A), while the anophthalmia phenotype is completely penetrant (Fig. S6; Kulesa and Hogan 2002). Molecular analysis reveals that genetic reduction of *Bmp4* (Fig. 4B) is paralleled by significantly lower *Grem1* expression in

the limb bud mesenchyme. In contrast, BMP signal transduction appears only slightly lowered and *Shh* expression is not affected (Fig. 4D and Fig. S6). These results establish that lowering of the *Bmp4* gene dosage is largely buffered by reducing *Grem1* expression in the limb bud mesenchyme. It has been previously shown that mesenchymal BMP signal transduction is required to up-regulate *Grem1* expression (Ovchinnikov et al. 2006) and that ectopic BMP signaling induces *Grem1* expression (Nissim et al. 2006), but the functional importance of this apparent cross-regulation remained unknown. The results shown in Fig. 3 (panels A to C) establish that regulation of *Grem1* expression by BMP4 buffers BMP signal transduction, which may contribute to robustness of the digit patterning system.

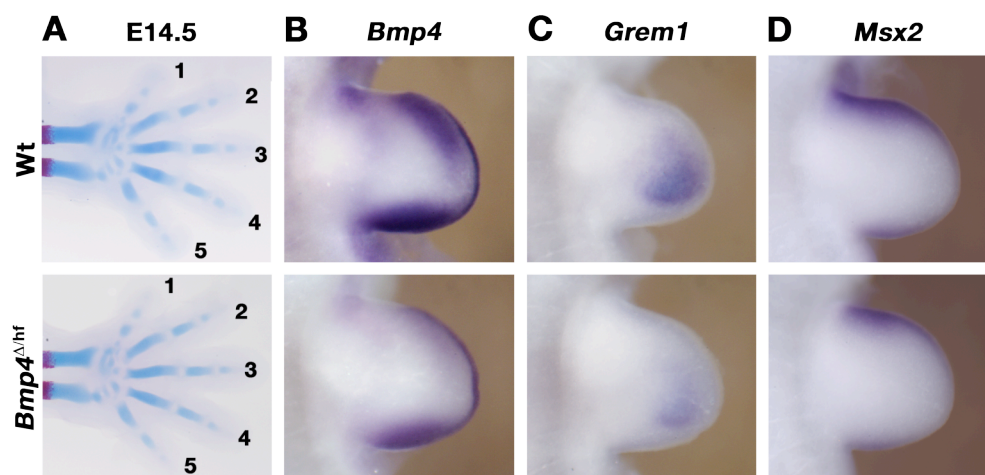


Fig. 4. Genetic reduction of BMP4 activity in *Bmp4*^{Δhf} embryos results in concurrent down-regulation of *Grem1* expression in limb buds.

(A) Forelimb skeletons; numbers indicate digit identities. Note that the identities of all five digits are maintained, however, a small post-axial condensation is frequently observed at later stages (see also Goldman et al. 2006). (B-D) Detection of *Bmp4*, *Grem1* and *Msx2* transcripts at E10.75 (37 somites). Note the global reduction of *Grem1* transcripts in *Bmp4*^{Δhf} limb buds (panel C), while the expression of *Msx2* is less affected (panel D).

To comparatively analyze the co-regulation of *Grem1* expression by BMP4 (Fig. 4) and SHH signaling (Zuniga et al. 1999; Panman et al. 2006; Nissim et al. 2006), carrier beads soaked with recombinant ligands were implanted into mouse limb buds and cultured up to 6 hours (Fig. 5). During this time period, mouse limb buds in culture develop with kinetics identical to embryonic limb buds *in utero* (Zuniga et al. 1999; Boot et al. 2008). Following implantation of a BMP4-soaked carrier bead into the mesenchyme, an initial transcriptional response is detected within one hour (Fig. 5A). Transcriptional up-regulation of *Grem1* is initiated within two hours (Fig. 5B) and in all cases significantly higher by 3 hours (Fig. 5C, D). Grafts into different positions within the anterior (Fig. 5B) and posterior limb bud show that *Grem1* expression is up-regulated within its normal domain in the distal mesenchyme (Fig. 5C, D). In contrast, SHH requires about 6 hours to up-regulate *Grem1* (Fig. 5E), and GREM1 in turn requires again around 6 hours to up-regulate AER-*Fgfs* (Fig. 5F). Taken together, the SHH/GREM1/FGF e-m feedback loop operates between the polarizing region, distal mesenchyme and AER with a loop time of about 12 hours, but our studies also reveal a fast and self-regulatory feedback with a loop time of around 2 hours that operates between BMP4 and GREM1 in the distal limb bud mesenchyme.

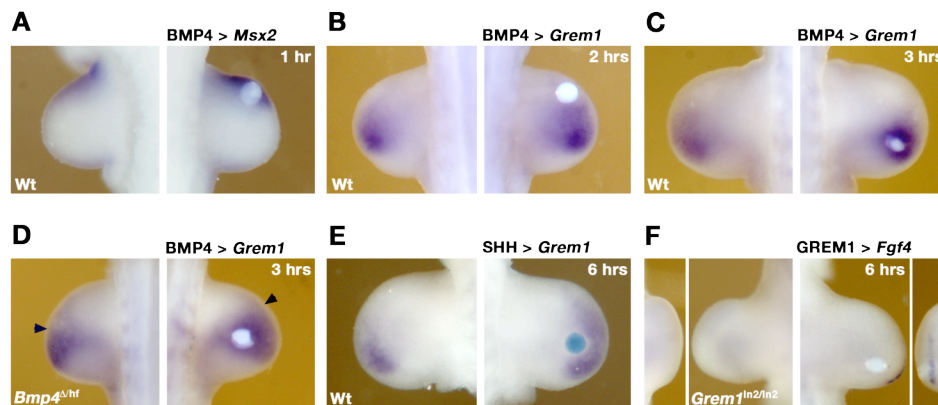


Fig. 5. Differential transcriptional regulation of *Grem1* by BMP4 and SHH signaling.

(A-F) Carrier beads soaked with recombinant BMP4, SHH or GREM1 recombinant proteins were grafted into the anterior or posterior mesenchyme of forelimb buds (E10.25-10.5; 33-35 somites) and cultured for 1 to 6 hours. Right panels show the expression of *Msx2*, *Grem1* or *Fgf4* in grafted limb buds after the culture time indicated. Left panels show the contra-lateral limb bud as an internal control. (A) BMP4-soaked beads induce transcriptional up-regulation of *Msx2* expression within 1 hour in wild-type limb buds. (B) BMP4 induces up-regulation of *Grem1* expression within 2 hours in wild-type limb buds. (C) Up-regulation of *Grem1* expression in response to a posterior BMP4 bead after 3 hours of culture. (D) BMP4-soaked beads normalize *Grem1* expression in *Bmp4*^{Δ/hf} limb buds. Note that BMP4 induces distal-anterior expansion of *Grem1* within its normal expression domain (arrowheads point to the anterior expression limits). (E) SHH-soaked beads require 6 hours to up-regulate *Grem1* expression in wild-type limb buds. (F) GREM1-soaked beads grafted into *Grem1* deficient limb buds induce *Fgf4* expression in the overlaying AER within 6 hours (dorsal and apical views are shown).

Interlinked feedback loops control specification of digit identities

To gain further insight into the properties of these interlinked signaling feedback loops (Fig. 6A), we simulated the dynamics of this apparent dual-time network using an ordinary differential equation model (Ben-Haim et al. 2006). The interactions of the BMP4/GREM1 module with the SHH/GREM1/FGF e-m feedback loop (Fig. 6A) were modeled in wild-type limb buds based on the expression patterns of the relevant mesenchymal signals and their experimentally determined induction kinetics (Fig. 5; Zuniga et al. 1999; Michos et al. 2004; Panman et al. 2006; Robert 2007). Firstly, our computational simulations indicate that high BMP4 (expressed prior to *Grem1* and *Shh*, Fig. S7) in contrast to SHH (data not shown) is

able to trigger up-regulation of *Grem1* expression via the fast BMP4/GREM1 module by about E9.0 (Fig. 6B). The increase in GREM1 lowers BMP4 activity rapidly, which in turn enables the rise of AER-FGF and SHH activities, i.e. establishment of the SHH/GREM1/FGF e-m feedback loop. This e-m feedback signaling loop in turn accelerates the rise in GREM1, SHH and AER-FGF activities, which plateau by about E10.0 in combination with low, but persistent BMP4 activity (Fig. 6B). Thus, this simulation nicely mimics the actually observed kinetics of the up-regulation of gene expression and signaling activities in mouse limb buds. Unexpectedly, these simulations predict a switch from BMP4-dependent initiation to predominant, SHH-dependent progression and stabilization of *Grem1* expression and morphogenetic signaling (Fig. 6B) encompassing the period critical for specification of digit identities (Zhu et al. 2008). This early requirement of BMP4 is even more apparent when the contributions of each feedback loop are simulated separately (Fig. 6C, D). A network lacking BMP4-mediated up-regulation of *Grem1* fails to initiate SHH/GREM1/FGF feedback signaling (Fig. 6C). In contrast, simulations without positive regulation of *Grem1* by SHH still result in a rise of SHH and AER-FGFs activities, while GREM1 remains lower and BMP4 higher than normal (Fig. 6D; compare to Fig. 6C). Last but not least, we tested the validity of our mathematical simulations with respect to the altered signaling activities in the different compound mutant limb buds analyzed as part of this study. In particular, simulation of *Grem1* deficient limb buds with genetically decreased *Bmp4* gene dosages mimic the observed *in vivo* restoration of SHH activity qualitatively well (Fig. 6E and Fig. S8 for complete simulations). These results identify the BMP antagonist GREM1 as a critical node (Kitano 2004) that links the fast BMP4/GREM1 initiator module to the slower but persistent SHH/GREM1/FGF e-m feedback loop (Fig. 6A) and unexpectedly, predict a requirement of mesenchymal BMP4 for initiation of e-m feedback signaling (Fig. 6B, C).

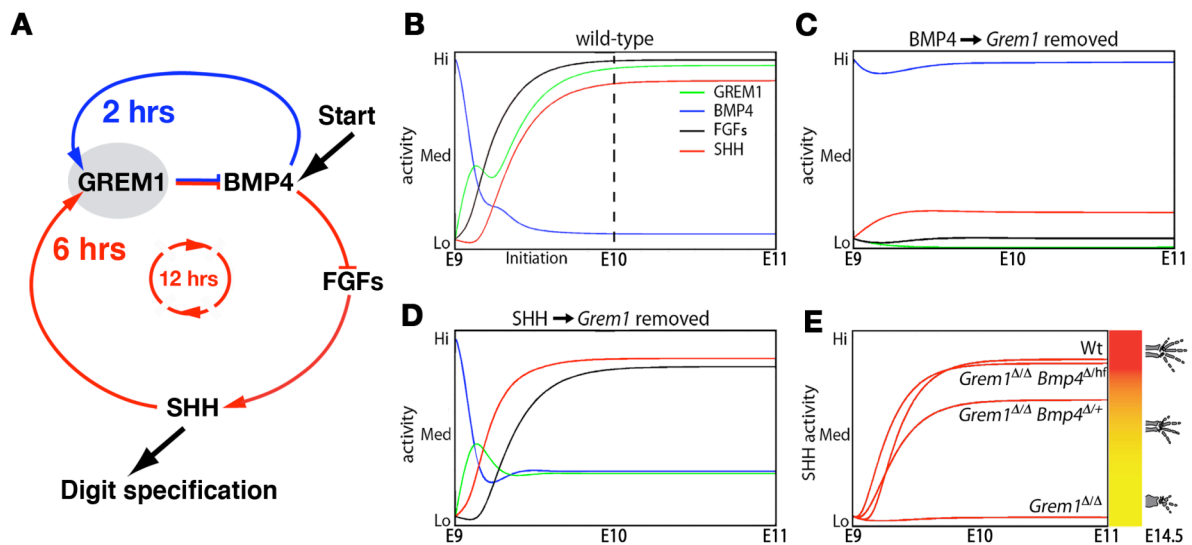


Fig. 6. Mathematical simulations of the dual-time feedback signaling interactions.

(A) The fast and auto-regulatory BMP4/GREM1 feedback module (2 hours loop time) is coupled to the slower SHH/GREM1/FGF e-m feedback loop (12 hours) via the GREM1 node, which is identified as the critical node (shaded grey). (B) Mathematical simulation describing the temporal kinetics of signaling activities in wild-type limb buds. BMP4, but not SHH, is initially able to up-regulate *Grem1* expression. This fast raise in GREM1 (green) lowers BMP4 activity (blue), which in turn enables the increase of FGF (black) in the AER and SHH (red) in the posterior mesenchyme. Such establishment of signaling interactions results in progressive up-regulation GREM by SHH as part of the SHH/GREM1/FGF e-m feedback loop. A stable state is reached around E10.0, which is characterized by high SHH/GREM1/FGF e-m feedback and low BMP4/GREM1 module activity. These simulations reveal an early requirement of BMP4 and subsequent switch to predominantly SHH controlled progression of limb bud development. (C) Simulation of specific disruption of the fast BMP4/GREM1 module by abolishing BMP4-mediated up-regulation of GREM1. Note that initiation of SHH/GREM1/FGF e-m feedback signaling is disrupted. (D) Disruption of the SHH/GREM1/FGF e-m feedback loop by specifically inactivating SHH-mediated up-regulation of GREM1 (but not its regulation by BMP4). Note that both AER-FGF and SHH activities are up-regulated as a consequence of the auto-regulatory reduction of BMP4 activity via BMP4/GREM1 module (panel B). This reduction relieves BMP4-mediated repression of AER-FGFs and results in up-regulation of SHH activity. (E) Simulation of SHH activity in different mutant genotypes. The SHH activity remains low in *Grem1* deficient limb buds, while the progressive genetic reduction of *Bmp4* in *Grem1^{Δ/Δ}* limb buds restores SHH activity similar to what is observed in compound mutant mouse limb buds.

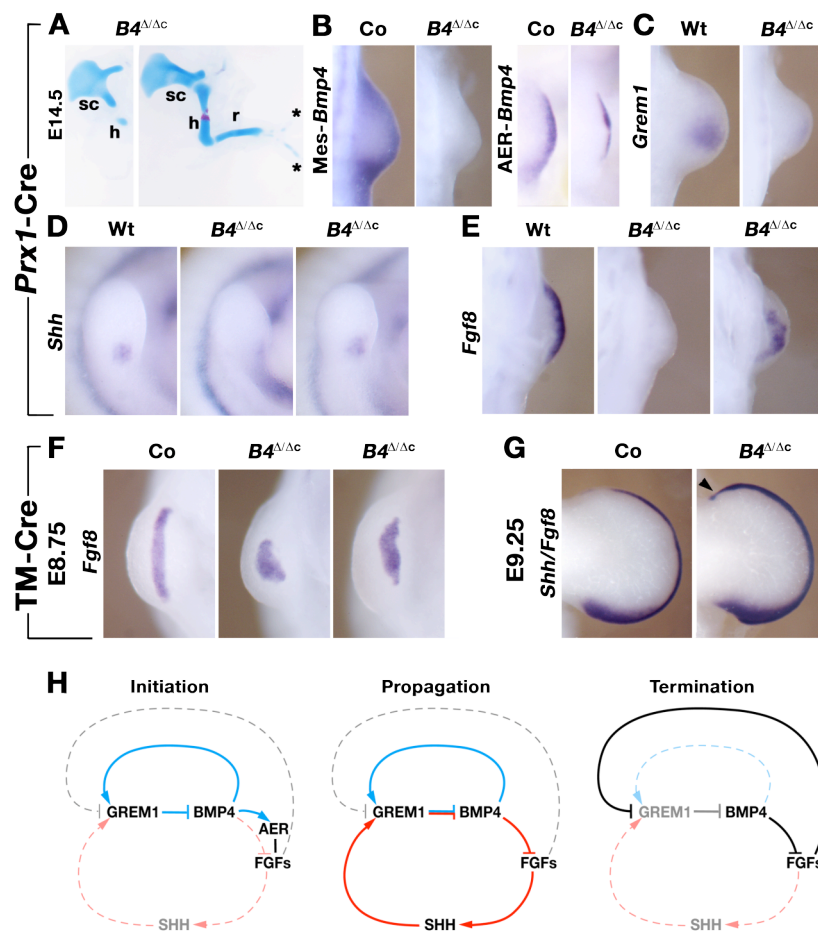


Fig. 7. BMP4 is required during initiation of limb bud development.

(A) Skeletal phenotypes of $Bmp4^{\Delta/\Delta c}$ forelimbs at E14.5 upon early inactivation of the conditional $Bmp4^{hf}$ allele using the $Prx1$ -Cre transgene. h: humerus; sc: scapula; r: radius, asterisks indicate rudimentary digital rays. (B) Detection of $Bmp4$ transcripts in control (Co: $Prx1$ -Cre^{tg/+} and $Bmp4^{\Delta/hf}$, respectively) and $Bmp4^{\Delta/\Delta c}$ forelimb buds (26 somites). Left panels show optimized detection of $Bmp4$ transcripts in the mesenchyme, right panels in the AER. As expected $Bmp4$ transcripts are lost from the mesenchyme of $Bmp4^{\Delta/\Delta c}$ limb

$Bmp4$ transcripts are lost from the mesenchyme of $Bmp4^{\Delta/\Delta c}$ limb buds (Mes- $Bmp4$), while expression remains in the AER (AER- $Bmp4$). (C to E) Detection of $Grem1$ (28 somites, dorsal view), Shh (27 somites, distal view), and $Fgf8$ (26 somites, ventral view) transcripts in wild-type (Wt) and $Bmp4^{\Delta/\Delta c}$ limb buds. (F) TM-Cre transgene mediated inactivation of $Bmp4$ by injecting pregnant mouse females with tamoxifen at about embryonic day E8.75, i.e. before initiation of forelimb bud development. Detection of $Fgf8$ transcripts in forelimb buds at E10.25 (32 somites). Control: TM-Cre heterozygous embryo. Experimental: forelimb bud of a $Bmp4^{\Delta/\Delta c}$ TM-Cre embryo. (G) Simultaneous detection of Shh and $Fgf8$ transcripts in forelimb buds at E11.75 (50 somites) following tamoxifen injection at E9.25, i.e. after initiation of forelimb bud outgrowth and AER formation. Control: $Bmp4^{\Delta c/+}$ TM-Cre forelimb bud, which is phenotypically wild-type. Experimental: $Bmp4^{\Delta/\Delta c}$ TM-Cre forelimb bud, note the anterior expansion of $Fgf8$ expression (arrowhead). (H) Schemes summarizing the predominant self-regulatory activities (solid lines) of the different interlinked feedback loops during limb bud development from initiation (high BMP4) to propagation of signaling and digit patterning (high SHH/ low BMP4) and termination of e-m feedback signaling (high FGF, ref. Verheyden and Sun 2008). Broken lines indicate low or inactive signaling interactions.

Mesenchymal BMP4 is required during the onset of limb bud development

To genetically test the prediction that BMP4 is required to establish e-m feedback signaling, we inactivated the remaining hypomorphic *Bmp4*^{hf} allele in *Bmp4*^{Δ/hf} mouse embryos from the onset of limb bud development in the mesenchyme using the *Prx1*-Cre transgene (Logan et al. 2002). Initially rather unexpected, most limb skeletons in *Bmp4*^{Δ/Δc} embryos are truncated distally to the scapula (Fig. 7A; n=8/14) or lack posterior skeletal elements (forming maximally one to three rudimentary anterior digits; Fig. 7A; n=6/14). In agreement with the expression patterns (Fig. S7) and simulation (Fig. 6B and 6C), *Bmp4* acts genetically upstream of both *Grem1* and *Shh* as its inactivation in *Grem1* and *Shh* deficient embryos reproduces the *Bmp4*^{Δ/Δc} forelimb phenotype (Fig. S7). Molecular analysis reveals that *Prx1*-Cre mediated recombination inactivates the floxed *Bmp4*^{hf} locus by E9.0 (22 somites, Fig. S6), which results in loss of mesenchymal *Bmp4* transcripts prior to E9.5 (26 somites, Fig. S9), and mesenchymal *Bmp4* transcript are lost prior to E9.5, while expression in the AER is maintained at early stages (Fig. 7B, left panel). This early loss of mesenchymal *Bmp4* expression disrupts both *Grem1* and *Shh* expression (Fig. 7C and 7D and Fig. S10). In addition, formation of the AER is disrupted (Fig. 7E and Fig S10) as revealed by the patchy (n=8/10) or absent *Fgf8* expression (n=2/10). These early molecular alterations are paralleled by massive apoptosis of mesenchymal progenitors (Fig. S9), which truncates the mutant limb buds (Fig S10). In agreement with the predictions of our mathematical simulations (Fig. 6), these results indicate that signaling by both AER and ZPA is disrupted, which results in early mesenchymal cell death and developmental arrest. The temporal requirement of BMP4 activity was further analyzed using an ubiquitously expressed tamoxifen-inducible Cre recombinase transgene to inactivate *Bmp4* from specific time points onwards (Hayashi and McMahon 2002). Inactivation from about E8.75 in both limb bud compartments (Fig. S9)

disrupts AER formation (Fig. 7F) similar to the activity of the *Prx1*-Cre transgene in the mesenchyme (Fig. 7E). In sharp contrast, tamoxifen-dependent inactivation from about E9.25 (Fig. S9) no longer affects AER formation, up-regulation of AER-FGF and SHH signaling and distal progression of limb bud development (Fig. 7G). The persistent low activity of the BMP4/GREM1 module (Fig. 6B) seems however relevant as inactivation of *Bmp4* causes anterior expansion of *Fgf8* (arrowhead, Fig. 7G), which is a known cause of polydactyly (Selever et al. 2004). In summary, this genetic analysis (Fig. 7) in agreement with the simulations (Fig. 6), indicates that BMP4 signaling from the mesenchyme to the ectoderm is required for formation of a functional AER. The mesenchymal BMP4 signal is likely transduced in the AER by BMP receptor 1A (BMPR1A) as its AER-specific inactivation results in similar, early disruption of limb bud development (Ahn et al. 2001). This early requirement of BMP4 (Fig. 4, F and G) may have been missed by the previous genetic studies (Selever et al. 2004; Bandyopadhyay et al. 2006) as *Bmp4* was probably not inactivated sufficiently early. In the limb bud mesenchyme, the BMP4 signal is most likely also transduced by BMPR1A to up-regulate *Grem1* expression (Ovchinnikov et al. 2006).

Prx1-Cre mediated inactivation of Bmp4 in the forelimb bud mesenchyme using different genetic make-ups

Our study reveals an early but transient requirement of BMP4 in the limb bud mesenchyme for AER formation and *Fgf8* expression. However, the limb phenotypes shown in Fig. 7A to 7F were not observed in two previous genetic studies of *Bmp4* functions in limb buds (Selever et al. 2004; Bandyopadhyay et al. 2006). In contrast to our genetic make-up requiring deletion of only one hypomorphic *Bmp4*^{hf} allele with significantly reduced activity (Fig. S1), the inactivation of *Bmp4* in these two studies was done either by *Prx1*-Cre-

mediated simultaneous deletion of one or two copies of another non-hypomorphic conditional *Bmp4* allele. It is possible BMP4 activity was only completely inactivated after its early and transient requirement. In support of this notion, no AER disruptions are observed when *Bmp4* is inactivated from E9.25 onwards (Fig. 7G). Several reasons may underlie such a delay in gene inactivation. For example, the genetic background may alter the activity of the *Prx1*-Cre transgene. In the BL6/J genetic background used for this study, the *Prx1*-Cre transgene is active very early in the forelimb field (data not shown; see ref. Hasson et al. 2007), while others have reported less efficient recombination (Lewis et al. 2001). For example, introduction of CD1 genome in our genetic background affect the efficiency of recombination (Fig. 8A). Inactivation of two floxed genes may also take longer as evidenced by *Prx1*-Cre mediated concurrent inactivation of two *Bmp4*^{hf} alleles (Fig. 8B). Such a genetic make-up allows for largely normal distal limb and autopod development (4-5 digits are formed in 50% of all forelimbs; n=8/16), similar to the results previously published by Bandyopadhyay et al. (2006). Finally, we have inactivated *Bmp4* in the limb bud mesenchyme by *Prx1*-Cre mediated deletion of one copy of the non-hypomorphic *Bmp4* allele (*Bmp4*^{f-Jfm}; ref. Selever et al. 2004) in the context of heterozygosity for the *Bmp4* null allele (mutant genotype: *Bmp4*^{Δ/f-Jfm}*Prx1*-Cre^{tg/+}=*Bmp4*^{Δ/Δc-Jfm}; Fig. 8C and 8D). Analysis of AER-*Fgf8* expression reveals the irregular AER morphology in *Bmp4*^{Δ/Δc-Jfm} forelimb buds in combination with ectopic cell death in the proximal limb bud mesenchyme (Fig. 8C; n=3/3). These phenotypes are reminiscent, but less striking than the ones of *Bmp4*^{Δ/Δc} forelimbs (Fig. 7 and Fig. S10). It is important to note that the *Bmp4* gene dosage in *Bmp4*^{Δ/Δc} embryos is reduced globally to significantly less than 50% already prior to activation of the *Prx1*-Cre transgene due to the hypomorphic nature of the *Bmp4*^{hf}

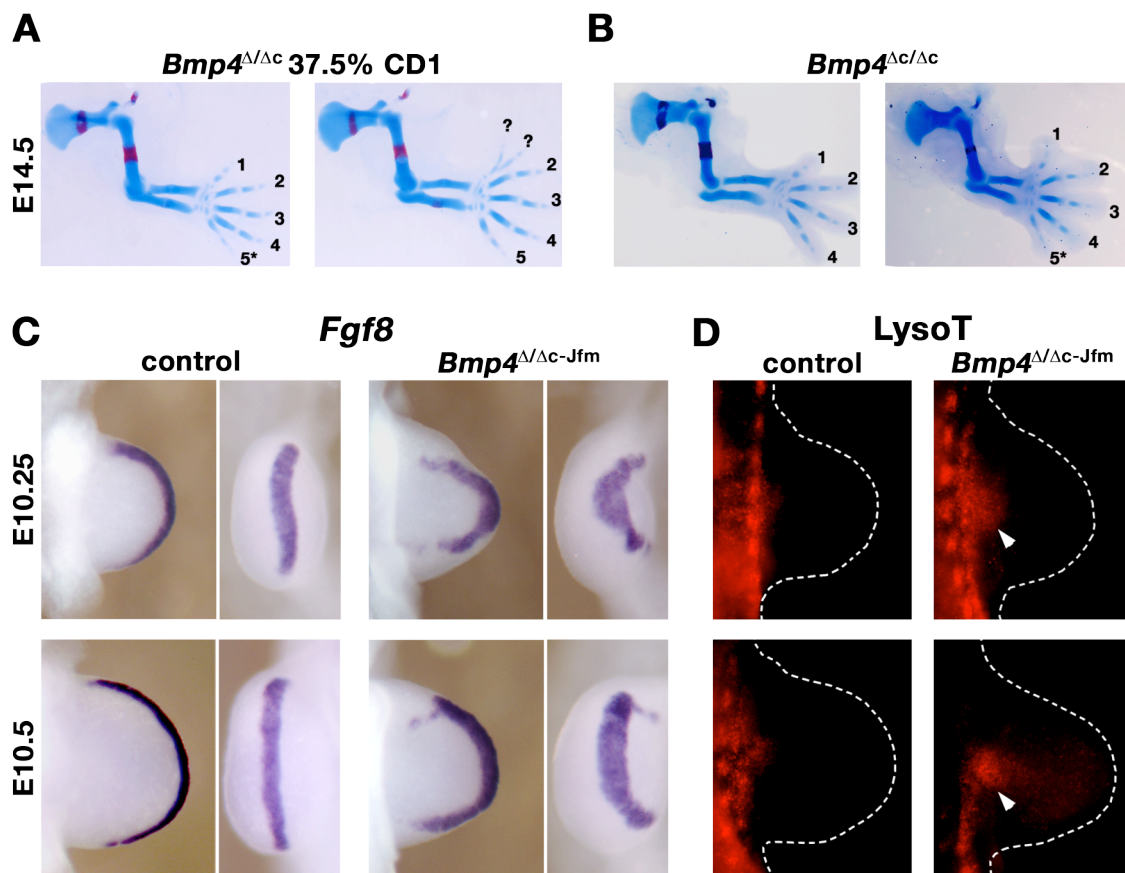


Fig. 8 Influence of genetic make up on the strength of the mesenchymal *Bmp4* null phenotype induced by the *Prx1*-Cre transgene.

(A) Introduction of CD1 genetic background weakens the mesenchymal *Bmp4*^{Δ/Δc} phenotype. While 13 out of 18 mutant limbs in a genetic background containing an average of 37.5% of the CD1 genome reproduce the skeletal phenotype described in Fig. 7, 5 limbs out of 13 appear rather normal or even develop polydactyly. These additional digits are likely the consequence of a late removal of BMP4 activity (see Fig 7G). (B) The number of conditional alleles to delete also influences the strength of the phenotype. A fraction of *Bmp4*^{Δc/Δc} mutant limb buds generate almost normal limb skeletons with 4 or 5 digits (n=8/16). Numbers indicate digit identities; asterisks indicate hypoplastic digits while question marks indicate digits with unclear identities in the polydactylous *Bmp4*^{Δ/Δc} mutant. (C, D) AER defects and apoptosis in forelimb buds lacking mesenchymal *Bmp4* as a consequence of *Prx1*-Cre mediated inactivation of the non-hypomorphic *Bmp4*^{f-Jfm} allele (*Bmp4*^{Δ/Δc-Jfm}). (C) *Fgf8* marks the AER in control (right panel) and *Bmp4*^{Δ/Δc-Jfm} forelimb buds (left panels) at E10.25 (33 somites, upper panels) and E10.5 (35 somites, lower panels). Ventral and apical views are shown. Note the aberrant AER morphology in both mutant forelimb buds. (D) Apoptosis patterns in contra-lateral limb buds. Note the premature and increased cell death in the proximal limb bud mesenchyme of *Bmp4*^{Δ/Δc-Jfm} forelimbs (white arrowheads, right panels) in comparison to age-matched controls (left panels).

allele (Fig. S1). Therefore, BMP4 activity is likely cleared faster from the limb bud mesenchyme upon inactivation of the *Bmp4*^{hf} than the *Bmp4*^{f-Jfm} allele. This difference provides a straightforward explanation for the phenotypic strength of both alleles upon their inactivation in agreement with the early, transient requirement of BMP activity (Fig. 7F). As *Bmp4* expression is also lost specifically from the mesenchyme of *Bmp4*^{Δ/Δc-Jfm} forelimb buds (data not shown), the results shown in Fig. 8 corroborate the early requirement of mesenchymal BMP4 for induction of a normal AER.

Supplementary figures

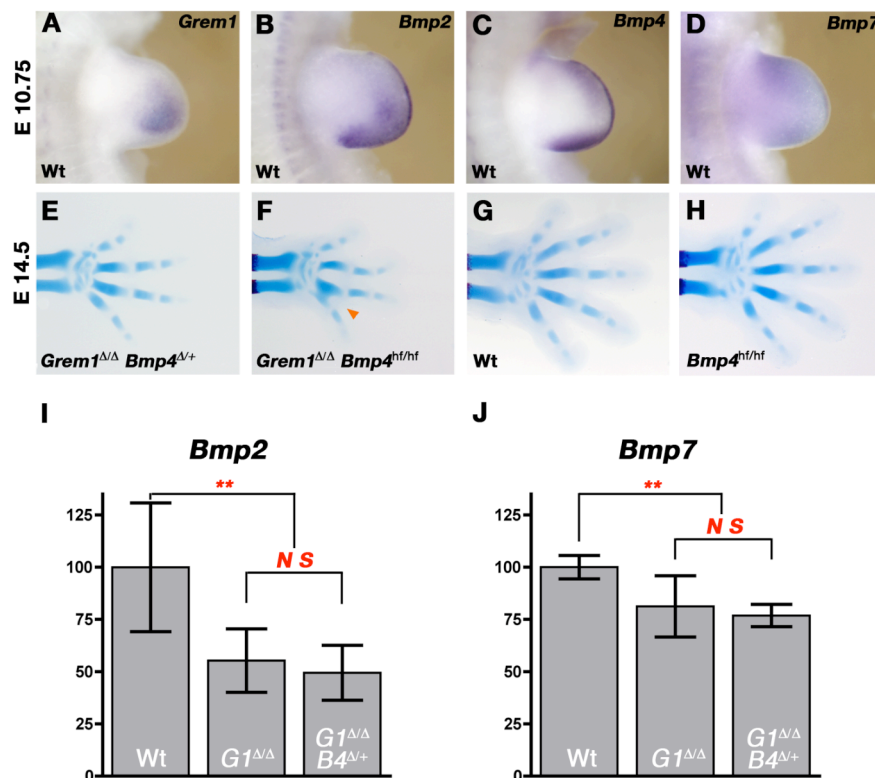


Fig. S1. Expression of *Grem1* and *Bmp* ligands and genetic assessment of the hypomorphic nature of the *Bmp4*^{hf} allele during mouse limb bud development.

(A to D) Distribution of *Grem1* (panel A), *Bmp2* (panel B), *Bmp4* (panel C) and *Bmp7* (panel D) transcripts in forelimb buds at E10.75 (37 somites). *Bmp4* is strongly expressed in the posterior limb bud mesenchyme and graded in the anterior-distal mesenchyme. *Grem1* expression is activated in the posterior-distal mesenchyme and expands anterior as limb bud development progresses. Within this domain, *Grem1* is restricted to the dorsal and ventral sub-ectodermal mesenchyme. (E, F) The partial restoration of distal forelimb and autopod development in *Grem1* deficient embryos carrying two copies of the *Bmp4*^{hf} allele (*Grem1*^{ΔΔ}*Bmp4*^{hf/hf}) is slightly less efficient than embryos carrying a *Bmp4* null allele (*Grem1*^{ΔΔ}*Bmp4*^{Δ/+}). The orange arrowhead points to the proximal fusion of the posterior digits 4 and 5 in *Grem1*^{ΔΔ}*Bmp4*^{hf/hf} forelimbs. This result shows that the hypomorphic nature of *Bmp4*^{hf} allele significantly reduces its activity. (G, H) The *Bmp4*^{hf} allele has no (semi-) dominant effects during limb bud development as the limbs of embryos homozygous for the *Bmp4*^{hf} allele are wild-type. This analysis reveals the hypomorphic nature of the *Bmp4*^{hf} allele with respect to limb bud development. (I, J) Genetic reduction of the *Bmp4* gene dosage in *Grem1* deficient embryos does not alter *Bmp2* and *Bmp7* expression levels as quantified by real time PCR in limb bud extracts (n= 8 limb bud pairs at E10.75, 36-39 somites). Wt: wild-type; *G1*^{ΔΔ}: *Grem1*^{ΔΔ}, *G1*^{ΔΔ} *B4*^{Δ/+}: *Grem1*^{ΔΔ}*Bmp4*^{Δ/+}; **: p-values ≤ 0.01; NS: not significantly altered. Note that *Bmp2* and *Bmp7* expression (for *Bmp4* see Fig. S2 and S5) are reduced in *Grem1*^{ΔΔ} limb buds.

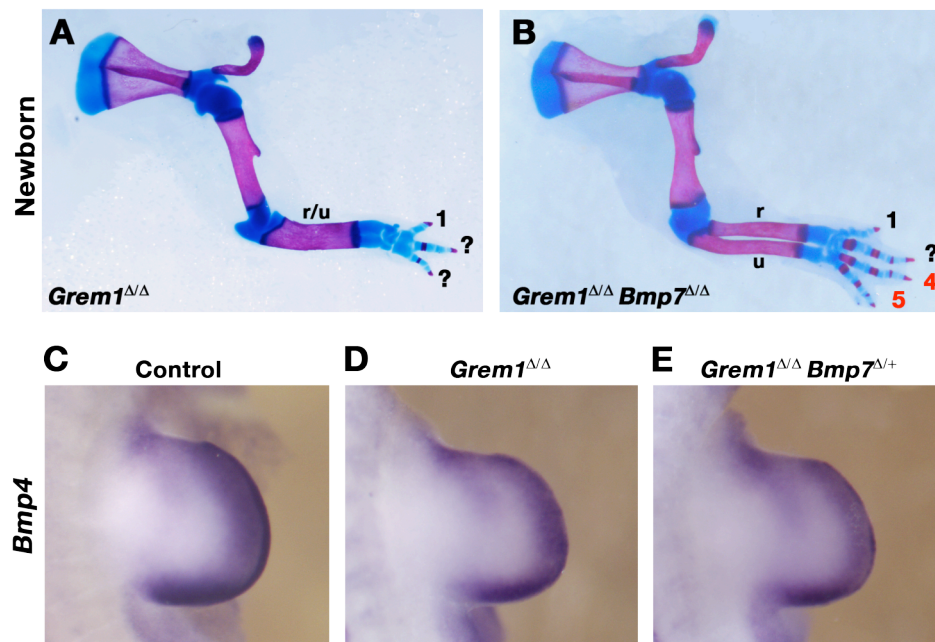


Fig. S2. Posterior, but not anterior digit identities are restored in forelimbs lacking both *Grem1* and *Bmp7*.

(A, B) Skeletal preparations of *Grem1*^{ΔΔ} and *Grem1*^{ΔΔ}*Bmp7*^{ΔΔ} forelimbs at birth (P0). Autopods of *Grem1*^{ΔΔ}*Bmp7*^{ΔΔ} forelimbs bear four digits and the restored identities of posterior digits are indicated in red. This restoration is comparable to one observed in *Grem1*^{ΔΔ}*Bmp4*^{Δ+} forelimbs (Fig. 1F). (C to E) Comparative analysis of *Bmp4* expression in control (*Grem1*^{Δ+}), *Grem1*^{ΔΔ} and *Grem1*^{ΔΔ}*Bmp7*^{ΔΔ} forelimb buds at E10.75 (37 somites). Note that the spatial distribution and levels of *Bmp4* transcripts are the same in *Grem1*^{ΔΔ} and *Grem1*^{ΔΔ} *Bmp7*^{Δ+} limb buds. This result shows that inactivation of *Bmp7* in *Grem1* deficient limb buds does not further alter *Bmp4* expression.

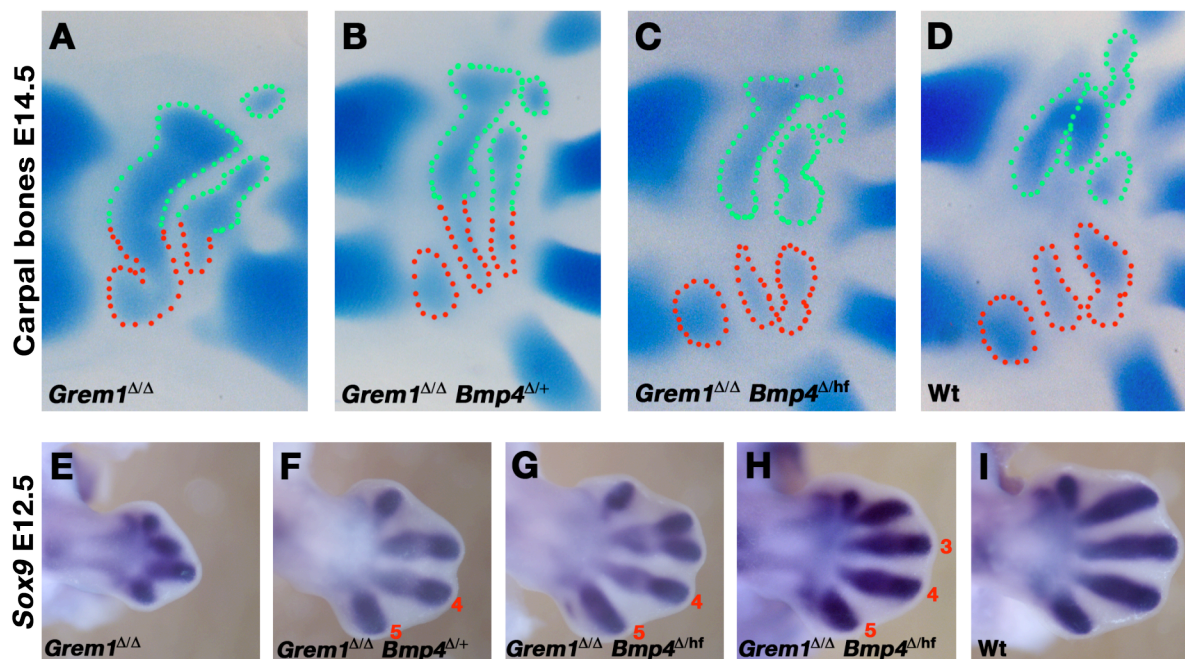


Fig. S3. Additional criteria used to determine digit identities in the different mutant contexts.

(A to D) Carpal bone morphology at E14.5 in forelimbs of the most relevant genotypes: *Grem1*^{Δ/Δ}; *Grem1*^{Δ/Δ}*Bmp4*^{Δ/+}; *Grem1*^{Δ/Δ}*Bmp4*^{Δ/hf} and wild-type (Wt). Red dots outline posterior and green dots anterior carpal elements. Note the extensive fusion and reduction of carpal bones in *Grem1*^{Δ/Δ} forelimbs (panel A), while progressive genetic reduction of the *Bmp4* restores carpal bone morphology (panels B to D). (E to F) Detection of *Sox9* transcripts in condensing cartilage elements of forelimb buds at E12.5. At this developmental stage digit identities are determined and the *Sox9* expression in digits prefigures the loss and restoration of the digit skeleton in *Grem1* deficient and compound mutant limb buds, respectively (compare to Fig. 1). In panels G to H, only the digit primordia with clearly restored morphological features are indicated (in comparison to wild-type and *Grem1*^{Δ/Δ} limb buds, panels E, I). Note that the overall size of the developing autopod and in particular the anterior digit primordia remain smaller in *Grem1*^{Δ/Δ}*Bmp4*^{Δ/hf} embryos (panel H) in comparison to age-matched wild-types (panel I). All panels are oriented with anterior to the top and posterior to the bottom.

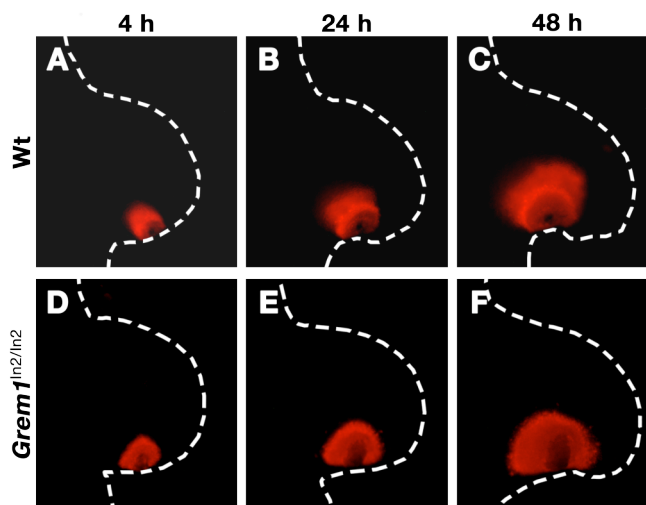


Fig. S4. Posterior mesenchymal cells expand normally in *Grem1* deficient limb buds.

Posterior mesenchymal cells in forelimb buds (E10.5; 34 somites) were labeled by DiI within the posterior most mesenchyme encompassing the ZPA region and cultured for up to 48 hrs ($n \geq 3$ for each genotype and stage). (A to C) Time course of a representative wild-type limb bud reveals the progressive expansion of posterior mesenchymal cells, which encompass a fraction of the *Shh* descendants. (D to F) The expansion of posterior mesenchymal cells in a *Grem1* deficient limb bud is indistinguishable from its wild-type counterpart (panels A to C). The *Grem1*^{ln2/ln2} allele was used for these studies, which corresponds to a limb bud specific *Grem1* loss-of-function mutation that is homozygous viable.

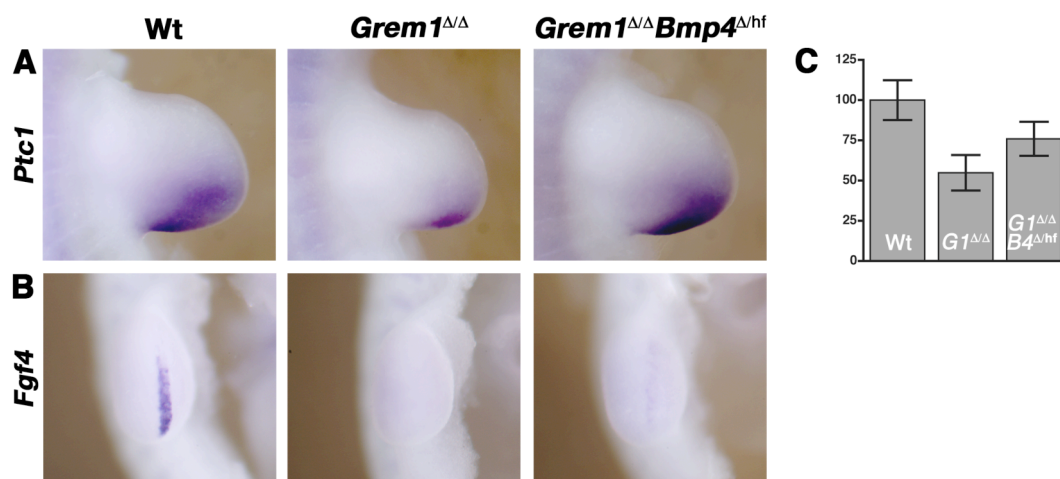


Fig. S5. Comparative and quantitative analysis of *Ptc1* and *Fgf4*.

(A, B) Detection of *Ptc1* (37 somites; dorsal view) and *Fgf4* (35 somites; apical view) transcripts by in situ hybridization in wild-type, *Grem1*^{ΔΔ} and *Grem1*^{ΔΔ}*Bmp4*^{Δhf} forelimb buds at E10.75. (C) Quantitative real time PCR was used to determine the relative expression levels of *Ptc1* in limb bud extracts ($n = 9$ at E10.75, 36-39 somites). Wt: wild-type: *G1*^{ΔΔ}: *Grem1*^{ΔΔ}, *G1*^{ΔΔ}*B4*^{Δhf}: *Grem1*^{ΔΔ}*Bmp4*^{Δhf}. Differences in expression levels between all the genotypes have P values ≤ 0.001 . Note the significant restoration of *Ptc1* and activation of *Fgf4* expression in *Grem1*^{ΔΔ}*Bmp4*^{Δhf} limb buds.

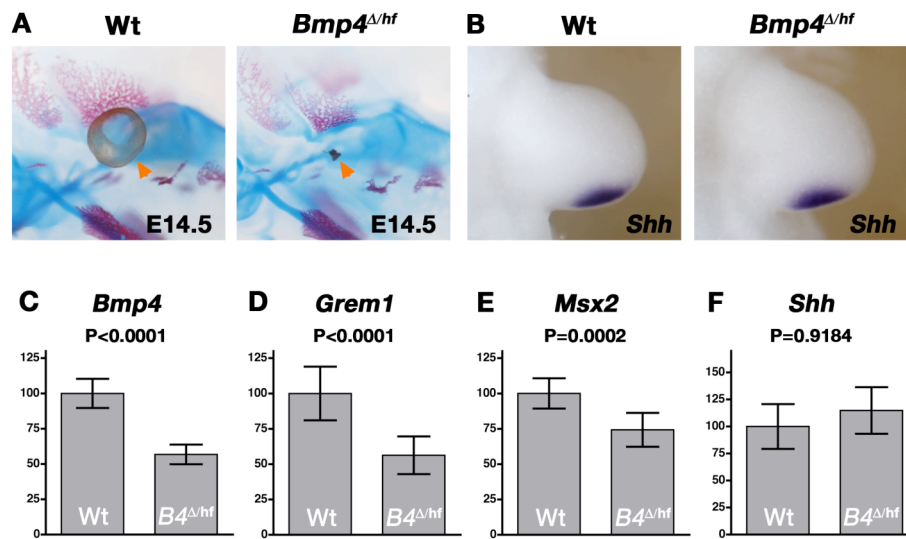


Fig. S6. Analysis of *Bmp4*^{Δ/hf} embryonic eyes and forelimb buds.

(A) Anophthalmia (eyeless) phenotype in *Bmp4*^{Δ/hf} embryos (arrowheads; E14.5). (B) *Shh* expression in wild-type and *Bmp4*^{Δ/hf} forelimb buds at E10.75 (37 somites). (C-F) Quantitative real time PCR was used to determine the relative expression levels of *Bmp4*, *Grem1*, *Msx2* and *Shh* in limb bud extracts (n= 9 at E10.75, 36-39 somites). Wt: wild type, *B4*^{Δ/hf}: *Bmp4*^{Δ/hf}. P-values are indicated.

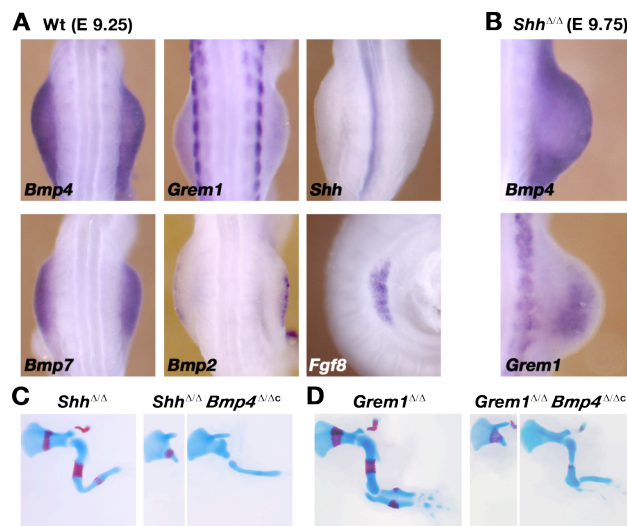


Fig S7. Expression and genetic hierarchies of *Bmp4*, *Grem1* and *Shh* during initiation of limb bud development.

(A) Activation of *Bmp4* expression precedes the one of *Grem1*, *Shh* and *Bmp2* in the forelimb bud mesenchyme (E9.25, 23 somites). In addition, *Bmp7* is expressed by the limb bud mesenchyme, while *Bmp2* and *Fgf8* expression are detected in the forming AER. (B) The activation of *Bmp4* and *Grem1* expression does not depend on SHH signaling as they remain expressed in *Shh* deficient limb buds at early stages (E9.75, 28 somites). (C, D) *Bmp4* acts genetically upstream of *Shh* and *Grem1* as the forelimb skeletal phenotypes of *Shh*^{Δ/Δ} *Bmp4*^{Δ/Δc} and *Grem1*^{Δ/Δ} *Bmp4*^{Δ/Δc} embryos are largely identical to the ones of *Bmp4*^{Δ/Δc} embryos (see Fig. 7). Taken together, these results corroborate the proposal that BMP4 initiates the interlinked feedback signaling interactions (Fig. 6) and is required upstream of SHH and GREM1 during AER formation (Fig. 7).

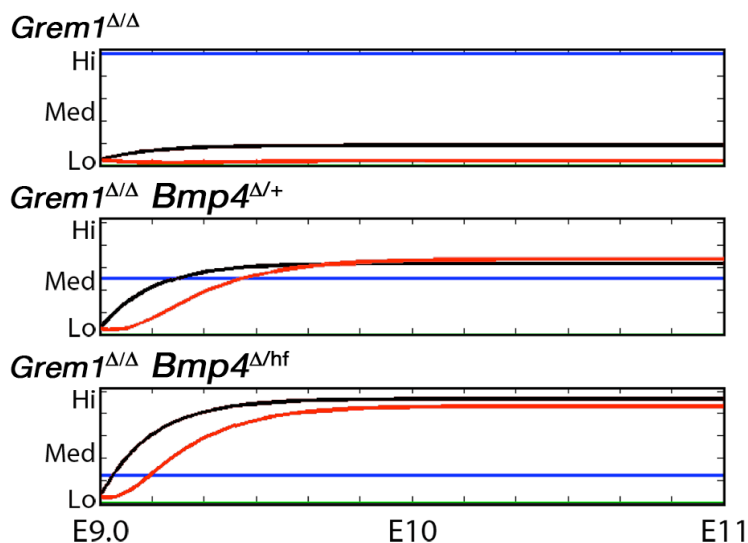


Fig. S8. Mathematical simulations of the different signaling activities in *Grem1* deficient limb buds upon genetic lowering of the *Bmp4* gene dosage. Reduction of the *Bmp4* gene dosage progressively restores SHH and FGF activities as is observed in vivo. Blue: BMP4, red: SHH, black: AER-FGFs.

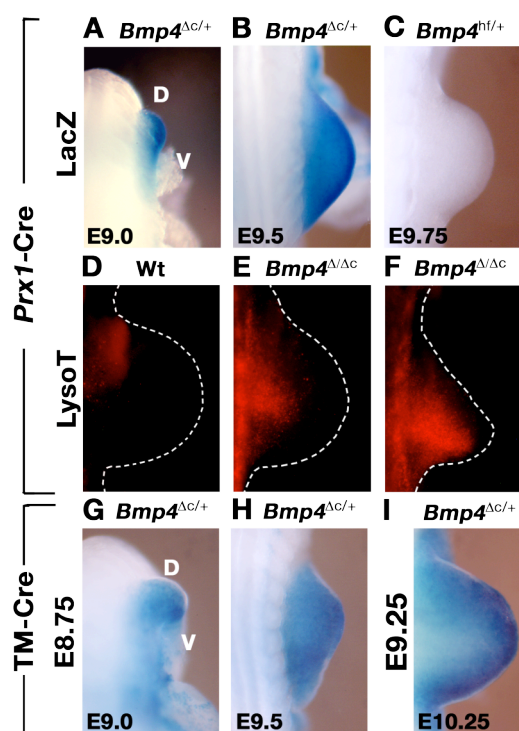


Fig. S9. Cre recombinase mediated inactivation of *Bmp4* is monitored by activation of the LacZ cassette.

(A, B) *Prx1*-Cre mediated inactivation of the *Bmp4* gene in the limb bud mesenchyme between E9.0 (22 somites) and E9.5 (26 somites). LacZ activity directly monitors *Bmp4* transcription as it is expressed as part of a fusion transcript with the recombined *Bmp4* gene. Therefore, the *Bmp4* locus is recombined throughout the limb bud mesenchyme by E9.0 (panel A). (C) *Bmp4*^{hf/+} limb bud as a negative control (E9.75; 28 somites). (D to F) Detection of apoptotic cells in limb buds at E10.0 (33 somites) by LysoTracker Red in wild-type and *Bmp4*^{Δ/Δc} limb buds. Note the massive apoptosis in the core mesenchyme (panels E, F) and abnormal morphology (panel F) of forelimb buds lacking mesenchymal *Bmp4*. (G, H) LacZ staining to monitor tamoxifen (TM)-Cre mediated inactivation of *Bmp4* in the entire embryo. Embryos were harvested 15-20h

after one tamoxifen injection into pregnant mothers at about E8.75. Recombination appears complete prior to E9.0 (22 somites, panel G). (I) TM injection at around E9.25 results in complete recombination prior to E10.25 (33 somites, panel I). D: dorsal; V: ventral.

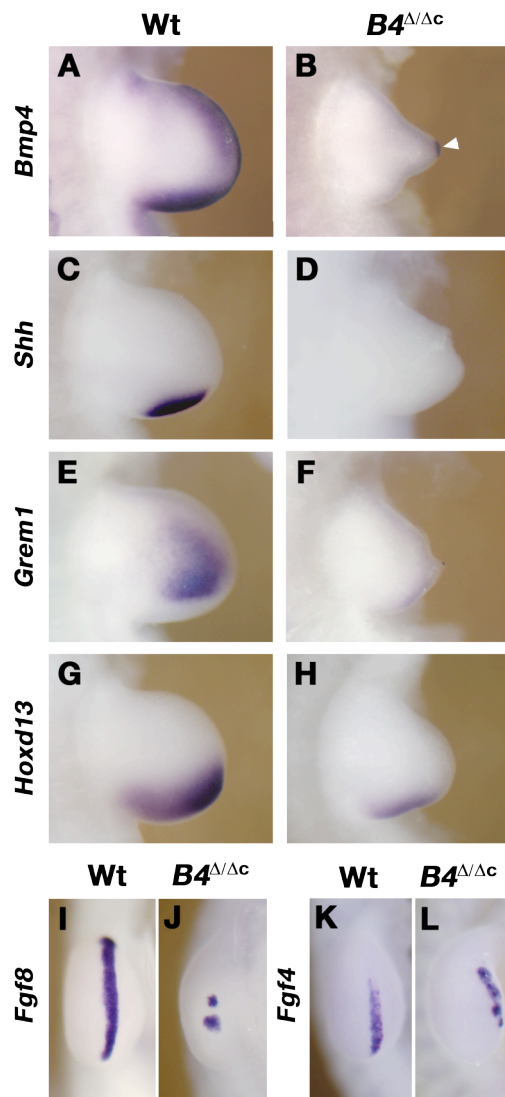


Fig. S10. Loss of key regulator genes from the mesenchyme of $Bmp4^{\Delta/\Delta c}$ forelimb buds by E10.75 (35-38 somites).

Bmp4 was inactivated specifically in the limb bud mesenchyme using the *Prx1*-Cre transgene. (A to L) Detection of *Bmp4* (A, B), *Shh* (C, D), *Grem1* (E, F), *Hoxd13* (G, H), *Fgf8* (I, J) and *Fgf4* (K, L) transcripts by in situ hybridization in wild-type and $Bmp4^{\Delta/\Delta c}$ forelimb buds. The residual AER continues to express *Bmp4* (panel B, arrowhead) *Fgf8* (panel J) and *Fgf4* (panel L).

Discussion

In this study, we use genetics and embryonic tissue culture in combination with mathematical simulations to show that BMP4 is transiently required during early mouse limb bud development, but its activity is tightly regulated by GREM1 antagonism to allow normal progression of limb development and patterning. We discover that during the onset of limb bud development, mesenchymal BMP4 activity is required for AER formation and survival of mesenchymal progenitors at early stages. In particular, BMP4 directly up-regulates the expression of its own antagonist *Grem1*, which results in fast and auto-regulatory lowering of BMP4 activity in the mesenchyme. This down-regulation of BMP4 activity is a pre-requisite for establishment of the dynamic e-m feedback signaling interactions that maintain AER-FGF and SHH signaling. Our studies identify the BMP antagonist GREM1 as the node (Kitano 2004), linking the fast BMP4/GREM1 initiator module to the slower but persistent SHH/GREM1/FGF e-m feedback to enable distal progression of limb bud morphogenesis. Furthermore, our genetic analysis and simulations reveal that tight regulation of BMP4 activity by GREM1 is critical. Early genetic inactivation of *Bmp4* disrupts AER formation and cell survival, while persistently high levels interfere with propagation of e-m feedback signaling and cell survival in *Grem1* deficient limb buds. In agreement with our mathematical simulations, TM-mediated inactivation of *Bmp4* from E9.25 onwards no longer affects progression of limb bud development. However, our molecular analysis and simulations show that low levels of BMP4 activity persist in the limb bud mesenchyme, which may be relevant with respect to fine-tuning autopod development. Indeed, increased AER-*Fgf* expression levels (this study) and mild and variable digit polydactylies are observed upon genetic inactivation of *Bmp4* during progression rather than initiation of limb bud development (Selever et al. 2004).

Taken together, our analysis provides good evidence that linking the fast and self-regulatory BMP4/GREM1 initiator module to the slower SHH/GREM1/FGF e-m feedback loop constitutes a crucial component of the limb pattern system that controls fail-safe specification of digit identities by coordinately controlling the opposing SHH and BMP4 activities. Therefore, the differential transcriptional regulation of *Grem1* expression by BMP4 and SHH is key to understanding the dynamic changes in signaling activities. In particular, BMP4 rapidly up-regulates the expression of its own antagonist *Grem1*, while the regulation of *Grem1* by SHH is slower and not direct (this study and Nissim et al. 2006), which according to our simulations promotes the switch from BMP4- to SHH-dependent morphogenetic signaling. The restricted transcriptional up-regulation of *Grem1* in the limb bud mesenchyme (this study and Panman et al. 2006) is likely to reflect the refractoriness of *Shh* descendants and cells exposed to high BMP levels (Scherz et al. 2004; Nissim et al. 2006). This differential regulation results in progressive expansion of the *Grem1* expression domain within the distal limb bud mesenchyme, which is a defining feature of enabling proper establishment of the pentadactylous digit territory (Zuniga et al. 1999; Panman et al. 2006). In particular, our mathematical simulations indicate that persistent up-regulation of *Grem1* by SHH continues to reduce BMP4 activity in the distal mesenchyme, thereby reinforcing e-m feedback signaling and enabling SHH-mediated specification of digit identities. Indeed, our genetic analysis reveals that high BMP4 activity opposes SHH-mediated specification of digit identities. The rapid self-regulatory lowering of BMP4 activity is possibly key as digit identities are being specified early and the autopod primordia is expanded subsequently under the influence of continued SHH signaling (Towers et al. 2008; Zhu et al. 2008). Furthermore, an experimental increase of SHH activity within its

normal domain is compensated by self-regulatory reduction of *Shh* levels and apoptosis of *Shh* expressing cells (Sanz-Ezquerro and Tickle 2000).

Another fascinating aspect of the SHH/GREM1/FGF e-m feedback loop concerns its self-terminating properties due to the fact that the expanding population of *Shh* descendants is refractory to *Grem1* expression and thereby increasingly separates *Shh* from *Grem1* expressing cells resulting in termination of morphogenetic signaling and autopod development (Scherz et al. 2004; Nissim et al. 2006). Verheyden and Sun (2008) recently showed that this refractoriness and the general down-regulation of *Grem1* expression during the terminal phase of limb bud outgrowth is caused by high FGF activity resulting from the activity of the SHH/GREM1/FGF feedback loop, which represses *Grem1* expression as part of an inhibitory FGF/GREM1 e-m feedback loop (Fig. 7H; Verheyden and Sun 2008). Mathematical simulation of all three phases of this limb signaling system (Fig. 9) reveals that distal limb bud development and digit specification progresses from BMP4-dependent initiation to predominantly SHH-dependent digit specification and growth and finally to FGF-induced termination in a largely self-regulatory manner and mainly as a consequence of the differential impact of these three signaling pathways on *Grem1* transcription (Fig. 7H). Interestingly, termination of morphogenetic signaling by the FGF/GREM1 feedback loop leads to an increase of BMP activity according to our simulations. This coincides with the requirement of BMP activity for fixing digits identities (Dahn and Fallon 2000; Suzuki et al. 2008) and initiating skeletal differentiation.

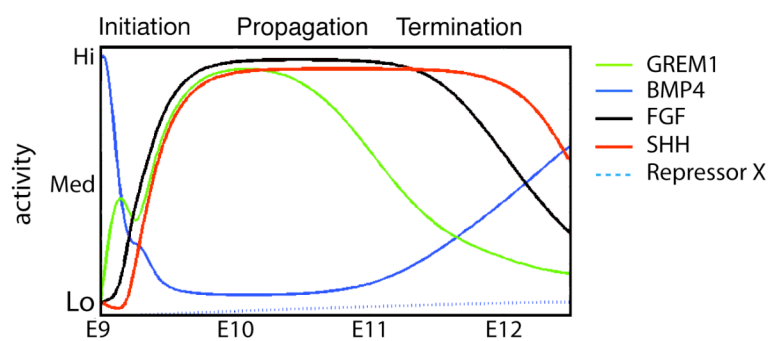


Fig. 9 Simulation of FGF-mediated termination of e-m SHH/GREM1/FGF feedback signaling.

While it is currently impossible to model spatial constraints such as the increasing separation of *Shh* and *Grem1* expressing cells, it was assumed that high FGF signaling

activity begins to inhibit *Grem1* expression as a consequence of the FGF-dependent accumulation of a repressor X (dotted line). This results in progressive down-regulation of GREM1 (green), SHH (red) and AER-FGFs (black), while BMP4 activity (blue) rises again. Interestingly, experimental evidence from analysis of chicken limb bud development indicates that BMP activity is required at these advanced stages to determine the definitive identities of digits and initiate chondrogenesis.

Most importantly, our analysis provides insight into how genetic variation of a morphogen signal such as SHH (Harfe et al. 2004; Towers et al. 2008; Zhu et al. 2008) is compensated by so-called distributed robustness (Wagner 2005) due to GREM1-mediated interconnectivity of the BMP, SHH and FGF signaling pathways and not simply by SHH pathway intra-regulation.

The absence of BMP4 completely disrupts limb bud development, which points to an essential role of BMP4 in formation of vertebrate paired appendages, most likely due to its role in AER induction. The GREM1-mediated switch from BMP4 to predominantly SHH dependent e-m feedback signaling links proximo-distal to antero-posterior limb patterning and promotes distal outgrowth and expansion of the autopod primordia. The innovation of the autopod represents a major step in evolution as it ultimately enabled tetrapods to conquer land (Shubin et al. 1997; Tickle 2006). Therefore, it is likely that GREM1-mediated fine-tuning of the temporal progression from BMP4 to predominant SHH and FGF-dependent signaling interactions would have contributed to shaping and stabilizing pentadactyly during

tetrapod evolution (Clark 2002). However, a large variety of derived and specialized limbs bearing less than five digits (oligodactyly) have evolved by modification of the initial bauplan (Shubin et al. 1997). For example, comparative analysis of closely related lizards reveals reductions and loss of particular digits, the severity of which has been correlated with a proportional shortening of the length and strength of SHH signaling (Shapiro et al. 2003). Significantly expanded forelimb autopod primordia, elongation of digits and interdigital webbing have enabled bats to fly. Interestingly, molecular analysis reveals that the timing of the SHH/GREM1/FGF e-m feedback loop is altered in comparison to mouse forelimb buds (Hockman et al. 2008). Following termination of e-m feedback signaling, all components of the SHH/GREM1/FGF feedback loop are reactivated in the interdigital mesenchyme of bat forelimb buds, where they most likely contribute to digit lengthening and interdigital webbing by their positive effect on cell survival and proliferation (Hockman et al. 2008). These two cases are prime examples of how adaptive diversification of pentadactylous limbs could involve direct alterations of the timing of signaling by changing the kinetics and interconnectivity of the self-regulatory and robust limb bud patterning system described here.

Publication:

Jean-Denis Bénazet, Mirko Bischofberger, Eva Tiecke, Alexandre Gonçalves, James F.

Martin, Aimée Zuniga, Felix Naef and Rolf Zeller. **A self-regulatory system of interlinked signaling feedback loops controls mouse limb patterning.** Science 2009. *In press.*

IX. CONCLUSION AND OUTLOOK

Despite the fact that the classical studies and models culminated in the identification of the relevant morphogenetic signals and their effectors, they have thus far not provided a comprehensive understanding of vertebrate limb bud morphogenesis. The molecular analysis in combination with experimental and genetic manipulation has provided important insights into how signals are emitted by ZPA and AER and are received and transduced by responding cells. These studies have now revealed the next level of complexity to be analyzed, namely how information is integrated from different signaling sources and pathways and memorized such that specification and growth of the whole limb bud occurs in a temporally and spatially coordinated manner (4D patterning). It is likely that early specified, positional information is “checked” continuously and “up-dated” as the territories are expanded by proliferation to generate the progenitors that form a particular skeletal element. Therefore, identities are likely only “fixed” at rather advanced developmental stages and this determination just precedes the initiation of differentiation. The signaling centers are now well defined both at the cellular and molecular level, which renders the developing limb bud well suited to systems biology-type research approaches. Such genome-wide and proteomics-driven functional-genetic approaches in combination with experimental manipulation and the predictive powers of modeling will hopefully provide definitive insights into how signals are sent and received and how information is integrated by cells during specification, proliferation and determination in time and space.

In this study, we show that the regulation of BMP activity over time is crucial for inducing and propagating morphogenetic signaling during limb development. The TGF β /BMP signals are usually transduced via the activation and nuclear translocation of the

SMAD transcriptional regulators. Upon binding of the BMPs and TGF β s ligands to their receptors, the regulatory SMADs (SMAD1, 5, 8 and SMAD2, 3, respectively) are phosphorylated, which results in their association with the co-factor SMAD4 and induces nuclear translocation. In the nucleus, the SMAD complexes bind to the regulatory sequences of target genes. Although some of the TGF β /BMP signals can be transduced via SMAD-independent pathways, SMAD4 appears as a central and unique mediator of the SMAD-dependant TGF β /BMP pathway (Derynck and Zhang 2003; Arnold et al. 2006). While our study reveals the architecture and the dynamics of the network that coordinates the key signals governing limb development, their integration in responding cells in terms of transcriptional regulation is less well understood. In a first attempt to unveil the underlying gene regulatory network controlling limb development, Vokes et al. (2008) have characterized the SHH/GLI-dependent *cis*-regulatory network by combining whole-genome chromatin immunoprecipitation (ChIP)-on-chip with transcriptional profiling. In light of our results, it is of prime importance to conduct similar studies with respect to BMP signal transduction. Transcriptional profiling in combination with temporally controlled *Smad4* inactivation (Yang et al. 2002) in developing limb buds and to ChIP-on-chip experiments using SMAD antibodies are a powerful tool to identify the SMAD-dependant *cis*-regulatory circuitry and its dynamics during the different phases of limb patterning (initiation, propagation and termination, see Fig. 9, chapter VIII).

Our study highlights the robust nature of the limb signaling network. Robustness is believed to be an essential feature of complex evolvable systems (Kitano 2004). This property allows a system to reliably functions despite external and internal perturbations. In terms of evolutionary processes, this implies that a robust biological system permits the accumulation of genetic variations without interfering with its function, at least in a limited range of

conditions (Kitano 2004). Thus, robustness is crucial for the generation and inheritance of non-lethal alleles as well as the establishment of new connections within a given gene regulatory networks (Isalan et al. 2008). The flexibility of a robust system favors the expansion of a reservoir of genetic variants, which ultimately facilitates evolvability if conditions change. However, it is of great importance to consider the robustness of biological systems in other fields such as drug design. The fact that biological systems are robust to a broad range of perturbations also implies that they can be robust, i.e. resistant to therapeutic drug treatment. For example, a disease can be viewed as a failure of a physiological system due to massive perturbations, which may result in the establishment of an alternate pathological robust state. Understanding system robustness in pathological conditions will be a powerful approach to identify points of fragility and design efficient therapeutic strategies (Kitano 2007). For example, tumor/stroma interactions and tumor angiogenesis depend on communication systems between distinct cell populations using identical or similar signaling interaction to those involved in limb patterning and other developmental processes (Bhowmick and Moses 2005; Kerbel 2008). It is likely that similar and robust networks mediate these interactions. The limb signaling system is robust against variations in *Bmps*, *Shh* and *Fgfs* dosages. However, in the absence of *Grem1* the system becomes particularly sensitive to such variations, making limb bud development labile. Identifying and targeting such points of fragility in diseases may break their robustness that confer i.e. drug resistance. In the emerging field of synthetic biology, a variety of artificial gene circuits have been designed to control and create *de novo* cellular behaviors (Andrianantoandro et al. 2006). These advances will probably lead to a wide range of applications in medicine and biotechnology. Most of the synthetic circuits that have been designed display simple behaviors such as oscillations or switches that influence the behavior of modified cells in a

cell-autonomous and asynchronous manner (for review see Hasty et al. 2002). A way to achieve more sophisticated and coordinated behaviors of cell population is to introduce self-regulatory communication systems as demonstrated by developmental systems. The architecture of the intercellular signaling network that we have described here and its properties (interlinked feedback loops with differential kinetics, self-regulatory switching behavior and robustness) can provide useful insights to engineer such artificial communication systems.

X. ACKNOWLEDGEMENTS

My first thanks are dedicated to Rolf Zeller for giving me the opportunity to do my PhD studies in his laboratory, for training me, for giving me independence and the freedom to develop my own ideas, for putting me back on track when I was getting lost and for his patience and support during these five years. Rolf, I would like particularly to thank you for the enthusiasm, talent, time and energy you dedicated to ensure that this work get published in the best possible way. Thank you for making a dream reality!

I would like to thank Mirko Bischorberger and Felix Naef for the fruitful collaboration; the mathematical modeling (Figs. 6, 9 and S8) lifted this project to higher levels (I mean the “Science” level!).

Many thanks to Alexandre Gonçalves for happily participating in this project, sometime at the expense of his own work. I thank Eva Tiecke for the bead grafting experiments (Fig. 5) and to Antonella Galli for taking care of me during the first year of my PhD. I thank Aimée Zuniga and Odysse Michos for their work during the initial phase of this project. A special thank to François Lehembre for teaching me how to make good quantitative PCR and Annette Roulier for the artwork in the book chapter. I thank Christine Müller-Thompson for proofreading this manuscript.

Many thanks to all group members for scientific advices, sharing reagents and for the nice daily atmosphere in the lab and great lab outing we had.

Many thanks to Prof. Dr. Markus Affolter and Prof. Dr. Antonius Rolink for being members of my thesis committee.

I would like to thank Valérie Lobjois, Fabienne Pituello, François Payre and Fernando Roch for guiding my first steps in science at the university Paul Sabatier in France.

Finally, I would like to thank my family and friends for their support throughout this time.

XI. REFERENCES

- Ahn, K., Mishina, Y., Hanks, M.C., Behringer, R.R., and Crenshaw, E.B., 3rd. 2001. BMPR-IA signaling is required for the formation of the apical ectodermal ridge and dorsal-ventral patterning of the limb. *Development* 128(22): 4449-4461.
- Ahn, S. and Joyner, A.L. 2004. Dynamic changes in the response of cells to positive hedgehog signaling during mouse limb patterning. *Cell* 118(4): 505-516.
- Andrianantoandro, E., Basu, S., Karig, D.K., and Weiss, R. 2006. Synthetic biology: new engineering rules for an emerging discipline. *Mol Syst Biol* 2: 2006 0028.
- Arnold, S.J., Maretto, S., Islam, A., Bikoff, E.K., and Robertson, E.J. 2006. Dose-dependent Smad1, Smad5 and Smad8 signaling in the early mouse embryo. *Dev Biol* 296(1): 104-118.
- Bandyopadhyay, A., Tsuji, K., Cox, K., Harfe, B.D., Rosen, V., and Tabin, C.J. 2006. Genetic Analysis of the Roles of BMP2, BMP4, and BMP7 in Limb Patterning and Skeletogenesis. *PLoS Genet* 2(12): e216.
- Barna, M. and Niswander, L. 2007. Visualization of cartilage formation: insight into cellular properties of skeletal progenitors and chondrodysplasia syndromes. *Dev Cell* 12(6): 931-941.
- Ben-Haim, N., Lu, C., Guzman-Ayala, M., Pescatore, L., Mesnard, D., Bischofberger, M., Naef, F., Robertson, E.J., and Constam, D.B. 2006. The nodal precursor acting via activin receptors induces mesoderm by maintaining a source of its convertases and BMP4. *Dev Cell* 11(3): 313-323.
- Bhowmick, N.A. and Moses, H.L. 2005. Tumor-stroma interactions. *Curr Opin Genet Dev* 15(1): 97-101.
- Boot, M.J., Westerberg, C.H., Sanz-Ezquerro, J., Cotterell, J., Schweitzer, R., Torres, M., and Sharpe, J. 2008. In vitro whole-organ imaging: 4D quantification of growing mouse limb buds. *Nat Methods* 5(7): 609-612.
- Boulet, A.M., Moon, A.M., Arenkiel, B.R., and Capecchi, M.R. 2004. The roles of Fgf4 and Fgf8 in limb bud initiation and outgrowth. *Dev Biol* 273(2): 361-372.

- Brugger, S.M., Merrill, A.E., Torres-Vazquez, J., Wu, N., Ting, M.C., Cho, J.Y., Dobias, S.L., Yi, S.E., Lyons, K., Bell, J.R., Arora, K., Warrior, R., and Maxson, R. 2004. A phylogenetically conserved cis-regulatory module in the *Msx2* promoter is sufficient for BMP-dependent transcription in murine and *Drosophila* embryos. *Development* 131(20): 5153-5165.
- Capdevila, J., Tsukui, T., Rodriguez Esteban, C., Zappavigna, V., and Izpisua Belmonte, J.C. 1999. Control of vertebrate limb outgrowth by the proximal factor *Meis2* and distal antagonism of BMPs by *Gremlin*. *Mol Cell* 4(5): 839-849.
- Capellini, T.D., Di Giacomo, G., Salsi, V., Brendolan, A., Ferretti, E., Srivastava, D., Zappavigna, V., and Selleri, L. 2006. *Pbx1/Pbx2* requirement for distal limb patterning is mediated by the hierarchical control of *Hox* gene spatial distribution and *Shh* expression. *Development* 133(11): 2263-2273.
- Charité, J., de Graaff, W., Shen, S., and Deschamps, J. 1994. Ectopic expression of *Hox-8* causes duplication of the ZPA in the forelimb and homeotic transformation of axial structures. *Cell* 78: 589-601.
- Charité, J., McFadden, D.G., and Olson, E.N. 2000. The bHLH transcription factor *dHAND* controls *Sonic hedgehog* expression and establishment of the zone of polarizing activity during limb development. *Development* 127: 2461-2470.
- Chen, M.H., Li, Y.J., Kawakami, T., Xu, S.M., and Chuang, P.T. 2004. Palmitoylation is required for the production of a soluble multimeric Hedgehog protein complex and long-range signaling in vertebrates. *Genes Dev* 18(6): 641-659.
- Chiang, C., Litingtung, Y., Harris, M.P., Simandl, B.K., Li, Y., Beachy, P.A., and Fallon, J.F. 2001. Manifestation of the Limb Prepattern: Limb Development in the Absence of *Sonic Hedgehog* Function. *Developmental Biology* 236: 421-435.
- Clark, J.A. 2002. An early tetrapod from "Romer's Gap". *Nature* 418: 72-76.
- Cohn, M.J. 2000. Giving limbs a hand. *Nature* 406: 953-954.
- Cross, J.C., Flannery, M.L., Blonar, M.A., Steingrimsson, E., Jenkins, N.A., Copeland, N.G., Rutter, W.J., and Werb, Z. 1995. *Hxt* encodes a basic helix-loop-helix transcription factor that regulates trophoblast cell development. *Development* 121(8): 2513-2523.
- Cserjesi, P., Brown, D., Lyons, G.E., and Olson, E.N. 1995. Expression of the novel basic helix-loop-helix gene *eHAND* in neural crest derivatives and extraembryonic membranes during mouse development. *Dev Biol* 170(2): 664-678.

- Dahn, R.D. and Fallon, J.F. 2000. Interdigital regulation of digit identity and homeotic transformation by modulated BMP signaling. *Science* 289(5478): 438-441.
- De Robertis, E.M. 2006. Spemann's organizer and self-regulation in amphibian embryos. *Nat Rev Mol Cell Biol* 7(4): 296-302.
- Derynck, R. and Zhang, Y.E. 2003. Smad-dependent and Smad-independent pathways in TGF-beta family signalling. *Nature* 425(6958): 577-584.
- Drossopoulou, G., Lewis, K.E., Sanz-Ezquerro, J.J., Nikbakht, N., McMahon, A.P., Hofmann, C., and Tickle, C. 2000. A model for anteroposterior patterning of the vertebrate limb based on sequential long- and short-range Shh signalling and Bmp signalling. *Development* 127(7): 1337-1348.
- Dudley, A.T., Ros, M.A., and Tabin, C.J. 2002. A re-examination of proximodistal patterning during vertebrate limb development. *Nature* 418(6897): 539-544.
- Dymecki, S.M. 1996. Flp recombinase promotes site-specific DNA recombination in embryonic stem cells and transgenic mice. *Proc Natl Acad Sci U S A* 93(12): 6191-6196.
- Eldar, A., Shilo, B.Z., and Barkai, N. 2004. Elucidating mechanisms underlying robustness of morphogen gradients. *Curr Opin Genet Dev* 14(4): 435-439.
- Fallon, J.F., Rowe, D.A., Frederick, J.M., and Simandl, B.K. 1983. Studies on epithelial-mesenchymal interactions during limb development. in *Epithelial- Mesenchymal Interactions in Development* (ed. R.H. Sawyer and J.F. Fallon), pp. 3-25. Praeger Scientific, New York.
- Fernandez-Teran, M., Piedra, M.E., Kathiriya, I.S., Srivastava, D., Rodriguez-Rey, J.C., and Ros, M.A. 2000. Role of dHAND in the anterior-posterior polarization of the limb bud: implications for the Sonic hedgehog pathway. *Development* 127: 2133-2142.
- Fernandez-Teran, M., Piedra, M.E., Rodriguez-Rey, J.C., Talamillo, A., and Ros, M.A. 2003. Expression and regulation of eHAND during limb development. *Dev Dyn* 226(4): 690-701.
- Ferrari, D., Lichtler, A.C., Pan, Z.Z., Dealy, C.N., Upholt, W.B., and Kosher, R.A. 1998. Ectopic expression of Msx-2 in posterior limb bud mesoderm impairs limb morphogenesis while inducing BMP-4 expression, inhibiting cell proliferation, and promoting apoptosis. *Dev Biol* 197(1): 12-24.

- Firulli, A.B. 2003. A HANDful of questions: the molecular biology of the heart and neural crest derivatives (HAND)-subclass of basic helix-loop-helix transcription factors. *Gene* 312: 27-40.
- Firulli, A.B., McFadden, D.G., Lin, Q., Srivastava, D., and Olson, E.N. 1998. Heart and extra-embryonic mesodermal defects in mouse embryos lacking the bHLH transcription factor Hand1. *Nat Genet* 18(3): 266-270.
- Firulli, B.A., Howard, M.J., McDaid, J.R., McIlreavey, L., Dionne, K.M., Centonze, V.E., Cserjesi, P., Virshup, D.M., and Firulli, A.B. 2003. PKA, PKC, and the protein phosphatase 2A influence HAND factor function: a mechanism for tissue-specific transcriptional regulation. *Mol Cell* 12(5): 1225-1237.
- Firulli, B.A., Krawchuk, D., Centonze, V.E., Vargesson, N., Virshup, D.M., Conway, S.J., Cserjesi, P., Laufer, E., and Firulli, A.B. 2005. Altered Twist1 and Hand2 dimerization is associated with Saethre-Chotzen syndrome and limb abnormalities. *Nat Genet* 37(4): 373-381.
- French, V., Bryant, P.J., and Bryant, S.V. 1976. Pattern regulation in epimorphic fields. *Science* 193(4257): 969-981.
- Goldman, D.C., Hackenmiller, R., Nakayama, T., Sopory, S., Wong, C., Kulesa, H., and Christian, J.L. 2006. Mutation of an upstream cleavage site in the BMP4 prodomain leads to tissue-specific loss of activity. *Development* 133(10): 1933-1942.
- Haramis, A.G., Brown, J.M., and Zeller, R. 1995. The limb deformity mutation disrupts the SHH/FGF-4 feedback loop and regulation of 5'HoxD genes during limb pattern formation. *Development* 121: 4237-4245.
- Harfe, B.D., Scherz, P.J., Nissim, S., Tian, H., McMahon, A.P., and Tabin, C.J. 2004. Evidence for an expansion-based temporal Shh gradient in specifying vertebrate digit identities. *Cell* 118(4): 517-528.
- Hasson, P., Del Buono, J., and Logan, M.P. 2007. Tbx5 is dispensable for forelimb outgrowth. *Development* 134(1): 85-92.
- Hasty, J., McMillen, D., and Collins, J.J. 2002. Engineered gene circuits. *Nature* 420(6912): 224-230.
- Hayashi, S. and McMahon, A.P. 2002. Efficient recombination in diverse tissues by a tamoxifen-inducible form of Cre: a tool for temporally regulated gene activation/inactivation in the mouse. *Dev Biol* 244(2): 305-318.

- Hockman, D., Cretekos, C.J., Mason, M.K., Behringer, R.R., Jacobs, D.S., and Illing, N. 2008. A second wave of Sonic hedgehog expression during the development of the bat limb. *Proc Natl Acad Sci U S A* 105(44): 16982-16987.
- Hofmann, C., Luo, G., Balling, R., and Karsenty, G. 1996. Analysis of limb patterning in BMP-7-deficient mice. *Dev Genet* 19(1): 43-50.
- Hollenberg, S.M., Sternglanz, R., Cheng, P.F., and Weintraub, H. 1995. Identification of a new family of tissue-specific basic helix-loop-helix proteins with a two-hybrid system. *Mol Cell Biol* 15(7): 3813-3822.
- Hornbruch, A. and Wolpert, L. 1991. The spatial and temporal distribution of polarizing activity in the flank of the pre-limb-bud stages in the chick embryo. *Development* 111: 725-731.
- Isalan, M., Lemerle, C., Michalodimitrakis, K., Horn, C., Beltrao, P., Raineri, E., Garriga-Canut, M., and Serrano, L. 2008. Evolvability and hierarchy in rewired bacterial gene networks. *Nature* 452(7189): 840-845.
- Jiao, K., Kulesa, H., Tompkins, K., Zhou, Y., Batts, L., Baldwin, H.S., and Hogan, B.L. 2003. An essential role of Bmp4 in the atrioventricular septation of the mouse heart. *Genes Dev* 17(19): 2362-2367.
- Karsenty, G., Luo, G., Hofmann, C., and Bradley, A. 1996. BMP 7 is required for nephrogenesis, eye development, and skeletal patterning. *Ann N Y Acad Sci* 785: 98-107.
- Kerbel, R.S. 2008. Tumor angiogenesis. *N Engl J Med* 358(19): 2039-2049.
- Kerszberg, M. 2004. Noise, delays, robustness, canalization and all that. *Curr Opin Genet Dev* 14(4): 440-445.
- Khokha, M.K., Hsu, D., Brunet, L.J., Dionne, M.S., and Harland, R.M. 2003. Gremlin is the BMP antagonist required for maintenance of Shh and Fgf signals during limb patterning. *Nat Genet* 34(3): 303-307.
- Kitano, H. 2004. Biological robustness. *Nat Rev Genet* 5(11): 826-837.
- Kitano, H. 2007. A robustness-based approach to systems-oriented drug design. *Nat Rev Drug Discov* 6(3): 202-210.
- Kmita, M., Tarchini, B., Zakany, J., Logan, M., Tabin, C.J., and Duboule, D. 2005. Early developmental arrest of mammalian limbs lacking HoxA/HoxD gene function. *Nature* 435(7045): 1113-1116.

- Knezevic, V., De Santo, R., Schughart, K., Huffstadt, U., Chiang, C., Mahon, K.A., and Mackem, S. 1997. *Hoxd-12* differentially affects preaxial and postaxial chondrogenic branches in the limb and regulates *Sonic hedgehog* in a positive feedback loop. *Development* 124: 4523-4536.
- Kolsch, V. and Paululat, A. 2002. The highly conserved cardiogenic bHLH factor Hand is specifically expressed in circular visceral muscle progenitor cells and in all cell types of the dorsal vessel during *Drosophila* embryogenesis. *Dev Genes Evol* 212(10): 473-485.
- Kraus, P., Fraidenraich, D., and Loomis, C.A. 2001. Some distal limb structures develop in mice lacking *Sonic hedgehog* signaling. *Mech Dev* 100(1): 45-58.
- Kulesa, H. and Hogan, B.L. 2002. Generation of a loxP flanked *bmp4loxP-lacZ* allele marked by conditional *lacZ* expression. *Genesis* 32(2): 66-68.
- Laufer, E., Nelson, C.E., Johnson, R.L., Morgan, B.A., and Tabin, C. 1994. *Sonic hedgehog* and *Fgf-4* act through a signaling cascade and feedback loop to integrate growth and patterning of the developing limb bud. *Cell* 79(6): 993-1003.
- Lewandoski, M., Sun, X., and Martin, G.R. 2000. *Fgf8* signalling from the AER is essential for normal limb development. *Nat Genet* 26(4): 460-463.
- Lewis, P.M., Dunn, M.P., McMahon, J.A., Logan, M., Martin, J.F., St-Jacques, B., and McMahon, A.P. 2001. Cholesterol modification of *sonic hedgehog* is required for long-range signaling activity and effective modulation of signaling by *Ptc1*. *Cell* 105(5): 599-612.
- Li, Y., Zhang, H., Litingtung, Y., and Chiang, C. 2006. Cholesterol modification restricts the spread of *Shh* gradient in the limb bud. *Proc Natl Acad Sci U S A* 103(17): 6548-6553.
- Litingtung, Y., Dahn, R.D., Li, Y., Fallon, J.F., and Chiang, C. 2002. *Shh* and *Gli3* are dispensable for limb skeleton formation but regulate digit number and identity. *Nature* 418(6901): 979-983.
- Logan, M., Martin, J.F., Nagy, A., Lobe, C., Olson, E.N., and Tabin, C.J. 2002. Expression of *Cre* recombinase in the developing mouse limb bud driven by a *Prxl* enhancer. *Genesis* 33(2): 77-80.

- Lu, P., Minowada, G., and Martin, G.R. 2006. Increasing Fgf4 expression in the mouse limb bud causes polysyndactyly and rescues the skeletal defects that result from loss of Fgf8 function. *Development* 133(1): 33-42.
- Ma, L. and Martin, J.F. 2005. Generation of a Bmp2 conditional null allele. *Genesis* 42(3): 203-206.
- Mann, R.K. and Beachy, P.A. 2004. Novel lipid modifications of secreted protein signals. *Annu Rev Biochem* 73: 891-923.
- Marazzi, G., Wang, Y., and Sassoon, D. 1997. Msx2 is a transcriptional regulator in the BMP4-mediated programmed cell death pathway. *Dev Biol* 186(2): 127-138.
- Mariani, F.V., Ahn, C.P., and Martin, G.R. 2008. Genetic evidence that FGFs have an instructive role in limb proximal-distal patterning. *Nature* 453(7193): 401-405.
- Martin, G.R. 1998. The roles of FGFs in the early development of vertebrate limbs. *Genes Dev* 12: 1571-1586.
- Massari, M.E. and Murre, C. 2000. Helix-loop-helix proteins: regulators of transcription in eucaryotic organisms. *Mol Cell Biol* 20(2): 429-440.
- McFadden, D.G., Barbosa, A.C., Richardson, J.A., Schneider, M.D., Srivastava, D., and Olson, E.N. 2005. The Hand1 and Hand2 transcription factors regulate expansion of the embryonic cardiac ventricles in a gene dosage-dependent manner. *Development* 132(1): 189-201.
- Mercader, N., Leonardo, E., Piedra, M.E., Martinez, A.C., Ros, M.A., and Torres, M. 2000. Opposing RA and FGF signals control proximodistal vertebrate limb development through regulation of Meis genes. *Development* 127(18): 3961-3970.
- Michos, O., Panman, L., Vintersten, K., Beier, K., Zeller, R., and Zuniga, A. 2004. Gremlin-mediated BMP antagonism induces the epithelial-mesenchymal feedback signaling controlling metanephric kidney and limb organogenesis. *Development* 131(14): 3401-3410.
- Min, H., Danilenko, D.M., Scully, S.A., Bonlon, B., Ring, B.D., Tarpley, J.E., DeRose, M., and Simonet, W.S. 1998. Fgf-10 is required for both limb and lung development and exhibits striking functional similarity to *Drosophila* branchless. *Genes & Development* 12(20): 3156-3161.
- Moon, A.M. and Capecchi, M.R. 2000. Fgf8 is required for outgrowth and patterning of the limbs. *Nat Genet* 26(4): 455-459.

- Niederreither, K., Subbarayan, V., Dolle, P., and Chambon, P. 1999. Embryonic retinoic acid synthesis is essential for early mouse post-implantation development. *Nat Genet* 21(4): 444-448.
- Niederreither, K., Vermot, J., Schuhbaur, B., Chambon, P., and Dolle, P. 2002. Embryonic retinoic acid synthesis is required for forelimb growth and anteroposterior patterning in the mouse. *Development* 129(15): 3563-3574.
- Nissim, S., Hasso, S.M., Fallon, J.F., and Tabin, C.J. 2006. Regulation of Gremlin expression in the posterior limb bud. *Dev Biol* 299(1): 12-21.
- Niswander, L. 2003. Pattern formation: old models out on a limb. *Nat Rev Genet* 4(2): 133-143.
- Niswander, L., Jeffrey, S., Martin, G.R., and Tickle, C. 1994. A positive feedback loop coordinates growth and patterning in the vertebrate limb. *Nature* 371: 609-612.
- Niswander, L., Tickle, C., Vogel, A., Booth, I., and Martin, G.R. 1993. FGF-4 replaces the apical ectodermal ridge and directs outgrowth and patterning of the limb. *Cell* 75(3): 579-587.
- Ohuchi, H.a.o. 1997. The mesenchymal factor FGF-10, initiates and maintains the outgrowth of the chick limb bud through interaction with FGF-8, an apical ectodermal factor. *Development* 124(11): 2235-2244.
- Ovchinnikov, D.A., Selever, J., Wang, Y., Chen, Y.T., Mishina, Y., Martin, J.F., and Behringer, R.R. 2006. BMP receptor type IA in limb bud mesenchyme regulates distal outgrowth and patterning. *Dev Biol* 295(1): 103-115.
- Panman, L., Galli, A., Lagarde, N., Michos, O., Soete, G., Zuniga, A., and Zeller, R. 2006. Differential regulation of gene expression in the digit forming area of the mouse limb bud by SHH and gremlin 1/FGF-mediated epithelial-mesenchymal signalling. *Development* 133(17): 3419-3428.
- Pizette, S., Abate-Shen, C., and Niswander, L. 2001. BMP controls proximodistal outgrowth, via induction of the apical ectodermal ridge, and dorsoventral patterning in the vertebrate limb. *Development* 128(22): 4463-4474.
- Reversade, B. and De Robertis, E.M. 2005. Regulation of ADMP and BMP2/4/7 at opposite embryonic poles generates a self-regulating morphogenetic field. *Cell* 123(6): 1147-1160.

- Riddle, R.D., Johnson, R.L., Laufer, E., and Tabin, C. 1993. *Sonic hedgehog* mediates the polarizing activity of the ZPA. *Cell* 75: 1401-1416.
- Robert, B. 2007. Bone morphogenetic protein signaling in limb outgrowth and patterning. *Dev Growth Differ* 49(6): 455-468.
- Ros, M.A., Lopez-Martinez, A., Simandl, B.K., Rodriguez, C., Izpisua Belmonte, J.C., Dahn, R., and Fallon, J.F. 1996. The limb field mesoderm determines initial limb bud anteroposterior asymmetry and budding independent of *sonic hedgehog* or apical ectodermal gene expressions. *Development* 122: 2319-2330.
- Sanz-Ezquerro, J.J. and Tickle, C. 2000. Autoregulation of Shh expression and Shh induction of cell death suggest a mechanism for modulating polarising activity during chick limb development. *Development* 127(22): 4811-4823.
- Sanz-Ezquerro, J.J. and Tickle, C. 2003. Fgf signaling controls the number of phalanges and tip formation in developing digits. *Curr Biol* 13(20): 1830-1836.
- Saunders, J.W., Jr. and Gasseling, M.T. 1968. Ectoderm-mesenchymal interaction in the origins of wing symmetry. in *Epithelial-Mesenchymal Interactions* (ed. R. Fleischmajer and R.E. Billingham), pp. 78-97. Williams Wilkins, Baltimore.
- Saunders, J.W.J. 1948. The proximo-distal sequence of origin of limb parts of the chick wing and the role of the ectoderm. *J Exp Zoology*(108): 363-404.
- Scherz, P.J., Harfe, B.D., McMahon, A.P., and Tabin, C.J. 2004. The limb bud Shh-Fgf feedback loop is terminated by expansion of former ZPA cells. *Science* 305(5682): 396-399.
- Scherz, P.J., McGlinn, E., Nissim, S., and Tabin, C.J. 2007. Extended exposure to Sonic hedgehog is required for patterning the posterior digits of the vertebrate limb. *Dev Biol* 308(2): 343-354.
- Schwenk, F., Baron, U., and Rajewsky, K. 1995. A cre-transgenic mouse strain for the ubiquitous deletion of loxP-flanked gene segments including deletion in germ cells. *Nucleic Acids Res* 23(24): 5080-5081.
- Sekine, K., Ohuchi, H., Fujiwara, M., Yamasaki, M., Yoshizawa, T., Sato, T., Yagashita, N., Matsui, D., Koga, Y., Itoh, N., and Kato, S. 1999. Fgf10 is essential for limb and lung formation. *Nature Genetics* 21(1): 138-141.

- Selever, J., Liu, W., Lu, M.F., Behringer, R.R., and Martin, J.F. 2004. Bmp4 in limb bud mesoderm regulates digit pattern by controlling AER development. *Dev Biol* 276(2): 268-279.
- Shapiro, M.D., Hanken, J., and Rosenthal, N. 2003. Developmental basis of evolutionary digit loss in the Australian lizard *Hemiergis*. *J Exp Zool B Mol Dev Evol* 297(1): 48-56.
- Shubin, N., Tabin, C., and Carroll, S. 1997. Fossils, genes and the evolution of animal limbs. *Nature* 388: 639-647.
- Srivastava, D. 1999. HAND Proteins: Molecular Mediators of Cardiac Development and Congenital Heart Disease. *Trends in Cardiovascular Medicine* 9: 11-18.
- Srivastava, D., Thomas, T., Lin, Q., Kirby, M.L., Brown, D., and Olson, E.N. 1997. Regulation of cardiac mesodermal and neural crest development by the bHLH transcription factor dHAND. *Nature Genetics* 16: 154-160.
- St-Jacques, B., Dassule, H.R., Karavanova, I., Botchkarev, V.A., Li, J., Danielian, P.S., McMahon, J.A., Lewis, P.M., Paus, R., and McMahon, A.P. 1998. Sonic hedgehog signaling is essential for hair development. *Curr Biol* 8(19): 1058-1068.
- Summerbell, D. 1979. The zone of polarizing activity: evidence for a role in normal chick limb morphogenesis. *J Embryol Exp Morphol* 50: 217-233.
- Summerbell, D. and Harvey, F. 1983. Vitamin A and the control of pattern in vertebrate limbs. in *Limb Development and Regeneration* (ed. J.F. Fallon and A.I. Caplan), pp. 109-118. Liss, A.R., New York.
- Summerbell, D., Lewis, J.H., and Wolpert, L. 1973. Positional information in chick limb morphogenesis. *Nature* 244(5413): 492-496.
- Sun, X., Mariani, F.V., and Martin, G.R. 2002. Functions of FGF signalling from the apical ectodermal ridge in limb development. *Nature* 418(6897): 501-508.
- Suzuki, T., Hasso, S.M., and Fallon, J.F. 2008. Unique SMAD1/5/8 activity at the phalanx-forming region determines digit identity. *Proc Natl Acad Sci U S A* 105(11): 4185-4190.
- Tabin, C. and Wolpert, L. 2007. Rethinking the proximodistal axis of the vertebrate limb in the molecular era. *Genes Dev* 21(12): 1433-1442.

- Tanaka, M., Cohn, M.J., Ashby, P., Davey, M., Martin, P., and Tickle, C. 2000. Distribution of polarizing activity and potential for limb formation in mouse and chick embryos and possible relationships to polydactyly. *Development* 127: 4011-4021.
- Tarchini, B., Duboule, D., and Kmita, M. 2006. Regulatory constraints in the evolution of the tetrapod limb anterior-posterior polarity. *Nature* 443(7114): 985-988.
- te Welscher, P., Fernandez-Teran, M., Ros, M.A., and Zeller, R. 2002a. Mutual genetic antagonism involving GLI3 and dHAND prepatterns the vertebrate limb bud mesenchyme prior to SHH signaling. *Genes Dev* 16(4): 421-426.
- te Welscher, P., Zuniga, A., Kuijper, S., Drenth, T., Goedemans, H.J., Meijlink, F., and Zeller, R. 2002b. Progression of Vertebrate Limb Development through SHH-Mediated Counteraction of GLI3. *Science* 298: 827-830.
- Thaller, C. and Eichele, G. 1987. Identification and spatial distribution of retinoids in the developing chick limb bud. *Nature* 327: 625-628.
- Theil, T., Kaesler, S., Grotewold, L., Bose, J., and Ruther, U. 1999. Gli genes and limb development. *Cell Tissue Res* 296(1): 75-83.
- Tickle, C. 1981. The number of polarizing region cells required to specify additional digits in the developing chick wing. *Nature* 289: 295-298.
- Tickle, C. 2006. Making digit patterns in the vertebrate limb. *Nat Rev Mol Cell Biol* 7(1): 45-53.
- Tickle, C., Alberts, B.M., Wolpert, L., and Lee, J. 1982. Local application of retinoic acid in the limb bud mimics the action of the polarizing region. *Nature* 296: 564-565.
- Tickle, C., Summerbell, D., and Wolpert, L. 1975. Positional signalling and specification of digits in chick limb morphogenesis. *Nature* 254(5497): 199-202.
- Towers, M., Mahood, R., Yin, Y., and Tickle, C. 2008. Integration of growth and specification in chick wing digit-patterning. *Nature* 452(7189): 882-886.
- Varjosalo, M. and Taipale, J. 2008. Hedgehog: functions and mechanisms. *Genes Dev* 22(18): 2454-2472.
- Verheyden, J.M. and Sun, X. 2008. An Fgf/Gremlin inhibitory feedback loop triggers termination of limb bud outgrowth. *Nature* 454(7204): 638-641.
- Vokes, S.A., Ji, H., Wong, W.H., and McMahon, A.P. 2008. A genome-scale analysis of the cis-regulatory circuitry underlying sonic hedgehog-mediated patterning of the mammalian limb. *Genes Dev* 22(19): 2651-2663.

- Wagner, A. 2005. Distributed robustness versus redundancy as causes of mutational robustness. *Bioessays* 27(2): 176-188.
- Wanek, N. and Bryant, S.V. 1991. Temporal pattern of posterior positional identity in mouse limb buds. *Developmental biology* 147: 480-484.
- Wang, B., Fallon, J.F., and Beachy, P.A. 2000. Hedgehog-Regulated Processing of Gli3 Produces an Anterior/Posterior Repressor gradient in the Developing Vertebrate Limb. *Cell* 100: 423-434.
- Wolpert, L. 1969. Positional information and the spatial pattern of cellular differentiation. *J Theor Biol* 25: 1-47.
- Wolpert, L., Tickle, C., and Sampford, M. 1979. The effect of cell killing by x-irradiation on pattern formation in the chick limb. *J Embryol Exp Morphol* 50: 175-193.
- Yang, X., Li, C., Herrera, P.L., and Deng, C.X. 2002. Generation of Smad4/Dpc4 conditional knockout mice. *Genesis* 32(2): 80-81.
- Yashiro, K., Zhao, X., Uehara, M., Yamashita, K., Nishijima, M., Nishino, J., Saijoh, Y., Sakai, Y., and Hamada, H. 2004. Regulation of retinoic acid distribution is required for proximodistal patterning and outgrowth of the developing mouse limb. *Dev Cell* 6(3): 411-422.
- Zakany, J. and Duboule, D. 2007. The role of Hox genes during vertebrate limb development. *Curr Opin Genet Dev* 17(4): 359-366.
- Zakany, J., Fromental-Ramain, C., Warot, X., and Duboule, D. 1997. Regulation of number and size of digits by posterior *Hox* genes: A dose-dependant mechanism with potential evolutionary implications. *Proc Natl Acad Sci USA* 94: 13695-13700.
- Zakany, J., Kmita, M., and Duboule, D. 2004. A dual role for Hox genes in limb anterior-posterior asymmetry. *Science* 304(5677): 1669-1672.
- Zeller, R. 2004. It takes time to make a pinky: unexpected insights into how SHH patterns vertebrate digits. *Sci STKE* 2004(259): pe53.
- Zeller, R. and Duboule, D. 1997. Dorso-ventral limb polarity and origin of the ridge: on the fringe of independence? *Bioessays* 19(7): 541-546.
- Zeng, X., Goetz, J.A., Suber, L.M., Scott, W.J., Jr., Schreiner, C.M., and Robbins, D.J. 2001. A freely diffusible form of Sonic hedgehog mediates long-range signalling. *Nature* 411(6838): 716-720.

- Zhu, J., Nakamura, E., Nguyen, M.T., Bao, X., Akiyama, H., and Mackem, S. 2008. Uncoupling Sonic hedgehog control of pattern and expansion of the developing limb bud. *Dev Cell* 14(4): 624-632.
- Zucker, R.M., Hunter, E.S., 3rd, and Rogers, J.M. 1999. Apoptosis and morphology in mouse embryos by confocal laser scanning microscopy. *Methods* 18(4): 473-480.
- Zuniga, A. and Galli, A. 2005. Limb Pattern Formation: Upstream and Downstream of Shh Signalling. in *Shh and Gli Signalling and Development* (ed. S. Howie and C. Fisher). Eureka.
- Zuniga, A., Haramis, A.P., McMahon, A.P., and Zeller, R. 1999. Signal relay by BMP antagonism controls the SHH/FGF4 feedback loop in vertebrate limb buds. *Nature* 401(6753): 598-602.
- Zuniga, A., Michos, O., Spitz, F., Haramis, A.P., Panman, L., Galli, A., Vintersten, K., Klasen, C., Mansfield, W., Kuc, S., Duboule, D., Dono, R., and Zeller, R. 2004. Mouse limb deformity mutations disrupt a global control region within the large regulatory landscape required for Gremlin expression. *Genes Dev* 18(13): 1553-1564.
- Zuniga, A. and Zeller, R. 1999. Gli3 (Xt) and formin (ld) participate in the positioning of the polarising region and control of posterior limb-bud identity. *Development* 126(1): 13-21.
- Zwilling, E. 1956. Interaction between Limb Bud Ectoderm and Mesoderm in the Chick embryo. II. Experimental Limb Manipulation. *JExp Zool*(132): 173-188.

XII. CURRICULUM VITAE AND PUBLICATION LIST

PERSONAL DETAILS

Name: Jean-Denis Bénazet

Date of birth: 08.06.1980

Nationality: French

address: Developmental Genetics group, Department of Biomedicine,
Mattenstrasse 28
4058 Basel, Switzerland

e-mail: Jean-Denis.Benazet@unibas.ch

Tel: +41 61 695 30 39

EDUCATION

Jan. 2004-Present: Ph.D student in the laboratory of Prof. Dr. Rolf Zeller, Developmental Genetics group, Department of Biomedicine, University of Basel Medical Faculty, Switzerland.

Sept. 2002-June 2003: Master's degree (DEA), speciality: molecular, cell and developmental biology, Toulouse University, Centre de Biologie du Développement (CBD), France.

Sept. 2001-June 2002: Maîtrise in Developmental and Cell Biology, Toulouse University, CBD, France.

Sept. 2000-June 2001: Bachelor's degree (Licence) in Cell Biology and Physiology, Toulouse University, France.

Sept. 1998-July 2000: 1st and 2nd years of “Classes Préparatoires aux Grandes Ecoles (Math. Sup., Math. Spe.)”, Lycée d’Auzeville, France.

RESEARCH ACTIVITIES

Jan. 2004-Present: Research assistant in the laboratory of Prof. Dr. Rolf Zeller, Developmental Genetics group, Department of Biomedicine, University of Basel Medical Faculty, Switzerland.

Thesis title: Interlinked signaling feedback loops and self-regulation during vertebrate limb development

Sept. 2002-Sept. 2003: Placement in the laboratory of Dr. F. Payre (signaling and cell morphogenesis) under the supervision of Dr. F. Roch at the Centre de Biologie du Développement, Toulouse, France.

Construction of transgenes coding for mutant forms of the small GTPase ARF6 and generation of drosophila strains carrying a loss-of-function allele of *Arf6*.

Feb. 2002-June 2002: Placement in the laboratory of Dr. F. Pituello (regionalisation of the vertebrate central nervous system) under the supervision of V. Lobjois at the Centre de Biologie du Développement, Toulouse, France.

Using microsurgical and pharmacological approaches, I studied the influence of the presomitic mesoderm and FGF signaling on the expression of cyclin D2 mRNA in the developing chicken spinal cord.

FELLOWSHIP

- Jan. 2004-Present: SNF Ph.D student fellowship
- Sept. 2002-June 2003: DEA studentship awarded by the Ministry of Education

TECHNICAL SKILLS

- Chick Embryo: Microsurgery (deletion and graft of presomitic mesoderm), Vibratome sectioning, mRNA *in situ* hybridization, embryo culture.
- Drosophila: Colony management, generation of loss-of-function mutants (hybrid dysgenesis), mRNA *in situ* hybridization, dissection of imaginal discs.
- Mouse: Colony management, genetics techniques including usage of the inducible Cre/LoxP system, genotyping, embryo isolation, mRNA *in situ* hybridization, cell death detection, embryonic limb bud culture, skeletal staining.
- Cell culture: Homologous recombination in mouse embryonic stem cells.
- Molecular biology: Genomic DNA extraction, Southern Blot, Western Blot, *in vitro* transcription, PCR, real time PCR, PCR-directed mutagenesis, cloning.
- Microscopy: General use of light and fluorescent microscopes.
- Software: MS Office (PowerPoint, Word, Excel), Adobe Photoshop and Illustrator, Mac Vector, Endnote...

LANGUAGES

French	Mother tongue
English	written and spoken
Spanish	Basic knowledge

POSTER PRESENTATIONS:

- 6th EMBL Mouse Molecular Genetics Meeting, EMBL Heidelberg, Germany, 2005.
- First Joint SFBD/ZMG Developmental Biology Meeting. Praz/Arly, France, 2006.
- Basel Computational Biology Conference, USGEB, Basel, Switzerland, 2007.
- “Cells into Organs” Meeting, Mechanisms of Early Development, Lisbon, Portugal, 2007.
- 10th International Conference on Limb Development and Regeneration. San Lorenzo de El Escorial, Madrid, Spain, 2008.

ORAL PRESENTATION:

- NCCR Frontiers in Genetics Annual Meeting, Saas-Fee, Switzerland, 2008.

PUBLICATIONS:

Research:

Jean-Denis Bénazet, Mirko Bischofberger, Eva Tiecke, Alexandre Gonçalves, James F. Martin, Aimée Zuniga, Felix Naef and Rolf Zeller. **A self-regulatory system of interlinked signaling feedback loops controls mouse limb patterning.** Science 20 February 2009: Vol. 323. no. 5917, pp. 1050 - 1053.

- Antonella Galli, Dimitri Robay, Marco Osterwalder, Jean-Denis Bénazet, Susan Mackem and Rolf Zeller. **Genetic dissection of the pre-patterning mechanism initiating polarity and *Shh* expression in mouse limb buds.** *In preparation.*

Book chapter:

- Jean-Denis Bénazet and Rolf Zeller. **Vertebrate limb development: moving from classical morphogen gradients to an integrated 4D patterning system.** In **Generating and interpreting gradient during development.** Cold Spring Harbor Laboratory Press 2009. *In press.*